AN ANALYTICAL AND EXPERIMENTAL STUDY OF ORTHOTROPIC STEEL BRIDGE DECKS

Abul Kalam Azad

A THESIS

in the

Faculty of Engineering

Presented in partial fulfilment of the requirements for
the Degree of Doctor of Engineering at
Sir George Williams University
Montreal, Canada

September, 1973

AN ANALYTICAL AND EXPERIMENTAL STUDY OF ORTHOTROPIC STEEL BRIDGE DECKS

AN ANALYTICAL AND EXPERIMENTAL STUDY OF ORTHOTROPIC STEEL BRIDGE DECKS

Abul Kalam Azad

ABSTRACT

A stiffness method of analysis of the conventional orthotropic steel bridge decks is proposed by idealizing the deck as a plate, stiffened only in the longitudinal direction and being continuous over flexible transverse floor beams. The main girders are assumed to provide simple supports to the deck. The basic theory of eccentrically stiffened plate is incorporated in this method, considering both open and closed type stiffeners. The proposed stiffness method and the design method of Pelikan-Esslinger are compared by applying them to solve several bridge decks of various proportions to check the sufficiency of the design method in a wide range of deck configurations.

An experimental investigation was conducted to observe the behaviour of the deck and the stress distribution under static loads. A twin plate girder bridge model with an orthotropic steel deck having closed ribs was fabricated for testing. The test results, when compared, showed a favourable agreement with results predicted by the proposed analytical method.

ACKNOWLEDGEMENTS

The entire work presented in this thesis was completed under the direct supervision of Dr. M.S. Troitsky, Professor of the Civil Engineering Department, to whom the author is deeply indebted for his valuable advice, suggestions and constant guidance throughout the course of this study.

The financial support provided by the National Research Council of Canada under Grant A4787 is gratefully acknowledged. The author also expresses his gratitude to all the Faculty members of the Civil Engineering Department, in particular to Dr. M. McC. Douglass and Dr. P.P. Fazio, for their co-operation and general interest in this study.

Thanks are also extended to Messrs. E. Heasman and L. Stankevicius, Structural Laboratory Technicians, who assisted in conducting experiments, to Mr. M. Wichterle, who helped to a great extent in operating the Data Acquisition System and to Miss M. Stredder and Mrs. D. Nathan for their typing of the manuscript.

CONTENTS

LIST OF FIGURES

LIST OF TABLES

NOTATIONS

A	area enclosed by the closed rib
A_w	effective web area of the floor beams
A_y	cross-sectional area of ribs in the y direction per unit length along the x axis
$[A]$	an 8 x 8 matrix containing coefficients
a	width of the deck in the x direction between supports
$\{B\}$	column vector containing amplitudes of the displacements u,v and w, and their derivatives
b	centre-to-centre spacing of the closed ribs
b_p	width of the deck plate within the closed rib
$\{C\}$	column matrix containing the arbitrary constants C_{1_m} to C_{8_m}
$\{C_f\}$	rectangular matrix of size 9 x 8 containing coefficients
$\{D_j\}$	Column matrix containing displacements corresponding to degrees of freedom
E	modulus of elasticity
F_a	shear flow in the closed rib
G	modulus of rigidity
I	moment of inertia of the deck plate per unit width
I_b	moment of inertia of the floor beams
I_y	moment of inertia of the area A_y about the middle surface of the deck plate

J_b	torsional constant of floor beams for pure torsion
J_p	torsional constant of the open type rib per unit length in the x direction for pure torsion
K_1, K_2, K_t	torsional constants used for the closed ribs
$K_{1_m}, K_{2_m}, K_{3_m}, K_{4_m}$	coefficients for the mth component of the series in the displacement u
K_{xy}	geometrical constant of the closed rib
ℓ	length of the deck between floor beams, i.e., the rib spans between floor beams
L_d	developed length of the closed rib
M_x, M_y	bending moments in the x and y directions with respect to the middle surface of the deck plate per unit length in the y and x directions, respectively.
M_{xy}, M_{yx}	torsional moments about the x and y axes per unit length in y and x directions respectively.
N_x, N_y	resultant normal forces in the x and y directions per unit length in the y and x directions
N_{xy}, N_{yx}	horizontal shear forces in the y and x directions per unit length in the x and y directions, respectively
P	arbitrary loading; $P = p(x,y)$
Q_m	amplitude of the mth component loading in the Fourier sine series
Q_{xz}, Q_{yz}	shear forces in the x and y directions per unit length in the y and x directions respectively
R_x, R_y	support reactions per unit length along the supports parallel to the y and x axes
$R_{1_m}, R_{2_m}, R_{3_m}, R_{4_m}$	coefficients for the mth component of the series in the displacement v

$[S]$	structure stiffness matrix
S_1, S_2, S_3, S_4	roots of the polynomial
$[S_p]$	panel stiffness matrix
t	thickness of the deck plate
t_r	thickness of the closed rib plate
u, v, w	displacements of a point on the middle surface of the deck plate in the x, y and z directions respectively
x, y, z	co-ordinates of a point on the deck; x-y plane is the middle surface of the plate and z is normal to the x-y plane
μ	Poisson's ratio
$\varepsilon_x, \varepsilon_y$	normal strains at a point in the deck in the x and y directions respectively
ε_{xy}	shear strain at a point in the deck plate
σ_x, σ_y	normal stresses at a point in the deck plate in the directions x and y respectively
σ'_y	normal stress at a point in the rib in the y direction
σ_{xy}, σ_{yx}	shear stress of a point in the deck plate
λ	rotation of the closed rib
θ, Φ	rotations
γ	relative rigidity ratio of the rib to the floor beams
α, β	coefficients

CHAPTER 1

INTRODUCTION

1.1 ORTHOTROPIC STEEL DECK BRIDGES - GENERAL

A new type of bridge construction, developed first in Europe after the Second World War as an answer to the shortage of steel and other materials, replaces the conventional concrete deck by a steel plate stiffened in both longitudinal and transverse directions together with a thin wearing surface on top. Bridges with this type of deck are often referred to as "Orthotropic Steel Deck" bridges.

An orthotropic plate, also known as orthogonal-anisotropic plate, possesses different elastic properties in two mutually perpendicular directions. Structurally, this may be achieved for a steel plate by stiffening it with closely spaced stiffeners in two perpendicular directions. The different rigidities of the plate in these directions characterize the behaviour of such a plate as being comparable to that of an orthotropic plate.

Aided by the improved welding and fabrication technique together with the experience from past construction, the orthotropic steel deck bridges are becoming increasingly popular in medium and long spans, because of some distinct advantages they have over other types. The substantial

reduction in the dead weight of such a bridge reflects in a considerable saving of the materials required for the structure. The participation of the deck in the action of the main members reduces the structural depth giving the bridge a slender appearance. The economy and structural efficiency of this system have led to numerous bridge constructions with these decks in the last two decades.

The deck plate performs several structural functions. It acts as top flange of the longitudinal stiffeners, the transverse floor beams and the main girders. The complex structural action and the resulting stress in the deck being of concern to the designers, the desirability of research on the subject has been apparent right from the beginning.

The early development of the theories and design methods for the orthotropic steel deck occurred in Europe, particularly in West Germany, where the first construction of such a bridge took place. It was only in the late 1950's and early 1960's that interest in this new concept spread to North America [1,2,3] and the first bridges were built [4,5]. Only recently, has interest in this type of construction and research on the subject gained a foothold in this continent. In the last decade, several major orthotropic steel deck bridges have been built in North America showing a diversified application of these decks in a variety of bridge systems, including box girder, cable stayed and suspension bridges. Four recently

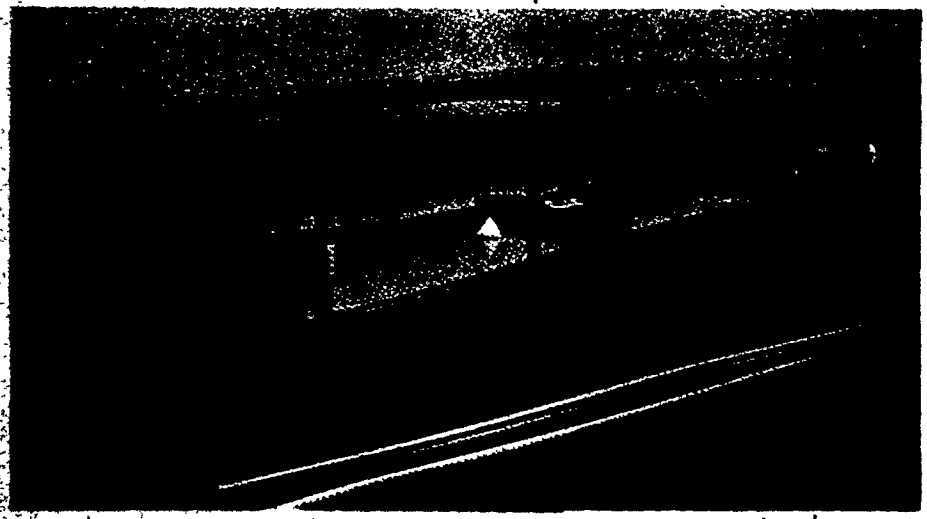

A. SAN MATEO-HAYWARD BRIDGE

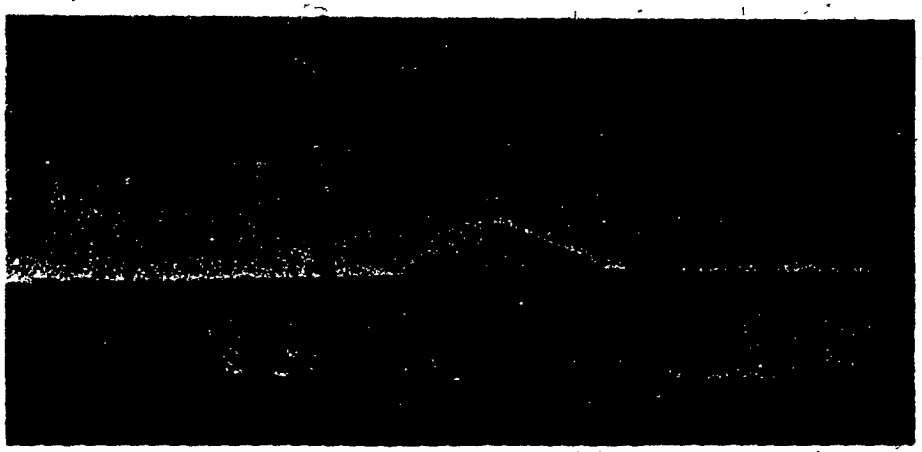

B. POPLAR BRIDGE

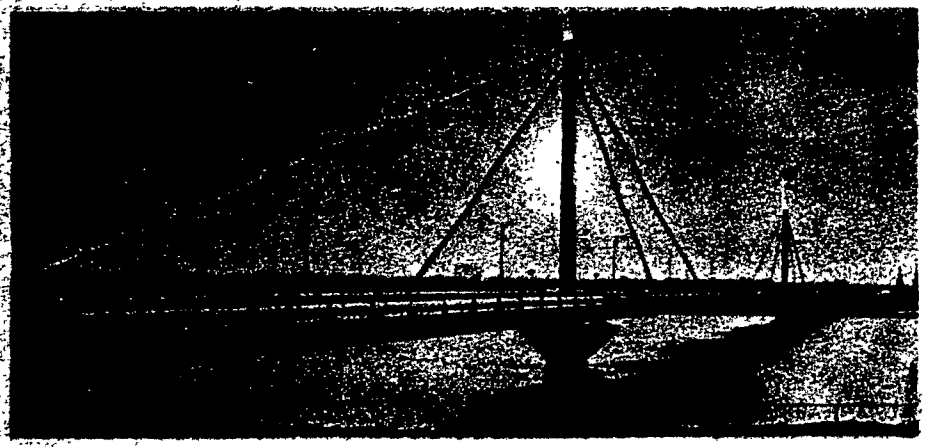

C. PAPINEAU-LEBLANC BRIDGE

D. A. MURRAY-MACKAY BRIDGE

FIG. 1.1 - FOUR RECENTLY BUILT NORTH AMERICAN BRIDGES

built orthotropic steel deck bridges are shown in Fig. 1.1.

1.2 STRUCTURAL SYSTEM

In the usual form of the construction, Fig. 1.2, the steel deck plate is stiffened by welding a series of closely spaced longitudinal stiffeners or ribs and transverse stiffeners or floor beams to the plate. Based on the types of stiffener, orthotropic steel decks are essentially of two types:

(i) Decks with torsionally soft or "open ribs" and

(ii) Decks with torsionally stiff or "closed ribs".

The first type consists of the open slender sections that have little torsional resistance, Fig. 1.3a. In Europe, the bulb-flat sections are preferred and frequently used due to their favourable structural properties. On the other hand, the closed ribs consist mainly of the box sections and Y-sections or the "Keltch" type stiffeners, Fig. 1.3b, which possess considerable torsional resistance.

The transverse floor beams are usually of inverted T-type sections, the upper flange of which is a portion of the deck plate. They are essentially of the same shape for both types of the deck. While the spacing of the longitudinal ribs, controlled mainly by the strength and deflection

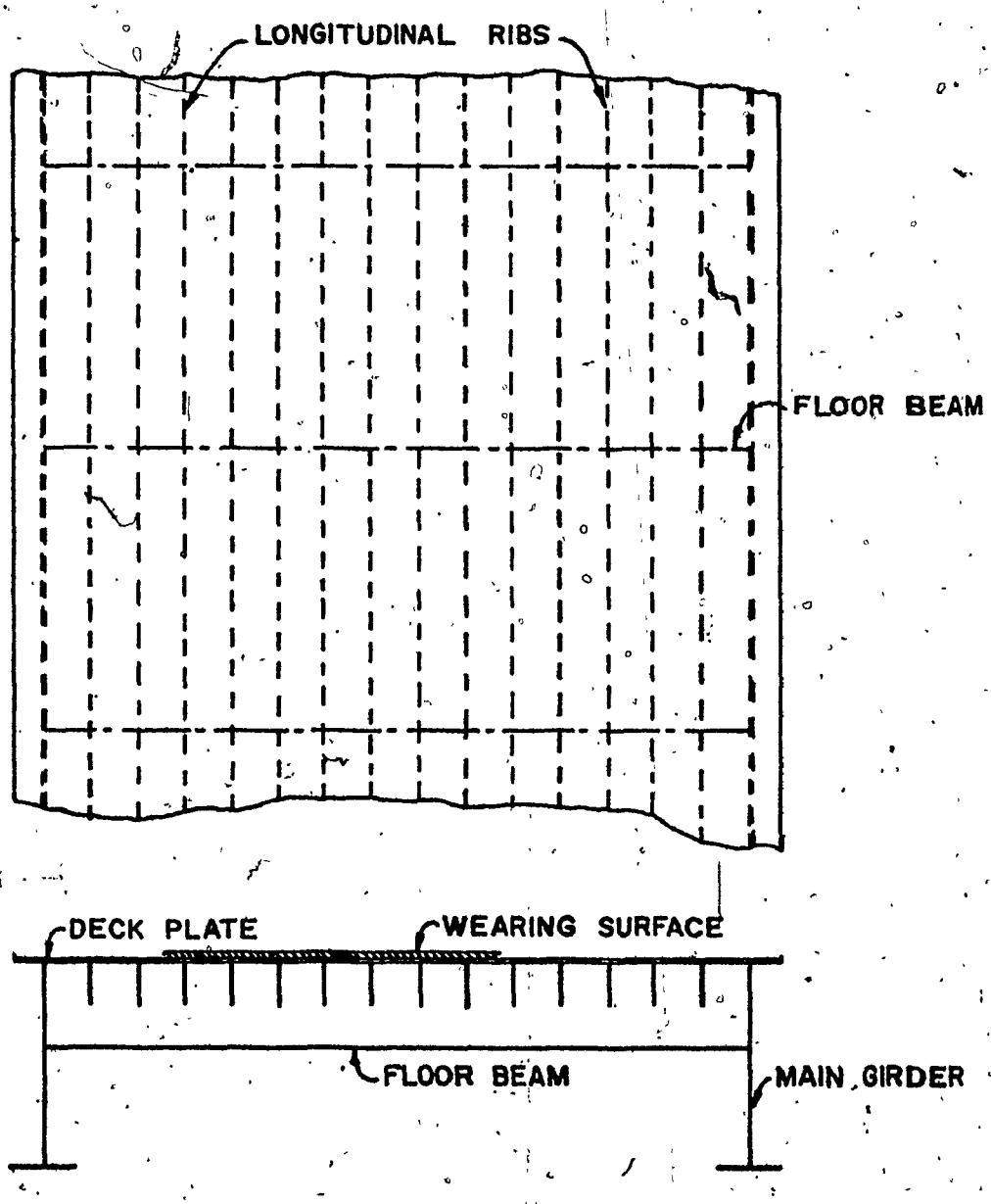

FIG. I.2 – GENERAL SCHEME OF ORTHOTROPIC STEEL DECK CONSTRUCTION

A. OPEN RIBS

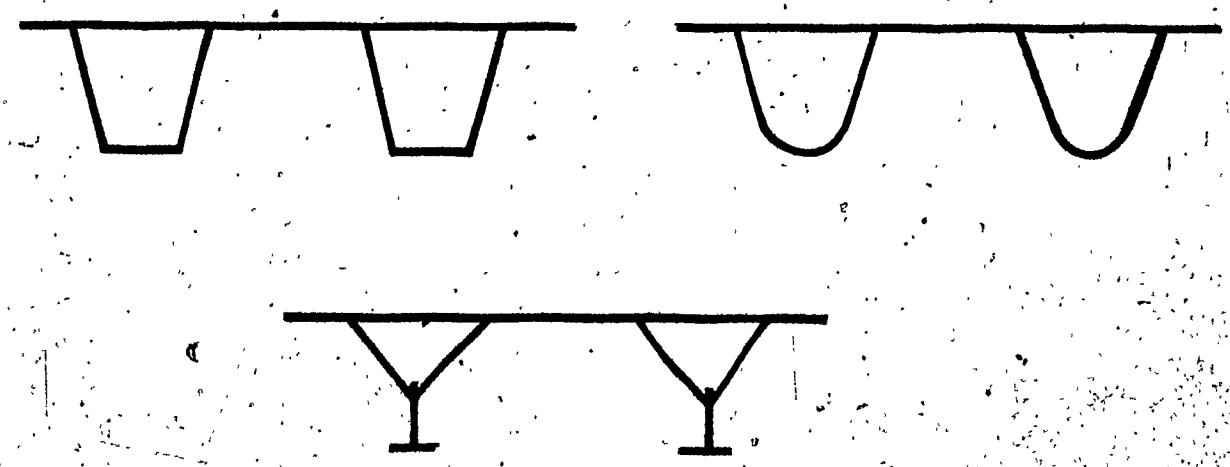

B. CLOSED RIBS

FIG. I-3 - TYPE OF RIBS

of the deck plate, is usually close, the floor beams are spaced at relatively large intervals and this depends upon the type of ribs, loading, and overall system of the structure. In the case of the deck with closed ribs, the floor beams are normally placed at larger spacing than that which would be required in a deck with open ribs, because of the better transverse load distribution capacity and higher stiffness of the former.

Both types of deck have their advantages and disadvantages, some of which are largely associated with the manner of construction [6,7]. In a recent article [8], the author has considered the use of open ribs as more favourable, in order to avoid the intensive local deformation and damage of the wearing surface due to sharper local deflections of the deck plate and larger differential deflection near the line of floor beam supports. It is worthwhile to mention here, that a comprehensive review of various possible forms of orthotropic deck construction made in Reference 9 concludes that there is a very little difference in weights between two types of deck under the same geometrical conditions.

The fabrication of such a complicated all-welded construction is of vital concern, as it controls largely the choice of the section and the cost involvement. Various methods have been used in fabricating these decks depending mainly on the practice of the company and the available equipment [6,8].

However, the general practice in North America so far has been to run the longitudinal ribs continuously through the floor beam cutouts which are carefully shaped to fit around the ribs.

1.3 PREVIOUS RESEARCH WORKS

Although research studies in the orthotropic steel bridge deck started after the Second World War, a considerable amount of work has been done in developing methods to analyze the deck. Most of the earlier work was done in Europe, particularly in West Germany. Whilst a great number of research work deals mainly with the mathematical models, relatively few are devoted to the experimental investigations on physical models. A comprehensive review of all existing mathematical and experimental works in this area is not intended, because many of them have been reported in References 6, 7 and 10. Consequently, only the significant highlights will be examined and a few of the latest works will be reviewed. For clarity, they are divided into two parts:

(i) Theoretical studies, and

(ii) Experimental studies.

1.3.1 Theoretical Studies

A survey of the available analytical methods proposed by numerous investigators to analyze the orthotropic deck shows that a large number of them are based basically on two

distinct approaches. In one approach, a widely used one, the "as built deck" is idealized as an equivalent orthotropic plate and the governing equations of such a plate are applied in various ways. The second approach is concerned with a rigorous treatment of the eccentrically stiffened plate which, however, involves more complicated mathematical analysis.

In the first approach, the rigidities of the longitudinal and transverse stiffeners are considered as distributed over the deck, thus transforming the actual discontinuous structural system into an equivalent orthotropic plate. This method of elastic equivalence was proposed first by Huber[11,12] and based on his theory of orthogonal anisotropic plate, the governing differential equation of such a plate is

$$D_x \frac{\partial^4 w}{\partial x^4} + 2H \frac{\partial^4 w}{\partial x^2 \partial y^2} + D_y \frac{\partial^4 w}{\partial y^4} = p(x,y) \qquad (1.1)$$

where D_x and D_y are the flexural rigidities in the x and y directions, respectively, H is the effective torsional rigidity and w is the deflection at coordinates x and y under the loading p. Solutions to many problems in orthotropic plate are given in the books of Lekhnitskii[13] and Timoshenko[14].

Cornelius[15] was the first to apply Huber's theory of equivalent orthotropic plate to analyze the orthotropic steel

bridge deck and derived the formulas necessary for the evaluation of moments and forces induced by various types of loadings. For torsional rigidity of the substitute system, a value determined empirically from the tests on a model was used.

In order to obtain the local stresses under loads between the floor beams which cannot be determined from the idealized plate with assumed continuously distributed rigidities, a refinement of the above method was proposed by Mader.[16]

In the course of time, various approaches were made by a number of investigators applying basically the orthotropic plate theory in different forms. Mention can be made of the grid method,[17] use of the influence surface[18] and the transformed coordinates method[19]. Evolution of these methods together with brief outlines are given in References 6 and 7.

All of the methods referred to above are, however, rather involved for design purposes. In 1957, Pelikan and Esslinger[20] developed a simplified method for the design of the stiffened steel plate decks, using an abbreviated form of Huber's equation. In this approach, the parameters of little influence in Equation (1.1) are disregarded. The method, due to its relative simplicity and reasonable accuracy, has been widely used in the design of many orthotropic deck bridges.

It is important to note that in all these methods, it has been customary to separate the deck structure from the

main carrying members, for which stresses are initially determined and then they are combined with those resulting from the action of the main carrying system. The latter is determined with the usual assumption that the deck plate with the longitudinal ribs acts as the top flange of the main members.

The design method of Pelikan-Esslinger is based on three independent structural component systems. In System 1, the deck acts as top flange of the main carrying members and in System II, the computation of moments and stresses in the deck alone, isolated as an independent structure, are carried out in two steps. First, the forces are calculated assuming that the deck plate with ribs are continuous over infinitely rigid floor beams and then to these values, additional effects due to the elastic flexibilities of floor beams are superimposed. In System III, the deck plate is considered to act locally between the ribs supporting the loads, and transmitting the reaction to the ribs.

Based primarily on this approach, in 1963, the American Institute of Steel Construction published a Design Manual[6] for the design of orthotropic steel plate deck bridges in order to promote interest on this continent in their construction and to provide criteria for the design of such structures. A comprehensive discussion of the basic theory and its engineering applications are also presented by Troitsky.[7]

The method of elastic equivalence, when applied to an orthotropic deck, represents an approximate treatment in the sense that the actual deck has stiffeners located only at the bottom of the plate, showing asymmetry with respect to the middle surface of the plate. As such, the neutral surfaces of the deck in bending about two axes parallel to the directions of the stiffeners do not usually coincide and increase the complexity of determining the orthotropic rigidity factors. Moreover, at the middle surface of the deck the strain is not zero and this indicates the presence of additional shear stresses that are disregarded in the orthotropic plate theory.

Pflüger [21,22] was the first to attack the problem rigorously. He obtained the force-displacement relations for such a typical plate element. His works, together with those of Trenks [23], Giencke [24-27], Massonnet [28] and others, have resulted in a refined analysis of the stiffened plate.

The elastic behaviour of such a deck under bending can be rigorously described by three simultaneous differential equations expressing three deformation components of the deck. The middle surface of the deck plate is taken as the reference plane for convenience and the displacements at any point in the deck, are measured in terms of the displacements of it. Expressing the displacements in trigonometric series, it is possible to combine the three differential equations into a single eighth order differential equation of the form

$$D_1\frac{\partial^8 w}{\partial x^8} + D_2\frac{\partial^8 w}{\partial x^6 \partial y^2} + D_3\frac{\partial^8 w}{\partial x^4 \partial y^4} + D_4\frac{\partial^8 w}{\partial x^2 \partial y^6} + D_5\frac{\partial^8 w}{\partial y^8} = Q \quad (1.2)$$

where D_1 to D_5 are expressed by the geometric and elastic characteristics of the plate and ribs and Q depends upon the fourth-order derivatives of loading $p(x,y)$. The development of the theory and the generalized solutions for various surface loadings are also presented by Clifton, Chang and Au [29] and Vitols, Clifton and Au [30].

It should be noted that these analytical investigations are based on the structural theory of the first order and may be considered rigorous as long as the deflection of the deck is small enough to eliminate the second order effect.

The effect of discontinuity of the rib arrangement in the deck was also considered in the case of open ribs by Schumann [31]. Attempts have been made by different authors [22,25,27] to determine rigorously the effective torsional rigidity of the closed rib system.

Most of the research works, published in the period 1961 to 1967, and pertaining to the structural action and design of the orthotropic bridge decks, are reviewed by Firmage [10], where the author has also presented briefly the state of knowledge in this field. Some of these analytical

methods are the modifications of Cornelius' solution by Chu and Krishnamoorthy [32], the application of eigen-functions by Schaefer [33] to determine stresses in the rib and plate due to bending, the inclusion of second-order membrane stress in the deck by Adotte [34] and the approach of Coull [35] who presented the direct stress analysis of orthotropic bridge slabs, by reducing the governing partial differential equation into a set of ordinary linear differential equations.

Further studies in this field show the application of such methods as the slope-deflection, the finite difference and the finite elements in analyzing the deck. Heins and Looney [36] employing the slope-deflection and the finite difference, and Dowling [37] utilizing the finite difference, have attempted to present solutions, basically using again the equivalent orthotropic plate theory. Heins and Yoo [38] have applied a grid technique to solve the entire bridge system, including the interaction of the main girders. The finite element method of analyzing the stiffened plate is presented by Williams and Scordelis [39], McBean [40], Powell and Ogden [41] and Tinawi [42]. While the approaches in References 39-41 are restricted to the open-type stiffeners, those of Reference 42 include both open and closed-type stiffeners.

1.3.2 Experimental Studies

Experimental investigations were also conducted to

investigate the performance and behaviour of the orthotropic bridge decks. Informative reports of some early experiments are contained in References 7 and 10. Among the earliest works, mention can be made of those done by Klöppel [43] in combination with others, from which useful data pertaining to the behaviour of the deck were obtained. He also showed that the ultimate load carrying capacity of the deck is many times greater than the load in the elastic range.

Test results reported by Nayuoka, Okabe and Hori [44] confirmed the plate-like behaviour of the orthotropic steel plate deck, and found satisfactory agreement between the computed and measured values for loading within the elastic range. Also, the problem of determining the effective width of the deck plate acting as the top flange of the main supporting girder has been looked into, both experimentally and theoretically, by Kondo, Kamatsy and Nakai [45]. Dowling [37] made some tests on an orthotropic deck model, the deck plate being stiffened by six closed ribs of trapezoidal shape. However, the model had little resemblance to an actual deck, due to the lack of any continuity of the ribs through a number of floor beams.

To perform major experimental works on the full-size structures, the California Division of Highways [46] has designed short-span bridges with orthotropic decks to investigate the overall structural behaviour, as well as fabrication

and erection problems. The studies of static and dynamic measurements of the Vacaville skew bridge have been reported by Bouwkamp [47]. Good agreement was claimed between the results of the experiment and the proposed theoretical analysis. Bouwkamp and Powell also conducted some field tests on an orthotropic steel deck bridge, the results of which can be found in Reference 48. Results of the field investigation on an aluminium orthotropic bridge deck is reported by Sharp [49]. For theoretical analysis, the method of Pelikan-Esslinger was used.

Fatigue tests were also conducted to find the behaviour of orthotropic steel decks under a fluctuating loading. The works of Davis and Toprac [50] and Erzurumlu and Toprac [51] can be mentioned in this connection. Decks stiffened both by conventional and biserrated trapezoidal ribs were considered in the later investigation.

An experimental investigation, conducted by Troitsky and Azad [52] on a plexiglass bridge model with an orthotropic deck found that the AISC Design Manual provides satisfactory methods of calculating bending stresses in the deck and suggested a procedure to determine the stresses in the cantilevered part of an orthotropic deck having open ribs. Test results from the experiment on a three panel orthotropic deck bridge model, reported by Glockner, Verma and de Paiva [53], concluded that Pelikan-Esslinger's method is adequate for safe

design of an orthotropic steel bridge deck.

1.4 SCOPE AND OBJECTIVES

Of all the various methods for analyzing the orthotropic bridge deck, the most practical one for design purposes is that of Pelikan-Esslinger. However, it is known that the method is essentially an approximate one, due to the many simplifying assumptions that are associated with it.

It is also known that Huber's equation for an orthotropic plate, if applied to an orthotropic steel bridge deck, introduces some error. The actual deck can be substituted as an equivalent orthotropic plate if the stiffeners are disposed symmetrically about the middle surface of the plate. Consequently, all methods based on the idealization of an equivalent orthotropic plate provide approximate solutions.

A look at existing orthotropic deck bridges will reveal that most of the deck configurations fall within a narrow range and a tendency may be observed to use somewhat similar deck proportioning. This is especially true for North American bridges, as seen from Table 1.1. The apparent reason is that design methods have been proven adequate in providing satisfactory solutions for these decks. However, for a wide range of the deck proportioning with a variety of variables, the reliability of the approximate method and its acceptability has not been carefully evaluated and compared with a more

TABLE 1.1

DECK PROPORTIONING IN SOME RECENT NORTH AMERICAN BRIDGES

Bridges	Year of erection	Deck plate thickness inch	Longitudinal ribs					Floor beams	
			Type	Thickness inch	Depth ins.	Width ins.	Spacing ins.	Type	Spacing
Concordia, Montreal	1965	7/16 - 1		5/16	13	12	24		15'-0"
Poplar Street, St. Louis	1968	9/16 -3/4		5/16	11	6½-13	26		15'-0"
San Mateo-Hayward, San Francisco	1968	5/8 -3/4		5/8 & 3/4	8 10 12		15		10'-5"
Coronado, San Diego	1969	3/8 &1/2		1/4 & 3/8	9 12	6 - 12	24		15'-0"
Papineau-Leblanc, Montreal	1969	7/16		1/4	13	12	24		15'-0"
A.Murray Mackay, Halifax	1970	3/8	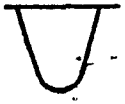	1/4	11	12	24		15'-10"

exact theory. This clearly indicates the desirability of a refined analysis, which should be based on a mathematical model closely resembling the actual structural system, and may form a good basis of evaluating the degree of reliability and accuracy of a design method in a wide range of deck configurations.

For this purpose, it is intended to use the rigorous theory of eccentrically stiffened plate[21-30] and apply it to analyze the decks. The structure will be idealized as a stiffened plate continuously supported by flexible floor beams. In the conventional orthotropic deck construction, the floor beams are spaced far apart and thus it would be inaccurate to assume their rigidities as distributed along the transverse direction over the entire width of floor beam spacing. It is more appropriate to consider them as elastic supports to the stiffened plate. Furthermore, to simplify the complex mathematical operations, it will be assumed that the deck is rectangular and the two opposite edges, supported by the main carrying members, are simply supported. The assumption of a simple support condition is generally satisfied if the bridge has two open type main girders having relatively small torsional rigidities, as shown in Fig. 1.4a. The idealized structure is then represented in Fig. 1.4b.

The primary objectives of this research are as follows:

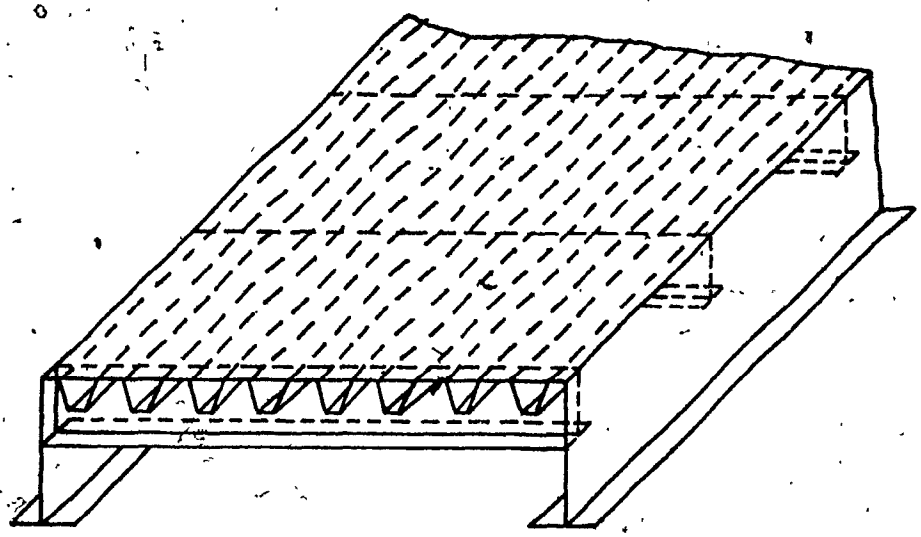

A. ACTUAL STRUCTURE

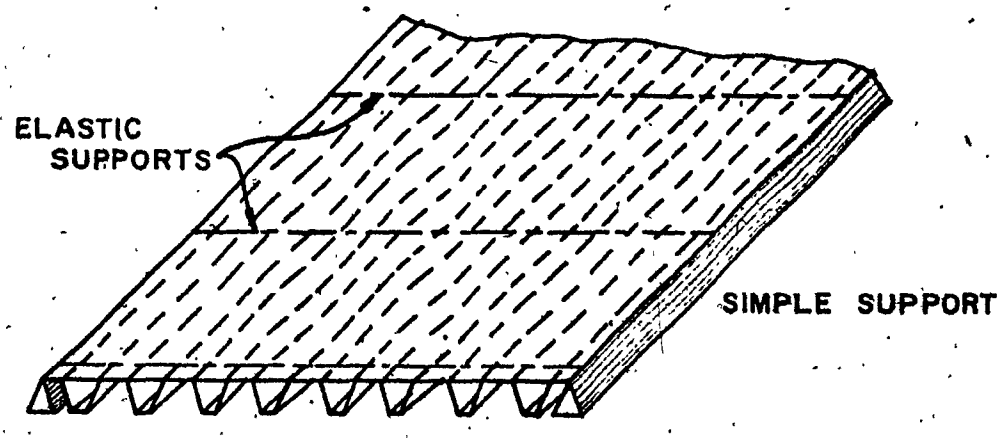

B. IDEALIZED STRUCTURE

FIG. I.4 – ACTUAL AND IDEALIZED STRUCTURE

(i) To develop a computerized method incorporating the basic theory of stiffened plate to readily analyze the conventional orthotropic steel bridge decks and find relevant solutions.

(ii) Compare the results of the proposed method with those obtained from the design method of Pelikan-Esslinger by applying both to analyze decks with various proportions.

(iii) Conduct an experimental investigation on a bridge model to check meaningfully the theoretical predictions and observe the deck behaviour under static loads.

(iv) Check the validity of the conventional procedure to determine the stresses in the deck due to girder bending.

In this analysis, the material is assumed to be elastic and homogeneous. For experimental investigation, all tests were confined within the elastic range of the material used.

1.5 OUTLINE OF THE THESIS

The contents of the thesis are briefly outlined here. In Chapter 2; the basic equations of eccentrically

stiffened plates are reviewed and modified to apply to the case of the conventional orthotropic bridge decks. Plates stiffened with both open and closed ribs are considered. Due to the mathematical complexity in incorporating the torsional rigidities of a closed rib, the approximate modified torsional rigidity of such a rib proposed by Giencke [27], is used in the governing differential equations.

Chapter 3 contains the proposed method of solution of an orthotropic deck. The widely spaced transverse floor beams are treated as elastic supports to the deck with appropriate spring constants to reflect their flexibilities. The stiffness matrix of a typical panel between floor beams and the simple supports of main girders is formulated, and a stiffness method of analysis for the entire deck, analogous to that of a continuous beam problem, is presented, together with a brief description of the main features of the computer program.

Chapter 4 contains the application of the proposed method and comparison with the design method of Pelikan-Esslinger by applying both of them to analyze several decks with different configurations. Both types of rib, open and closed, are considered, and parameters such as stiffener size, span and spacing etc., are varied.

In Chapter 5, the experimental part of this investigation is described in detail. Beginning with the model

material and fabrication, the entire test program with all instrumentations and experimental techniques is systematically presented.

Chapter 6 contains the test results and their presentation with a comprehensive discussion. Test measurements are in the form of strains and deflections. The results are compared with the analytical values obtained both from the proposed method and that of Pelikan-Esslinger.

Finally, in Chapter 7, the entire work is briefly summarized followed by a set of conclusions derived from this research. In the light of this study, some recommendations are made for future research work in this area.

CHAPTER 2

BASIC EQUATIONS OF ECCENTRICALLY STIFFENED PLATE

2.1 ASSUMPTIONS

The "as built orthotropic steel deck" is idealized as indicated in Figure 1.4 and will be treated basically as a plate stiffened eccentrically only in the longitudinal or the y-direction. The following assumptions are made in the development of the basic equations.

(i) The material is homogeneous, isotropic and linearly elastic.

(ii) The deck plate is flat and is of constant thickness.

(iii) The stiffeners are rigidly connected to the plate and are geometrically identical with uniform but close spacing.

(iv) The torsional resistance of the ribs due to warping is neglected.

(v) The plane sections remain plane with respect to the middle surface of the plate before and after bending.

2.2 DECK STIFFENED BY OPEN RIBS

A typical orthotropic plate element stiffened eccentrically with open ribs in the y-direction is shown in Figure 2.1, together with the forces acting on the positive faces. Due to asymmetry, the middle surface of the plate does not coincide with the centroidal axis in the y-direction. Thus, the forces N_x, N_y and N_{xy} or N_{yx} are present and increase the complexity of the problem.

In the refined analysis of such a plate, the governing differential equations are expressed in terms of the displacements, u, v and w, of the middle surface of the plate in the directions x, y and z, respectively. The displacements at any point are related to those at the middle surface.

Referring to Figure 2.1, the basic equations are written as follows:

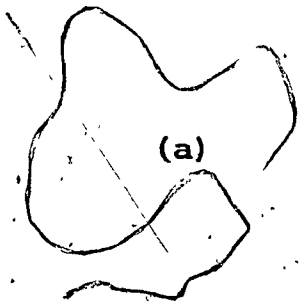

(a) Strain-displacement relations

$$\varepsilon_x = \frac{\partial u}{\partial x} - z\frac{\partial^2 w}{\partial x^2} \qquad (2.1)$$

$$\varepsilon_y = \frac{\partial v}{\partial y} - z\frac{\partial^2 w}{\partial y^2} \qquad (2.2)$$

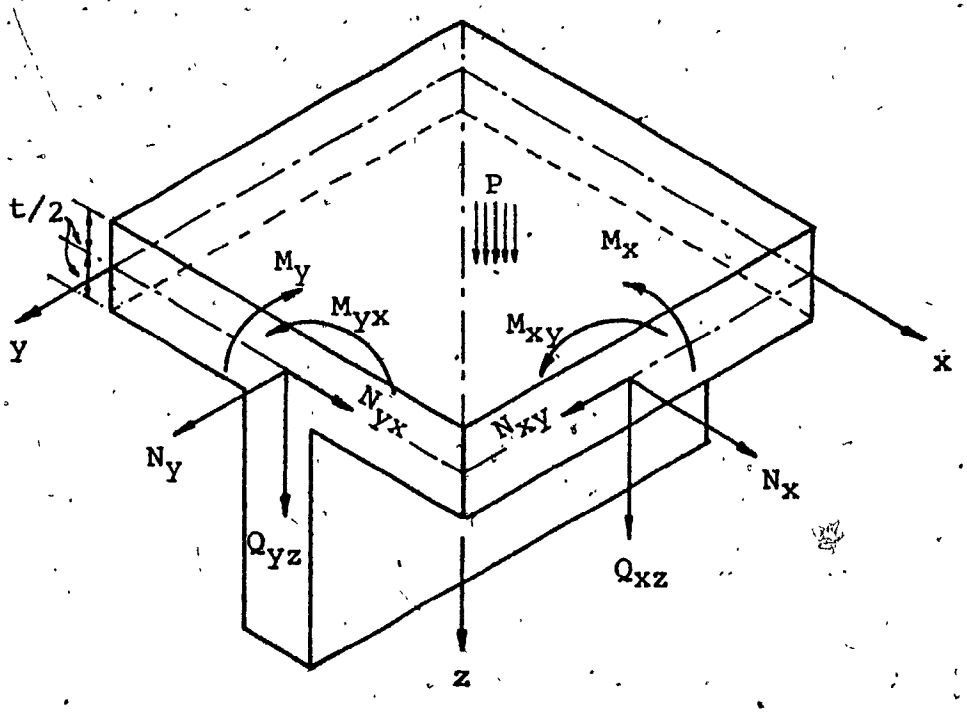

FIG. 2.1 – ORTHOTROPIC PLATE ELEMENT STIFFENED BY OPEN RIBS

$$\gamma_{xy} = \frac{\partial u}{\partial y} + \frac{\partial v}{\partial x} - 2z \frac{\partial^2 w}{\partial x \partial y} \qquad (2.3)$$

ε_x and ε_y are the normal strains in the x and y directions, respectively, and γ_{xy} is the shearing strain at ordinate z.

(b) Stress - displacement relations

for the plate

$$\sigma_x = \frac{E}{1-\mu^2} \left[\frac{\partial u}{\partial x} - z \frac{\partial^2 w}{\partial x^2} + \mu \left(\frac{\partial v}{\partial y} - z \frac{\partial^2 w}{\partial y^2}\right)\right] \qquad (2.4)$$

$$\sigma_y = \frac{E}{1-\mu^2} \left[\frac{\partial v}{\partial y} - z \frac{\partial^2 w}{\partial y^2} + \mu \left(\frac{\partial u}{\partial x} - z \frac{\partial^2 w}{\partial x^2}\right)\right] \qquad (2.5)$$

$$\sigma_{xy} = \frac{E}{2(1+\mu)} \left(\frac{\partial u}{\partial y} + \frac{\partial v}{\partial x} - 2z \frac{\partial^2 w}{\partial x \partial y}\right) \qquad (2.6)$$

and for the rib

$$\sigma'_y = E\left(\frac{\partial v}{\partial y} - z \frac{\partial^2 w}{\partial y^2}\right) \qquad (2.7)$$

(c) Force-displacement relations

$$N_x = Et^*\left(\frac{\partial u}{\partial x} + \mu\frac{\partial v}{\partial y}\right) \tag{2.8}$$

$$N_y = E\left(\bar{A}_y \frac{\partial v}{\partial y} + \mu t^*\frac{\partial u}{\partial x} - S_y\frac{\partial^2 w}{\partial y^2}\right) \tag{2.9}$$

$$N_{xy} = N_{yx} = Et_2^* \left(\frac{\partial u}{\partial y} + \frac{\partial v}{\partial x}\right) \tag{2.10}$$

$$Q_{xz} = -EI\left(\frac{\partial^3 w}{\partial x^3} + \frac{\partial^3 w}{\partial x \partial y^2}\right) \tag{2.11}$$

$$Q_{yz} = -E\left(\bar{I}_y \frac{\partial^3 w}{\partial y^3} + I \frac{\partial^3 w}{\partial x^2 \partial y} - S_y \frac{\partial^2 v}{\partial y^2}\right) \tag{2.12}$$

$$R_x = -EI\left[\frac{\partial^3 w}{\partial x^3} + (2-\mu) \frac{\partial^3 w}{\partial x \partial y^2}\right] \tag{2.13}$$

$$R_y = -E\left[\bar{I}_y \frac{\partial^3 w}{\partial y^3} + \{I'(2-\mu) + J^*\}\frac{\partial^3 w}{\partial x^2 \partial y} - S_y \frac{\partial^2 v}{\partial y^2}\right] \tag{2.14}$$

(d) Moment-Displacement Relations

$$M_x = -EI\left(\frac{\partial^2 w}{\partial x^2} + \mu\frac{\partial^2 w}{\partial y^2}\right) \tag{2.15}$$

$$M_y = -E\left(\bar{I}_y \frac{\partial^2 w}{\partial y^2} + \mu I\frac{\partial^2 w}{\partial x^2} - S_y \frac{\partial v}{\partial y}\right) \tag{2.16}$$

$$M_{xy} = EI(1-\mu)\frac{\partial^2 w}{\partial x \partial y} \qquad (2.17)$$

$$M_{yx} = -E[I(1-\mu) + J^*]\frac{\partial^2 w}{\partial x \partial y} \qquad (2.18)$$

In the above equations

E = modulus of elasticity,

μ = Poisson's ratio,

t = thickness of isotropic plate,

A_y = area of the rib in the y-direction per unit width in the x-direction

$t^* = \dfrac{t}{1-\mu^2}$

$t_2 = \dfrac{t}{2(1+\mu)}$

$\bar{A}_y = A_y + t^*$

$I = \dfrac{t^3}{12(1-\mu^2)}$ = moment of inertia per unit width of plate

S_y = moment of area A_y about the middle surface of the plate

I_y = moment of inertia of area A_y about the middle surface of the plate

$\bar{I}_y = I_y + I$

J_p = torsional constant of the open rib per unit length in the x-direction for pure torsion

$$J^* = \frac{J_p}{2(1+\mu)}$$

R_x, R_y = reactions at the supported edges parallel to the y-axis and x-axis, respectively.

Satisfying the equilibrium conditions of a plate element when acted upon by any normal loading $P = p(x,y)$, the following three differential equations are obtained:

$$t^*\frac{\partial^2 u}{\partial x^2} + t_1\frac{\partial^2 y}{\partial x \partial y} + t\frac{\partial^2 u}{\partial y^2} = 0 \qquad (2.19)$$

$$\bar{A}_y\frac{\partial^2 v}{\partial y^2} + t_1\frac{\partial^2 u}{\partial x \partial y} + t\frac{\partial^2 v}{\partial x^2} - S_y\frac{\partial^3 w}{\partial y^3} = 0 \qquad (2.20)$$

$$I\frac{\partial^4 w}{\partial x^4} + (2I+J^*)\frac{\partial^2 w}{\partial x^2 \partial y^2} + \bar{I}_y\frac{\partial^4 w}{\partial y^4} - S_y\frac{\partial^3 v}{\partial y^3} = \frac{P}{E} \qquad (2.21)$$

where

$$t_1 = \frac{t}{2(1-\mu)}$$

Eliminating u and v from the above differential equations, an eighth order differential equation in terms of w can be obtained in the form

$$a_1\frac{\partial^8 w}{\partial x^8} + a_2\frac{\partial^8 w}{\partial x^6 \partial y^2} + a_3\frac{\partial^8 w}{\partial x^4 \partial y^4} + a_4\frac{\partial^8 w}{\partial x^2 \partial y^6} + a_5\frac{\partial^8 w}{\partial y^8} =$$

$$= \frac{t_2}{t_1} Q \qquad (2.22)$$

where Q depends upon the fourth order derivative of loading P and the coefficients a_1 to a_5 are given as follows:

$$\begin{aligned}
a_1 &= t_2 t^* I \\
a_2 &= t_1^2 I - t_2^2 I - 2t_2 t^* I - t^* \bar{A}_y I - t^* t_2 J_p \\
a_3 &= 2t_2^2 I - 2t_1^2 I + 2t^* \bar{A}_y I + t_2 \bar{A}_y I + t_2 t^* \bar{I}_y \\
&\quad + t^* \bar{A}_y J^* - 2t_1^2 I J^* + 2t_2^2 I J^* \qquad (2.23) \\
a_4 &= t^* S_y^2 + t_1^2 \bar{I}_y - t_2^2 \bar{I}_y - 2t_2 \bar{A}_y I - t^* \bar{A}_y \bar{I}_y \\
&\quad - \bar{A}_y t_2 J^* \\
a_5 &= t_2 \bar{A}_y \bar{I}_y - t_2 S_y^2
\end{aligned}$$

The set of three simultaneous partial differential Equations (2.19 - 2.21) of fourth order or the single differential equation of eighth order (Eq. 2.22), describes the deformation of a stiffened plate with open stiffeners subjected to a normal loading.

2.3 DECK STIFFENED WITH CLOSED RIBS

The forces acting on the positive faces of a typical plate element stiffened by closed ribs are shown in Figure 2.2. Due to the geometrical characteristics of such a

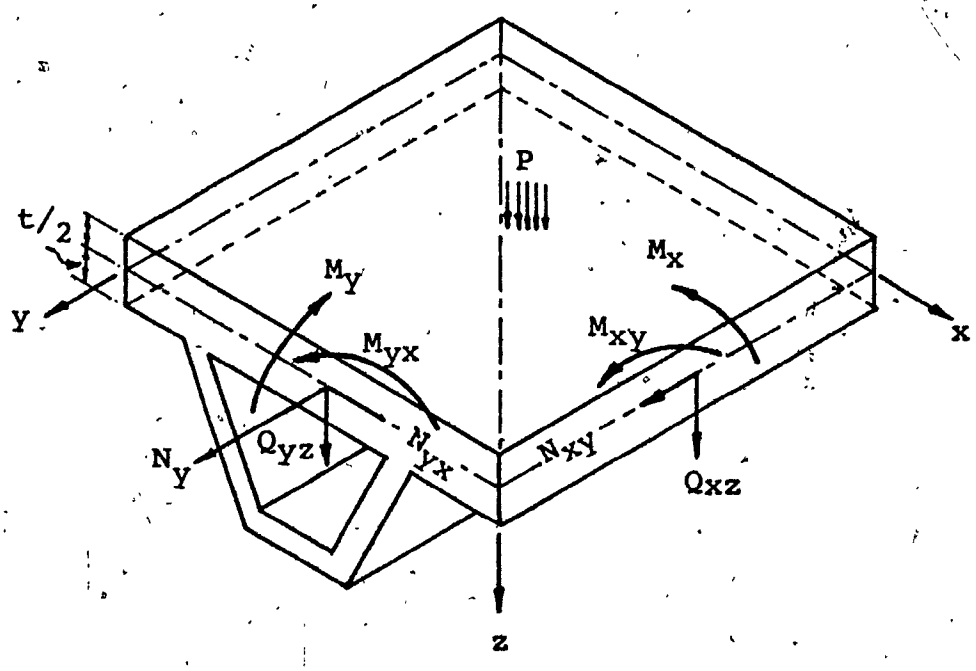

FIG. 2.2 – ORTHOTROPIC PLATE ELEMENT STIFFENED BY CLOSED RIBS

rib, of all quantities shown in Figure 2.2, only N_{yx} and M_{yx} may possibly have force displacement relations different from those in the case of open ribs.

If the angle of twist per unit length of the closed rib is assumed to be the same as that of the middle surface of the plate, the geometrical configuration of the deformed deck would be represented by the dotted line in Figure 2.3a. The expression for M_{yx} can be written then, with relative simplicity, as given in References (22) and (29). However, this assumption overestimates the actual value of the torsional rigidity of the structural system and is valid only in the case of a sufficiently thick or rigid plate which would permit the deck to have a smooth deflection curve, as indicated by the dotted line.

In an actual case, however, the deck plate is relatively thin and flexible and deforms due to shear transfer in the transverse or the x-direction. The geometry of the deck after bending thus corresponds to the wavy curve as shown by the solid line in Figure 2.3a. As a result, the full theoretical torsional rigidity of the ribs, corresponding to their geometry and plate thickness, is not fully utilized.

As shown in Figure 2.3b, the torsional rotation of the deformed rib per unit length is not the same as that of the deck plate and is smaller than the latter. This in-

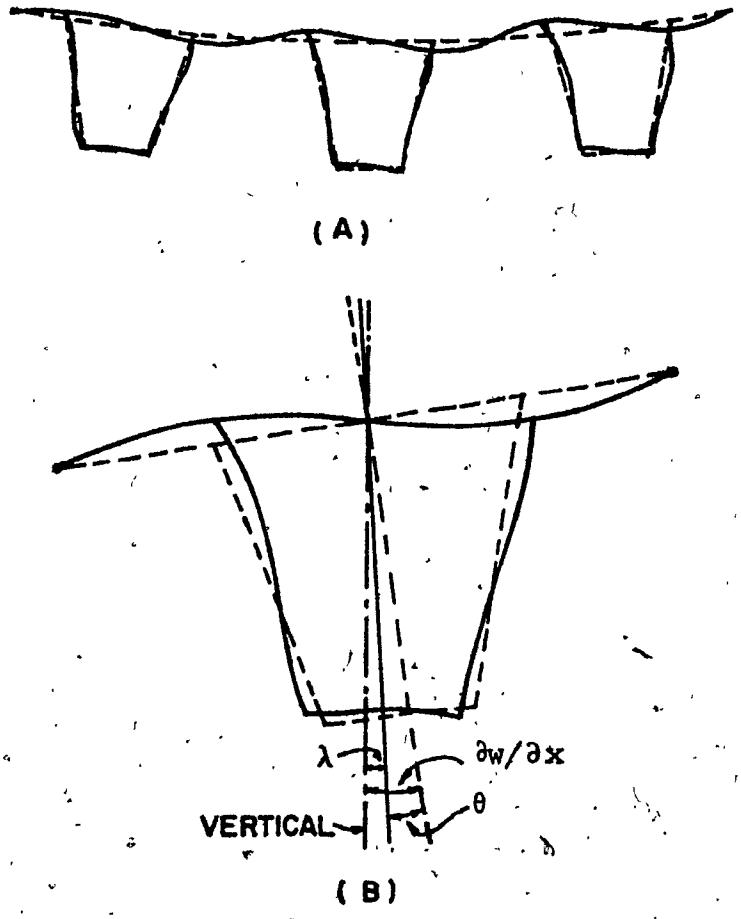

FIG. 2.3 – DEFORMATION OF DECK PLATE AND RIB AFTER BENDING

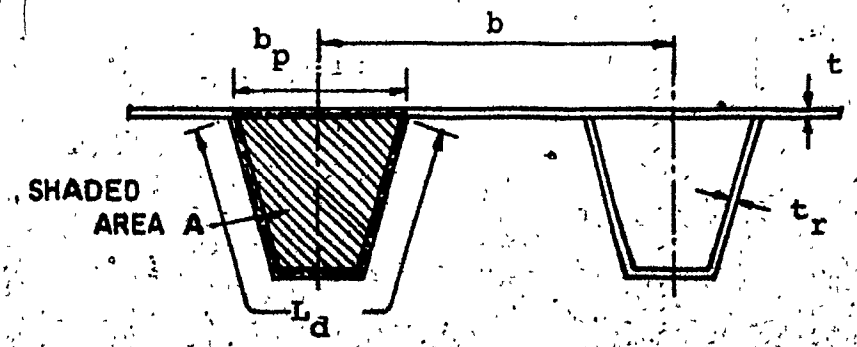

FIG. 2.4 – DIMENSIONS OF CLOSED RIB

equality in the angle of twist constitutes a rather difficult problem to correctly express and use the value of the torsional rigidity. The actual rib rotation, λ, is related to the plate rotation as

$$\lambda = \frac{\partial w}{\partial x} - \theta \qquad (2.24)$$

In order to write the general expression for M_{yx} considering the deformation of the rib in Figure 2.3b, three effects are to be distinguished. First, the deck plate alone undergoing a twist of $\frac{\partial^2 w}{\partial x \partial y}$ will be subjected to a torsional moment $M_{yx,1}$ given by

$$M_{yx,1} = EI(1-\mu)\frac{\partial^2 w}{\partial x \partial y} \qquad (2.25)$$

The torsional moment $M_{yx,2}$, due to the twisting of the rib alone, can be expressed by the formula for torsion of thin-walled hollow members as [54]

$$M_{yx,2} = K_t G \frac{\partial \lambda}{\partial y} = \frac{EK_t}{2(1+\mu)} \frac{\partial \lambda}{\partial y} \qquad (2.26)$$

with

$$K_t = \frac{4A^2}{\frac{b_p}{t} + \frac{L_d}{t_r}} \qquad (2.27a)$$

Where G is the shear modulus, A is the area enclosed by the box rib, b_p is the width of the plate within the rib, t_r is the thickness of the rib and L_d is the developed length of the rib section, as shown in Figure 2.4. With notation

$$K' = \frac{K_t}{2(1+\mu)} \qquad (2.27b)$$

$$M_{yx,2} = EK' \frac{\partial \lambda}{\partial y} \qquad (2.28)$$

The horizontal shear force N_{yx} acting at the middle surface of the plate is eccentric with respect to the shear centre of the closed rib and therefore, an additional torsional moment $M_{yx,3}$, must be applied to satisfy the equilibrium requirement. If the shear flow in the closed section due to this twisting moment is designated by F_a, then from membrane analogy [54]

$$M_{yx,3} = -2A F_a \qquad (2.29)$$

and

$$F_a = \frac{\frac{b_p}{t}}{\frac{b_p}{t} + \frac{L_d}{t_r}} N_{yx} \qquad (2.30)$$

Due to the shear flow caused by the torsional moments $M_{yx,2}$ and $M_{yx,3}$, the horizontal shearing force at the middle surface of the deck plate is not given by the

same expression over the entire width of the plate, b. However, as the sum of the horizontal components of the shear flow due to $M_{yx,2}$ and $M_{yx,3}$ around the perimeter of the closed rib is zero, the net horizontal shear force per unit length in the x-direction still remains the same. For relative simplicity, therefore, the same expression for N_{yx} as used in the case of open ribs can also be applied in this case.

With the values of N_{yx} from Eq. (2.10) and F_a from Eq. (2.30)

$$M_{yx,3} = - \frac{Ab_p}{b\, t\left(\frac{p}{t} + \frac{L_d}{t_r}\right)} \frac{Et}{(1+\mu)} \left(\frac{\partial u}{\partial y} + \frac{\partial v}{\partial x}\right) \qquad (2.31)$$

Designating

$$K_2 = \frac{Ab_p}{b\left(\frac{p}{t} + \frac{L_d}{t_r}\right)(1+\mu)} \qquad (2.32)$$

$$M_{yx,3} = - EK_2 \left(\frac{\partial u}{\partial y} + \frac{\partial v}{\partial x}\right) \qquad (2.33)$$

Total torsional moment M_{yx} acting per unit length in the x-direction is

$$M_{yx} = - \left(M_{yx,1} + \frac{M_{yx,2} + M_{yx,3}}{b}\right) \qquad (2.34)$$

which leads to

$$M_{yx} = -EI(1-\mu)\frac{\partial^2 w}{\partial x \partial y} - EK'\frac{\partial \lambda}{\partial y} + Ek_2\left(\frac{\partial u}{\partial y} + \frac{\partial v}{\partial x}\right) \quad (2.35)$$

The expression of M_{yx} involves the partial derivatives of the displacements u, v and w, as well as the angle λ which is related to w by Eq. (2.24). Giencke [26] has attempted to solve the general differential equations, taking into consideration the rotation λ, but the treatment is too complicated to apply in the analysis of an actual bridge deck. The problem, however, can be simplified considerably if the value $EK' \frac{\partial \lambda}{\partial y}$ is replaced by a modified value $EK_1 \frac{\partial^2 w}{\partial x \partial y}$, where EK_1 is a more reduced value than EK'. The value of K_1 can be used approximately in the following form [26], using only the first component

$$EK_1 = \frac{EK'}{1 + \left(\frac{\pi}{\ell}\right)^2 \frac{EK'}{K_{xy}}} \quad (2.36)$$

where K_{xy} is a geometrical constant of the rib and the plate, as given in Reference (26), and ℓ is the span length of the rib.

The rearranged equation for M_{yx} is then

$$M_{yx} = -E\left[\{I(1-\mu) + K_1\}\frac{\partial^2 w}{\partial x \partial y} - K_2\left(\frac{\partial u}{\partial y} + \frac{\partial v}{\partial x}\right)\right] \quad (2.37)$$

Consequently, the reaction R_y at the supported edge parallel to the x-axis, is given as

$$R_y = - E[\bar{I}_y \frac{\partial^3 w}{\partial y^3} + \{I(2-\mu) + K_1\} \frac{\partial^3 w}{\partial x^2 \partial y} - S_y \frac{\partial^2 v}{\partial y^2} + K_2 (\frac{\partial^2 v}{\partial x \partial y} + \frac{\partial^2 v}{\partial x^2})] \quad (2.38)$$

The value of M_{xy} remains the same as in the case of open ribs. Using the new value of M_{yx} from Eq. (2.37), the governing differential Eq. (2.21) becomes in the case of closed ribs

$$I \frac{\partial^4 w}{\partial x^4} + (2I + K_1) \frac{\partial^4 w}{\partial x^2 \partial y^2} + \bar{I}_y \frac{\partial^4 w}{\partial y^4} - S_y \frac{\partial^3 v}{\partial y^3} - K_2 (\frac{\partial^3 u}{\partial x \partial y^2} + \frac{\partial^3 v}{\partial x^2 \partial y}) = \frac{P}{E} \quad (2.39)$$

It is seen that Eq. (2.39) reduces to Eq. (2.21) by letting $K_1 = J^*$ and $K_2 = 0$. Eqs. (2.19), (2.20) and (2.39), describe the deformation of a plate stiffened by closed ribs and being subjected to an arbitrary normal loading P.

2.4 SOLUTION OF DIFFERENTIAL EQUATIONS

It is necessary only to consider the differential equations for the closed ribs, namely Eqs. (2.19), (2.20) and

(2.39), as these equations can be modified easily to apply them in the case of open ribs, by simply substituting $K_1 = J^*$ and $K_2 = 0$.

In the case of a rectangular plate with two opposite edges, $x = 0$ and $x = a$, being simply supported, Figure 2.5, a single series solution of Levy type can be formulated for the displacements u, v and w representing the homogeneous solution of the differential Eqs. (2.19), (2.20) and (2.39), which are expressed as

$$W_h = \sum_{m=1}^{\infty} W_m \sin \bar{m}x$$

$$U_h = \sum_{m=1}^{\infty} U_m \cos \bar{m}x \qquad (2.40)$$

$$V_h = \sum_{m=1}^{\infty} V_m \sin \bar{m}x$$

where $\bar{m} = m\pi/a$ and W_m, U_m and V_m are the functions in y only.

As presented in Reference (30), the functions W_m, U_m and V_m can be written in the following form for the mth component of the series:

$$W_m = \sum_{j=1}^{4} [C_{jm} e^{s_j \bar{m} y} + C_{(j+4)m} e^{-s_j \bar{m} y}] \qquad (2.41)$$

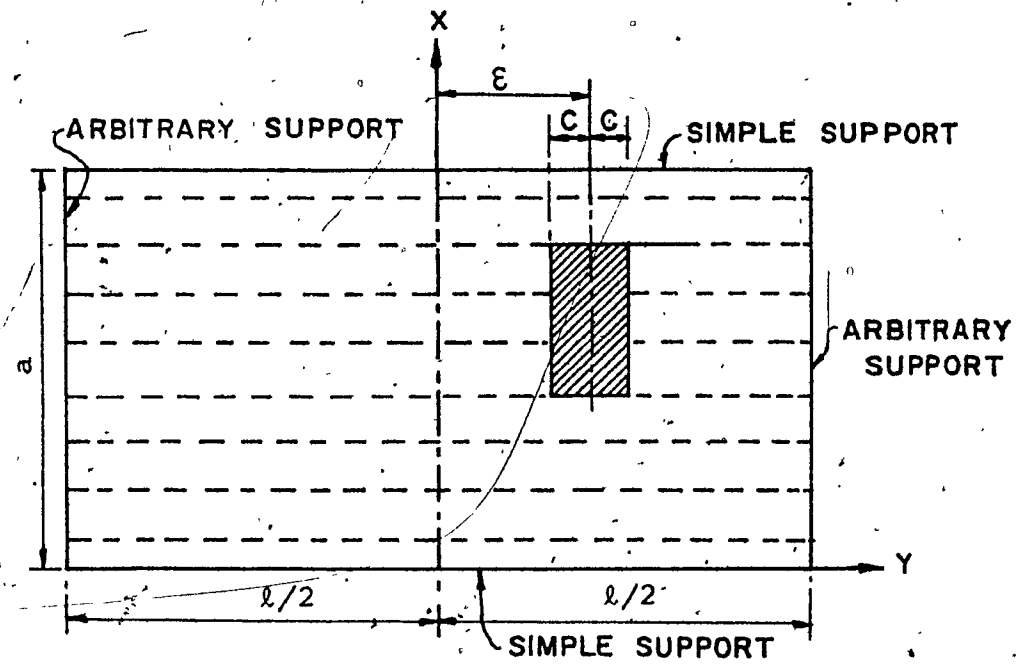

A. PLAN

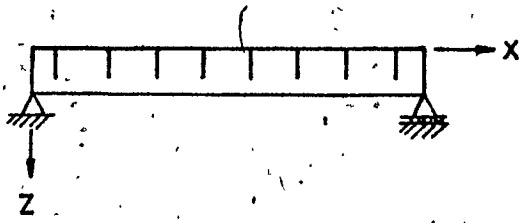

B. CROSS SECTION

FIG. 2.5 - RECTANGULAR STIFFENED PLATE PANEL WITH SURFACE LOADING

$$U_m = \sum_{j=1}^{4} [K_{jm} C_{jm} e^{s_j \bar{m} y} + K_{(j+4)m} C_{(j+4)m} e^{-s_j \bar{m} y}] \quad (2.42)$$

$$V_m = \sum_{j=1}^{4} [R_{jm} C_{jm} e^{s_j \bar{m} y} + R_{(j+4)m} C_{(j+4)m} e^{-s_j \bar{m} y}] \quad (2.43)$$

where $C_{1m}, \ldots\ldots, C_{8m}$ are the arbitrary constants to be determined from the boundary conditions at $y = \pm \frac{\ell}{2}$ and

$$K_{jm} = \frac{-\bar{m}^* S_y t_1 S_j^4}{-(t^* - t_2 S_j^2)(\bar{A}_y S_j^2 - t_2) + t_1^2 S_j^2} \quad (2.44)$$

$$R_{jm} = \frac{-\bar{m} S_y (t^* - t_2 S_j^2)}{-(t^* - t_2 S_j^2)(\bar{A}_y S_j^2 - t_2) + t_1^2 S_j^2}$$

also

$$K_{jm} = K_{(j+4)m}$$

$$R_{jm} = -R_{(j+4)m} \quad (j=1, \ldots\ldots, 4) \quad (2.45)$$

The values of $\pm S_1$, $\pm S_2$, $\pm S_3$ and $\pm S_4$ are the eight roots of the eighth order polynomial

$$a_5' S^8 + a_4' S^6 + a_3' S^4 + a_2' S^2 + a_1' = 0 \quad (2.46)$$

where the coefficients a_5' to a_1' are given as follows:

$$
\begin{aligned}
a_5' &= t_2(\bar{A}_y\bar{I}_y - S_y^2) \\
a_4' &= t^*S_y^2 + t_2^2\bar{I}_y - t_2^2\bar{I}_y - 2t_2\bar{A}_y I - t^*\bar{A}_y\bar{I}_y \\
&\quad - A_y t_2 K_1 - S_y t_1 K_2(t_1 - t_2) \\
a_3' &= 2t_2^2 I - 2t_1^2 I + 2t^*\bar{A}_y I + t_2\bar{A}_y\bar{I}_x + t_2 t^*\bar{I}_y \\
&\quad + K_1 t^*\bar{A}_y - K_1(t_1^2 - t_2^2) - K_2 t^* S_y \\
a_2' &= t_1^2 I - t_2^2 I - 2t_2 t^* I - t^*\bar{A}_y I - K_1 t^* t_2 \\
a_1' &= t_2 t_3 t^* I
\end{aligned}
\tag{2.47}
$$

The above coefficients a_5' to a_1' reduce to a_5 to a_1 as given by the expressions in Eqs. (2.23) in the case of open ribs, by letting $K_1 = J^*$ and $K_2 = 0$.

For an actual bridge deck with open type ribs, out of eight roots from Eq. (2.46), two pairs, say, $\pm S_1$ and $\pm S_2$, are always real and the remaining pairs, $\pm S_3$ and $\pm S_4$, are complex conjugates. A proof of this is given in Appendix I.

However, for an orthotropic deck with closed ribs, such a distinction among the roots cannot be made. There are only two possible variations. Either two pairs of roots are

real and the remaining two pairs are complex conjugate or all the four pairs are real. In the case of all pairs of roots being real, the expressions for displacement functions in Eqs. (2.41-2.43) become relatively simple. However, they become somewhat complicated, if the two pairs of roots are complex conjugates. Dealing with this case and designating the complex conjugate roots as

$$S_3 = \alpha + i\beta$$

and (2.48)

$$S_4 = \alpha - i\beta$$

where both α and β are real, Eqs. (2.41-2.43) can be rearranged, realizing that the constants C_{jm} associated with the complex conjugate roots are also complex conjugate. This leads to the following expressions of the displacement functions in terms of the new constants, C_{im} (i,....., 8).

$$W_m = C_{1m}e^{s_1\bar{m}y} + C_{2m}e^{s_2\bar{m}y} + 2C_{3m}e^{\alpha\bar{m}y}.\cos\beta\,\bar{m}y$$

$$+ 2C_{4m}e^{\alpha\bar{m}y}.\sin\beta\,\bar{m}y + C_{5m}e^{-s_1\bar{m}y} + C_{6m}e^{-s_2\bar{m}y} \quad (2.49)$$

$$+ 2C_{7m}e^{-\alpha\bar{m}y}.\cos\beta\,\bar{m}y + 2C_{8m}e^{-\alpha\bar{m}y}.\sin\beta\,\bar{m}y$$

$$U_m = K_{1m} C_{1m} e^{s_1 \bar{m} y} + K_{2m} C_{2m} e^{s_2 \bar{m} y} + 2C_{3m} e^{\alpha \bar{m} y}$$
$$[K_{3mr} \cos\beta \bar{m} y - K_{3mi} \sin\beta \bar{m} y] - 2C_{4m} e^{\alpha \bar{m} y}$$
$$[K_{3mr} \sin\beta \bar{m} y + K_{3mi} \cos\beta \bar{m} y] + K_{1m} C_{5m} e^{-s_1 \bar{m} y}$$
$$+ K_{2m} C_{6m} e^{-s_2 \bar{m} y} + 2C_{7m} e^{-\alpha \bar{m} y} [K_{3mr} \cos\beta \bar{m} y \quad (2.50)$$
$$+ K_{3mi} \sin\beta \bar{m} y] + 2C_{8m} e^{-\alpha \bar{m} y} [K_{3mr} \sin\beta \bar{m} y$$
$$- K_{3mi} \cos\beta \bar{m} y]$$

$$V_m = R_{1m} C_{1m} e^{s_1 \bar{m} y} + R_{2m} C_{2m} e^{s_2 \bar{m} y} + 2C_{3m} e^{\alpha \bar{m} y}$$
$$[R_{3mr} \cos\beta \bar{m} y - R_{3mi} \sin\beta \bar{m} y] - 2C_{4m} e^{\alpha \bar{m} y}$$
$$[R_{3mr} \sin\beta \bar{m} y + R_{3mi} \cos\beta \bar{m} y] - R_{1m} C_{5m} e^{-s_1 \bar{m} y}$$
$$- R_{2m} C_{6m} e^{-s_2 \bar{m} y} - 2C_{7m} e^{-\alpha \bar{m} y} [R_{3mr} \cos\beta \bar{m} y \quad (2.51)$$
$$+ R_{3mi} \sin\beta \bar{m} y] + 2C_{8m} e^{-\alpha \bar{m} y} [- R_{3mr} \sin\beta \bar{m} y$$
$$+ R_{3mi} \cos\beta \bar{m} y]$$

In the above equations

$$K_{3m} = K_{3mr} + i K_{3mi}$$

$$K_{4m} = K_{3mr} - i K_{3mi}$$

$$R_{3m} = R_{3mr} + i R_{3mi} \qquad (2.52)$$

and

$$R_{4m} = R_{4mr} - i R_{4mi}$$

In the case of the applied loading width being symmetric with respect to the x-axis, the above displacement functions are reduced to the following forms, knowing that the displacements W_m and U_m must be symmetric and V_m must be antisymmetric with respect to the x-axis. Therefore

$$W_m = 2C_{1m} \cosh s_1\bar{m}y + 2C_{2m} \cosh s_2\bar{m}y + 4C_{3m} \cosh\alpha\bar{m}y \cos\beta\bar{m}y - 4C_{4m} \sinh\alpha\bar{m}y \sin\beta\bar{m}y \qquad (2.53)$$

$$U_m = 2K_{1m}C_{1m}\cosh S_1\bar{m}y + 2K_{2m}C_{2m}\cosh S_2 my$$
$$+ 4C_{3m}[K_{3mr}\cos\beta\bar{m}y \cosh\alpha\bar{m}y -$$
$$K_{3mi}\sin\beta\bar{m}y \sin\alpha\bar{m}y - 4C_{4m}[K_{3mr}\sin\beta\bar{m}y \quad (2.54)$$
$$\sinh\alpha\bar{m}y + K_{3mi}\cos\beta\bar{m}y \cosh\alpha\bar{m}y]$$

$$V_m = 2R_{1m}C_{1m}\sinh S_1\bar{m}y + 2R_{2m}C_{2m}\sinh S_2\bar{m}y +$$
$$4C_{3m}[R_{3mr}\cos\beta\bar{m}y \sinh\alpha\bar{m}y - R_{3mi}\sinh\beta\bar{m}y$$
$$\cosh\alpha\bar{m}y] - 4C_{4m}[R_{3mr}\sin\beta\bar{m}y \cosh\alpha\bar{m}y + \quad (2.55)$$
$$+ R_{3mi}\cos\beta\bar{m}y \sinh\alpha\bar{m}y]$$

For the case of an antisymmetric loading about the x-axis

$$W_m = 2C_{1m}\sinh S_1\bar{m}y + 2C_{2m}\sinh S_2\bar{m}y +$$
$$4C_{3m}\sinh\alpha\bar{m}y \cos\beta\bar{m}y - 4C_{4m}\cosh\alpha\bar{m}y, \quad (2.56)$$
$$\sin\beta\bar{m}y$$

$$U_m = 2K_{1m}\,C_{1m}\sinh S_1\bar{m}y + 2K_{2m}\,C_{2m}\sinh S_2\bar{m}y + 4C_{3m}\,[K_{3mr}\sinh\alpha\bar{m}y\ \cos\beta\bar{m}y - K_{3mi}\cosh\alpha\bar{m}y \sin\beta\bar{m}y] - 4C_{4m}\,[K_{3mr}\cosh\alpha\bar{m}y\ \sin\beta\bar{m}y + K_{3mi}\sinh\alpha\bar{m}y\ \cos\beta\bar{m}y] \tag{2.57}$$

$$V_m = 2R_{1m}\,C_{1m}\cosh S_1\bar{m}y + 2R_{2m}\,C_{2m}\cosh S_2\bar{m}y - 4C_{3m}\,[R_{3mr}\cos\beta\bar{m}y\ \cosh\alpha\bar{m}y - R_{3mi}\sin\beta\bar{m}y.\sinh\alpha\bar{m}y] - 4C_{4m}\,[R_{3mr}\sin\beta\bar{m}y\ \sinh\alpha\bar{m}y + R_{3mi}\cos\beta\bar{m}y\ \cosh\alpha\bar{m}y] \tag{2.58}$$

For the particular solution of Eqs. (2.19), (2.20) and (2.39), the loading P on the deck is expressed by the Fourier sine series, covering the entire width, a, of the plate as

$$P = \sum_{m=1}^{\infty} Q_m \sin\bar{m}x \tag{2.59}$$

where Q_m is the amplitude of the mth component loading of the Fourier sine series.

It can be shown with the aid of the differential

Equations (2.19), (2.20) and (2.39), that the particular solutions for the displacements W_p, U_p and V_p, in order to be compatible, both U_p and V_p must be zero and that only W_p exists. W_p is expressed as

$$W_p = \sum_{m=1}^{\infty} a_m \sin \bar{m}x \qquad (2.60)$$

where

$$a_m = \frac{Q_m}{\bar{m}^4 EI} \qquad (2.61)$$

The final displacements are then

$$w = \sum_{m=1}^{\infty} (W_m + a_m) \sin \bar{m}x \qquad (2.62)$$

$$u = \sum_{m=1}^{\infty} U_m \cos \bar{m}x \qquad (2.63)$$

$$v = \sum_{m=1}^{\infty} V_m \sin \bar{m}x \qquad (2.64)$$

In order to complete the general solution of the plate subjected to a loading $P = p(x,y)$, the arbitrary constants C_{im} are to be determined from the boundary conditions at supports $y = \pm \ell/2$ and the conditions of continuity at either edges of the loaded strip. For a loading width being asymmetric with respect to x-axis, Figure 2.5, the complete solution for the plate involves 24 unknown constants to be

determined, there being 8 new constants for each of three regions of the loaded and unloaded strips. However, if the loading width is placed symmetrically about the x-axis, $\varepsilon = 0$ in Figure 2.5, the number of arbitrary constants to be determined, reduces to 12.

CHAPTER 3.

METHOD OF ANALYSIS OF ORTHOTROPIC BRIDGE DECK

3.1 INTRODUCTION

Due to any loading on the deck of the idealized structure, Figure 3.1, the deck plate will undergo a vertical deflection and rotation at each of the floor beam supports. Free body of a distorted panel of this system, Figure 3.2, indicates certain indeterminate end forces, as well as the resulting deflections and slopes which would conform with the geometry of the deformed structure. The slope-deflection equations at a support line relating the end displacements to the end actions can be set up, if the panel stiffness corresponding to the degrees of freedom, namely the rotation and deflection, are somehow determined. For each support then, there will be two equations and for a structure with n numbers of floor beams, 2 n numbers of simultaneous equations are available to solve for the unknown displacements at supports. Thus, the approach of the stiffness method, as applied to a continuous beam analysis, may also be extended in this case.

This objective can be achieved if the applied load on the deck is represented by a series of sinusoidal component loads extending over the entire width, a, of the deck. Such a sinusoidal loading for a plate panel with edges x = 0 and

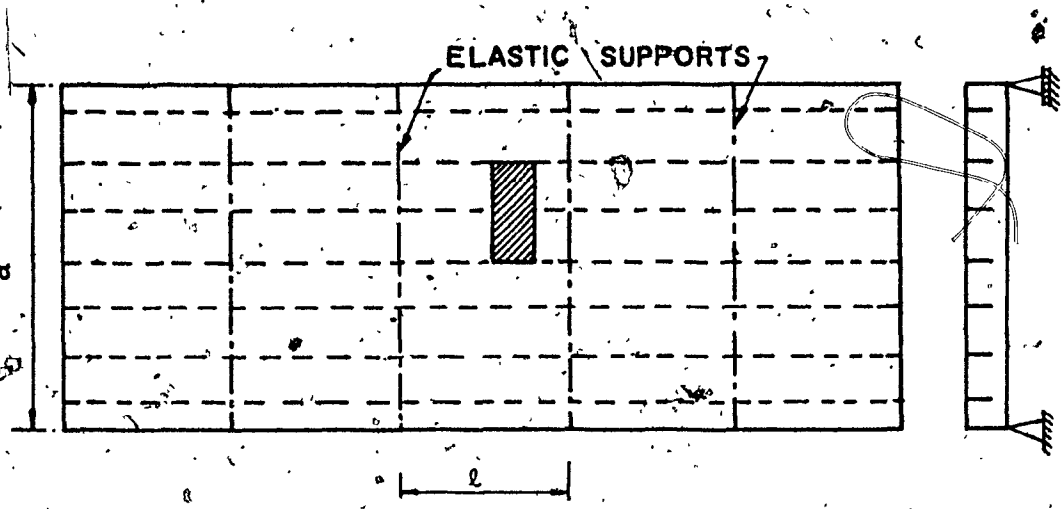

FIG. 3.1 - IDEALIZED DECK STRUCTURE

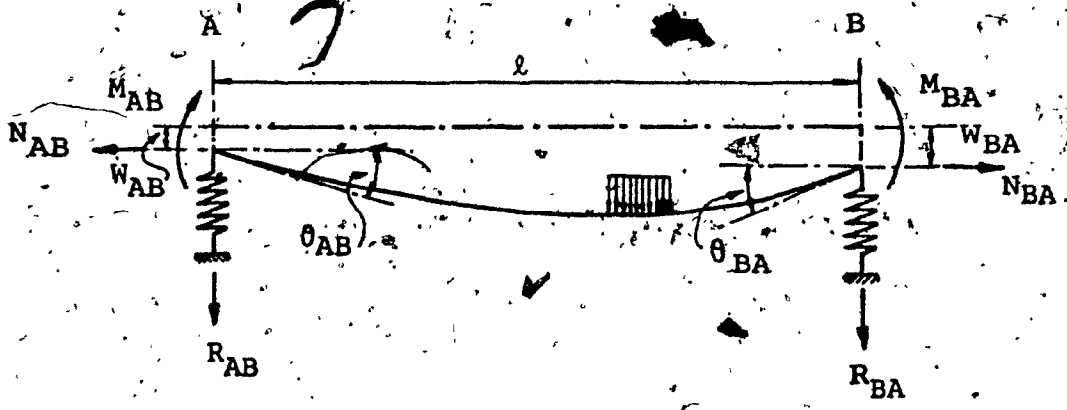

FIG. 3.2 - FREE BODY OF A TYPICAL DEFORMED DECK PANEL

$x = a$ and with arbitrary support conditions at the edges $y = \pm \frac{\ell}{2}$, will produce sinusoidal deflections, rotations, moments, and shears in the y-direction at any location y. This is apparent by observing that the expressions for the moment, shear and rotation in the y-direction contain the term $\sin \bar{m}x$. The sinusoidal affinity between the load and deformations in the y-direction is an important factor in obtaining the stiffness matrix for a typical panel.

3.2 TRANSFORMATION OF EQUATIONS IN MATRIX FORM

For the computer applications, it is necessary to express the equations of the displacements, forces and stresses as given in Chapter 2, in the more convenient matrix forms. If the amplitudes of the displacements and the necessary derivatives of these functions are assembled in a single column vector, the forces and stresses, which are directly related to them, can be obtained by simply pre-multiplying the vector with a transformation matrix.

If $\{B\}$ is the column vector containing the amplitudes of the displacements and their partial derivatives in the order, w, u, v, $\frac{\partial w}{\partial y}$, $\frac{\partial^2 w}{\partial y^2}$, $\frac{\partial^3 w}{\partial y^3}$, $\frac{\partial v}{\partial y}$, $\frac{\partial^2 v}{\partial y^2}$ and $\frac{\partial u}{\partial y}$, then

$$\{B\} = [C_f]\{C\} \qquad (3.1)$$

where $[C_f]$ is a rectangular matrix of the size 9 x 8 whose

elements are the values of the coefficients associated with {C} in the expressions of the displacement functions and their derivatives, for a given y.

The necessary forces and stresses are obtained by premultiplying {B} with a transformation matrix. For the moments and reactions, the amplitudes are given as

$$\begin{Bmatrix} M_x \\ M_y \\ M_{yx} \\ R_y \end{Bmatrix} = -E \begin{bmatrix} b_{11} & 0 & 0 & 0 & b_{15} & 0 & 0 & 0 & 0 \\ b_{21} & 0 & 0 & 0 & b_{25} & 0 & b_{27} & 0 & 0 \\ 0 & 0 & b_{33} & b_{34} & 0 & 0 & 0 & 0 & b_{39} \\ 0 & 0 & b_{43} & b_{44} & 0 & b_{46} & 0 & b_{48} & b_{49} \end{bmatrix} \begin{Bmatrix} B \end{Bmatrix} \quad (3.2)$$

and for the stresses

$$\begin{Bmatrix} \sigma_x \\ \sigma_y \\ \sigma_{xy} \\ \sigma_y' \end{Bmatrix} = \frac{E}{1-u^2} \begin{bmatrix} d_{11} & d_{12} & 0 & 0 & d_{15} & 0 & d_{17} & 0 & 0 \\ d_{21} & d_{22} & 0 & 0 & d_{25} & 0 & d_{27} & 0 & 0 \\ 0 & 0 & d_{33} & d_{34} & 0 & 0 & 0 & 0 & d_{39} \\ 0 & 0 & 0 & 0 & d_{45} & 0 & d_{47} & 0 & 0 \end{bmatrix} \begin{Bmatrix} B \end{Bmatrix} \quad (3.3)$$

where

$$b_{11} = -\bar{m}^2 I; \quad b_{15} = \mu I$$

$$b_{21} = -\mu\bar{m}^2 I; \quad b_{25} = \bar{I}_y; \quad b_{27} = -S_y$$

$$b_{33} = -\bar{m}k_2; \quad b_{34} = \{(1-\mu)I + k_1\}\bar{m}; \quad b_{39} = -k_2$$

$$b_{43} = \bar{m}^2 k_2; \quad b_{44} = -\{(2-u)I + k_1\}\bar{m}^2, \quad b_{46} = \bar{I}_y$$

$$b_{48} = -S_y; \quad b_{49} = \bar{m}k_2$$

.....

$$d_{11} = \bar{m}^2 z; \quad d_{12} = -\bar{m}; \quad d_{15} = -\mu z; \quad d_{17} = \mu$$

$$d_{21} = -\bar{m}^2 \mu z; \quad d_{22} = -\bar{m}\mu; \quad d_{25} = -z; \quad d_{17} = 1$$

$$d_{33} = \bar{m}(1-\mu)/2; \quad d_{34} = -\bar{m}z(1-\mu); \quad d_{39} = (1-\mu)/2$$

$$d_{45} = -z(1-\mu^2); \quad d_{47} = 1-\mu^2 \qquad (3.4)$$

It should be noted that in the above expressions for M_{yx} and R_y, those applicable for closed ribs are used. By equating $k_1 = J^*$ and $k_2 = 0$, the above formulae can be used for open ribs.

3.3 PANEL STIFFNESS MATRIX

The stiffness matrix for a typical panel can be determined by solving the individual plate problems, as shown in Figure 3.3. From the nature of the displacement functions w, u and v, and Eqs. (2.16) and (2.14) or (2.38) for the moments and reactions in the y-direction, it is evident that for a given sinusoidal rotation at one edge, Figure 3.3(b), the moments and reactions at the edge rotated and at the fixed edge are also sinusoidal. Likewise, if one fixed edge is subjected to a sine-wave type deflection, Figure 3.3(c), the induced moments, and reactions at both fixed edges, are also distributed as sine curves.

3.3.1 Unit Sinusoidal Rotation at an Edge

The following are the eight boundary conditions to determine the eight unknown constants of Eqs. (2.41-2.43)

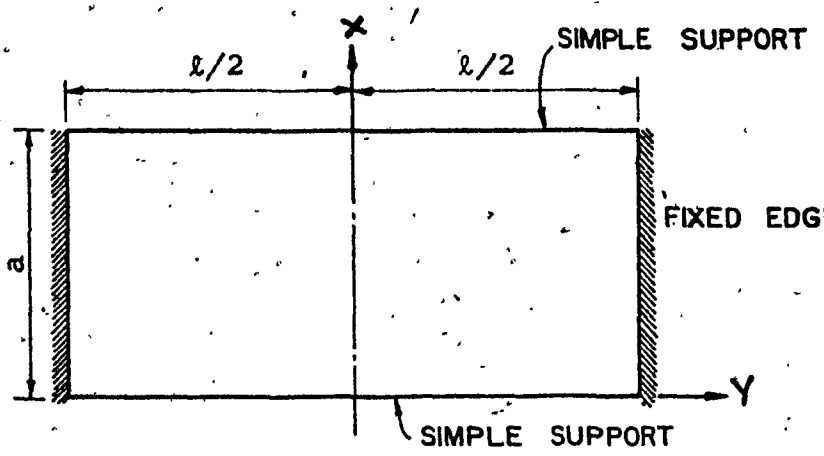

A. TYPICAL DECK PANEL

$M_{AB} = \theta_{mn} \text{ SIN } \bar{m}X$ $\qquad$ $M_{BA} = \theta_{mf} \text{SIN } \bar{m}X$

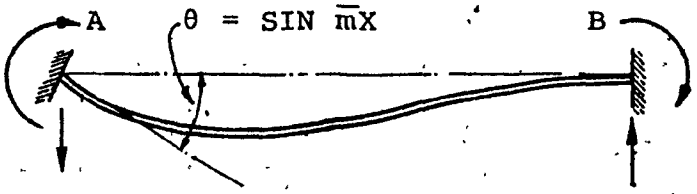

$R_{AB} = \theta_{rn} \text{ SIN } \bar{m}X$ $\qquad$ $R_{BA} = \theta_{rf} \text{ SIN } \bar{m}X$

B. INDUCED MOMENTS AND REACTIONS DUE TO UNIT SINUSOIDAL ROTATION AT EDGE A

$\Delta = 1.\text{SIN } \bar{m}X$ $\qquad$ $M_{BA} = \delta_{mf} \text{SIN } \bar{m}X$

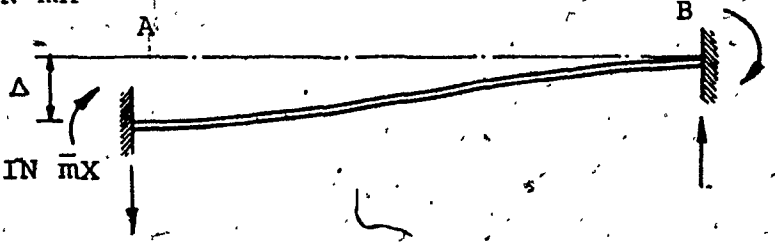

$M_{AB} = \delta_{mn} \text{SIN } \bar{m}X$

$R_{AB} = \delta_{rn} \text{SIN } \bar{m}X$ $\qquad$ $R_{BA} = \delta_{rf} \text{SIN } \bar{m}X$

C. INDUCED MOMENTS AND REACTIONS DUE TO UNIT SINUSOIDAL DEFLECTION AT EDGE A

FIG. 3.3 - END MOMENTS AND REACTIONS OF A TYPICAL DECK PANEL DUE TO UNIT SINUSOIDAL DISPLACEMENTS

representing the homogeneous solution for an unloaded plate subjected only to a rotation. $\theta = 1 \sin \bar{m}x$, at the edge $y = \frac{\ell}{2}$, as shown in Figure 3.3(b).

At the edge $y = -\frac{\ell}{2}$

$$w = 0 \tag{3.5a}$$

$$u = 0 \text{ (supported along the x-direction)} \tag{3.5b}$$

$$v = \bar{v} \sin \bar{m}x \text{ (assumed)} \tag{3.5c}$$

$$\frac{\partial w}{\partial y} = 1. \sin \bar{m}x \tag{3.5d}$$

and at the edge $y = + \frac{\ell}{2}$

$$w = 0 \tag{3.5e}$$

$$u = 0 \tag{3.5f}$$

$$v = 0 \text{ , and} \tag{3.5g}$$

$$\frac{\partial w}{\partial y} = 0 \tag{3.5h}$$

Due to the rotation of the edge $y = -\frac{\ell}{2}$, accompanied by the end forces, the displacement amplitude $\bar{v}$ associated with the rotation has to be determined. This can be obtained from the condition that at the neutral line parallel to the x-axis, located at distance z_e from the middle surface of the plate, the strain is zero. It is possible to determine the value of z_e in the conventional manner due to the condition that, at the rotated edge, the strain $\frac{\partial u}{\partial x}$ is zero.

For the rotated edge then

$$\frac{\partial v}{\partial y} = z_e \frac{\partial^2 w}{\partial y^2} \tag{3.6}$$

Simultaneous equations relating the boundary values in (3.5) can be written in the matrix form as

$$[A]\{C\} = \{F\} \tag{3.7}$$

where A is an 8 x 8 matrix containing the coefficients associated with eight constants {C} in the linear Eqs. (3.5) and F is a column matrix of the form

$$\{F\} = \{0,0,\bar{v},1,0,0,0,0\}^T \tag{3.8}$$

Therefore

$$\{C\} = [A]^{-1}\{F\} \tag{3.9}$$

If the elements in the matrix $[A]^{-1}$ are denoted by a'_{ij} $(i,j = 1, \ldots 8)$, the matrix multiplication of Eq. (3.9) yields

$$\begin{aligned} C_{1m} &= a'_{13}\,\bar{v} + a'_{14} \\ C_{2m} &= a'_{23}\,\bar{v} + a'_{24} \end{aligned} \tag{3.10}$$

In suffix notation

$$C_{jm} = a'_{j3}\,\bar{v} + a'_{j4} \tag{3.11}$$

Designating the values of derivatives $\frac{\partial^2 w}{\partial y^2}$ and $\frac{\partial v}{\partial y}$ at the edge $y = -\frac{\ell}{2}$ as

$$\frac{\partial^2 w}{\partial y^2} = b_1 C_{1m} + b_2 C_{2m} + \ldots + b_8 C_{8m} = b_j C_{jm}$$

$$\frac{\partial v}{\partial y} = d_1 C_{1m} + d_2 C_{2m} + \ldots + d_8 C_{8m} = d_j C_{jm} \qquad (3.12)$$

where b_j and d_j are the coefficients associated with C_{jm} in the expression of the derivatives.

Using the values of C_{jm} from Eq. (3.11), we obtain

$$\frac{\partial^2 w}{\partial y^2} = b_j a'_{j3} \bar{v} + b_j a'_{j4}$$

$$\frac{\partial v}{\partial y} = d_j a'_{j3} \bar{v} + d_j a'_{j4} \qquad (3.13)$$

Substituting expressions (3.13) into the relationship of (3.6)

$$d_j a'_{j3} \bar{v} + d_j a'_{j4} = z_e (b_j a'_{j3} \bar{v} + b_j a'_{j4}) \qquad (3.14a)$$

which on simplification yields

$$\bar{v} = \frac{d_j a'_{j4} - z_e b_j a'_{j4}}{z_e b_j a'_{j3} - d_j a'_{j3}} \qquad (3.14b)$$

$\bar{v}$ being determined, the unknown constants C_{jm} can then be evaluated from Eq. (3.11). The required amplitudes $\theta_{mn}, \theta_{rn}, \theta_{mf}$ and θ_{rf} of the end moments and reactions in Figure 3.3(b), which form part of the panel stiffness matrix, can thus be calculated from Eq. (3.2). The displacements and stresses at any desired location on the deck can also be determined from Eqs. (3.1) and (3.3), respectively.

3.3.2 Unit Sinusoidal Deflection at an Edge

With the edge $y = -\frac{\ell}{2}$ subjected to a unit sinusoidal deflection $\bar{w} = 1 \sin \bar{m}x$, as shown in Figure 3.3(c), the plate problem can be solved using the following boundary conditions:

At the edge $y = -\frac{\ell}{2}$

$$w = 1 \sin \bar{m}x \qquad (3.15a)$$

$$u = 0 \qquad (3.15b)$$

$$v = 0 \qquad (3.15c)$$

$$\frac{\partial w}{\partial y} = 0 \text{ and} \qquad (3.15d)$$

at the edge $y = +\frac{\ell}{2}$

$$w = 0 \qquad (3.15e)$$

$$u = 0 \qquad (3.15f)$$

$$v = 0 \text{ and} \qquad (3.15g)$$

$$\frac{\partial w}{\partial y} = 0 \qquad (3.15h)$$

The unknown constants C_{jm} are given by

$$\{C\} = [A]^{-1} \{F\} \qquad (3.16)$$

where $[A]^{-1}$ is the same matrix as obtained in the case of unit rotation with no deflection at the edge $y = -\frac{\ell}{2}$ and the matrix $\{F\}$ contains all zero elements except for the first one, f_1, which has the value of 1.

Therefore

$$C_{jm} = a_{j1}$$

$$(j = 1, \ldots 8) \qquad (3.17)$$

Determining C_{jm}, the fixed end moments and reactions as well as the displacements and stresses at any point, can be evaluated. The values of $\delta_{mn}, \delta_{rn}, \delta_{mf}$ and δ_{rf} determined from this analysis provide the remaining part of the stiffness matrix.

The stiffness matrix, S_r, is then constructed in terms of amplitudes of forces as follows, using the new sign conventions and indexing sequence, as depicted in Figure 3.4.

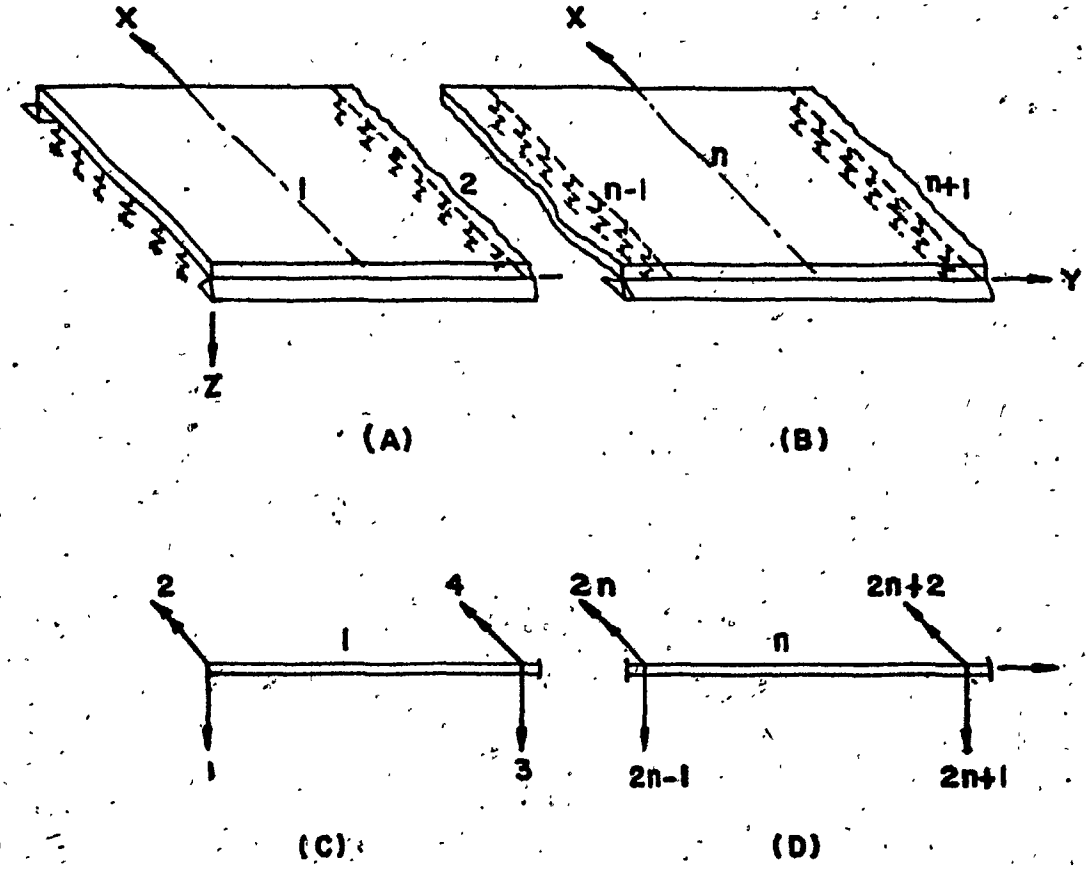

FIG. 3.4 - SIGN CONVENTION AND NUMBERING SYSTEM FOR DECK CONTINUOUS OVER FLEXIBLE SUPPORTS

$$S_r = \begin{bmatrix} \delta_{rn} & \theta_{rn} & -\delta_{rf} & \theta_{rf} \\ \delta_{mn} & \theta_{mn} & -\delta_{mf} & \theta_{mf} \\ -\delta_{rf} & -\theta_{rf} & \delta_{rn} & \theta_{rn} \\ \delta_{mf} & \theta_{mf} & -\delta_{mn} & \theta_{mn} \end{bmatrix} \qquad (3.18)$$

3.4 FLOOR BEAM STIFFNESS

In the previous development of the panel stiffness matrix, S_r, only the stiffened plate action has been considered. However, the interaction of the flexible floor beams has to be taken into account, in order to generate the overall structure stiffness matrix.

The flexibility effects of the beams can be computed assuming that it possesses both the flextural and torsional stiffness. In the case of floor beams with shorter spans and web cutouts for the passage of the ribs, which is a common fabrication practice in North America, the shear deflection in the beam may not be negligible and should be considered in calculating the vertical flexibility of the beams.

The vertical stiffness of the simply supported floor beams can be computed by examining again the sinusoidal affinity between the load and deflection. For a sinusoidal load, $F_n = F' \sin \bar{m}x$, on the beam, the deflection at any point due to bending, δ_b, is given by

$$\delta_b = F' \iiiint \frac{\sin \bar{m}x}{EI_b} = \frac{1}{\bar{m}^4 EI_b} \cdot F' \sin \bar{m}x \qquad (3.19)$$

where EI_b = flextural rigidity of the beam, is assumed uniform.

The deflection due to shear, δ_s, is given as

$$\delta_s = \frac{1}{\bar{m}^2 \ GA_w} \sin \bar{m}x \qquad (3.20)$$

in which GA_w represents the effective shear rigidity of the beam.

The total deflection δ, of the beam is then

$$\delta = \delta_s + \delta_b = \frac{\bar{m}^2 \ GA_w + \bar{m}^4 \ EI_b}{\bar{m}^2 \ GA_w \cdot \bar{m}^4 \ EI_b} F' \sin \bar{m}x \qquad (3.21)$$

The vertical stiffness or the spring constant of the beam K_s, becomes equal to

$$K_s = \frac{\text{load}}{\text{deflection}} = \frac{\bar{m}^2 \ GA_w \cdot \bar{m}^4 \ EI_b}{\bar{m}^2 \ GA_w + \bar{m}^4 \ EI_b} \qquad (3.22)$$

In the case where shear deflection is neglected, K_s is given as

$$K_s = \bar{m}^4 \ EI_b \qquad (3.23)$$

If the same beam is subjected to a sinusoidal rotation, $\Phi = \Phi' \sin \bar{m}x$, the distributed torque on the beam, m_t, considering only the effect of pure torsion, becomes

$$m_t = - GJ_b \frac{d^2\phi}{dx^2} = \bar{m}^2 \; GJ_b \; \phi' \sin \bar{m}x \quad (3.24)$$

where GJ_b = the torsional rigidity of the floor beam.

Rotational stiffness of the floor beam, k_t, is then

$$K_t = \frac{\text{load}}{\text{rotation}} = \bar{m}^2 \; GJ_b \quad (3.25)$$

Therefore, if a simply supported beam is subjected to a sinusoidally varying deflection and rotation, the sinusoidal vertical load and torsional moment of amplitudes F_n and m_t are given as

$$\begin{Bmatrix} F_n \\ m_t \end{Bmatrix} = \begin{bmatrix} \dfrac{\bar{m}^2 \; GA_w \cdot \bar{m}^4 \; EI_b}{\bar{m}^2 \; GA_w + \bar{m}^4 \; EI_b} & 0 \\ 0 & m^{-2} GJ_b \end{bmatrix} \begin{Bmatrix} \delta \\ \phi \end{Bmatrix} \quad (3.26)$$

3.5 FIXED END ACTIONS DUE TO LOAD

Expressing the applied load on the particular panel into Fourier sine series, the plate problem with the edges $y = \pm \frac{\ell}{2}$ as fixed, can be solved, applying the conditions of continuity at the junctions of loaded and unloaded strips, as indicated in Chapter 2, and using the

boundary conditions at each fixed edge as

$$w = u = v = \frac{\partial w}{\partial y} = 0 \qquad (3.27)$$

For the highway bridges, the applied wheel loads can be considered as loads distributed on relatively small areas. If the loading width in the y-direction $2c$, is not symmetrical about the x-axis of the panel, the solution for each component loading requires 24 simultaneous linear equations to solve for 24 unknown constants for the displacement functions. Thus, the size of the input matrix, containing the values of the coefficients associated with these constants becomes 24 x 24. This is a rather large matrix which, however, can be reduced to the size of 12 x 12 by replacing the applied loading into a pair of symmetrical and antisymmetrical loadings with respect to the x-axis, as shown in Figure 3.5. When the solutions for the four substituted loading cases are superposed, the actual results for the particular loading component is obtained for the plate. The fixed end moments and the reactions are thus known as well as any desired displacement and stresses in the plate.

3.6 SOLUTION BY STIFFNESS METHOD

After establishing the panel stiffness matrix and fixed end actions due to the applied loading on the panels, the stiffness method can be readily applied to solve the

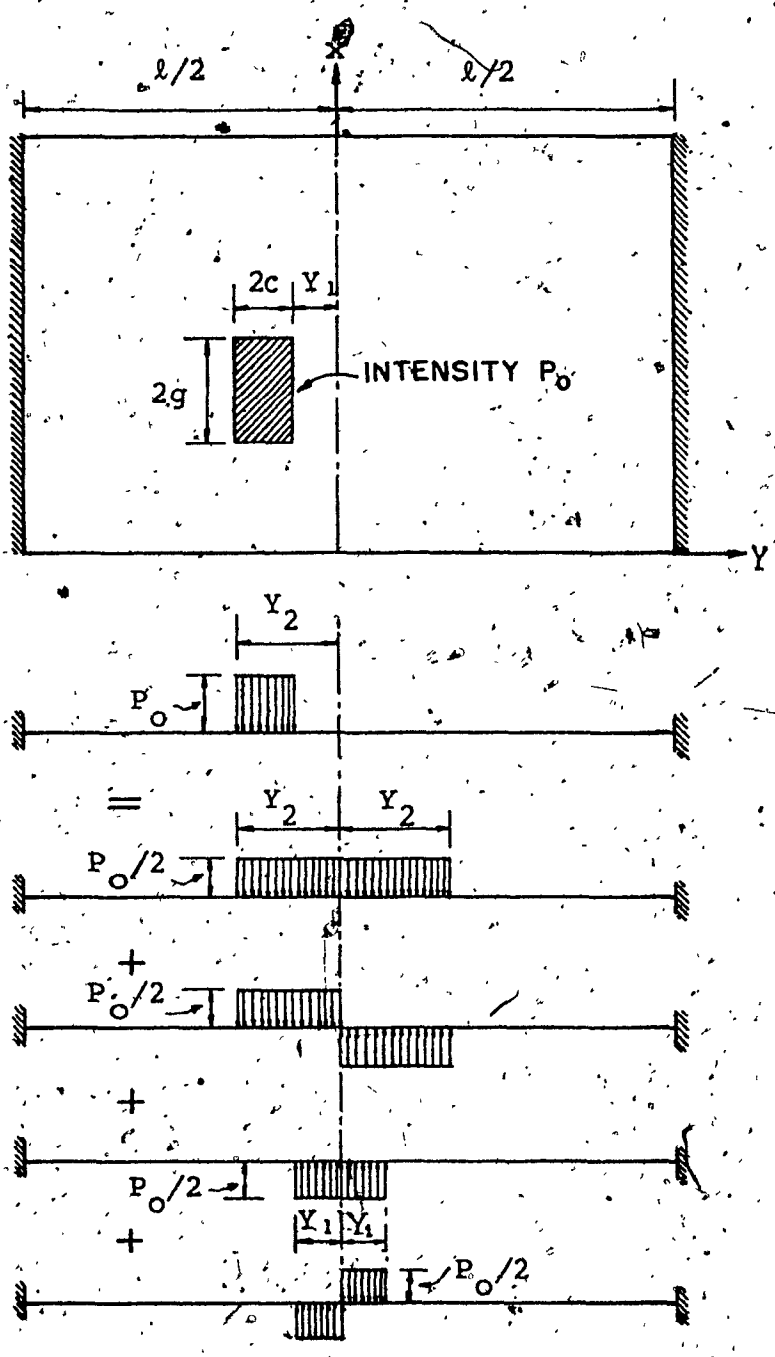

FIG. 3.5 – BREAKDOWN OF A LOADING INTO A PAIR OF SYMMETRIC AND ANTISYMMETRIC LOADINGS

entire structure. The technique of such a computerized approach can be found in References (55) and (56).

The overall stiffness matrix, S, for a bridge structure with n numbers of floor beams will be 2n x 2n, and can be assembled following the arbitrary numbering index, as indicated in Figure 3.4. The terms in the leading diagonal of the matrix S will also contain the values representing the stiffness of the floor beam in proper sequence. If the fixed-end actions due to the applied loading are designated by the matrix $\{A_m\}$ assembled in accordance with the numbering system, as depicted in Figure 3.4, the matrix $\{D_j\}$ containing the unknown displacements at floor beam supports, is given by

$$\{D_j\} = [S]^{-1} \{A_m\} \qquad (3.28)$$

The unknown displacements at each support being determined, the final deflection at any point can be evaluated from the following relation.

$$w = w_f + \lfloor w_s \rfloor \{D_m\} \qquad (3.29)$$

where w is the final deflection, w_f is the deflection due to the load acting on the fixed-end panel, $\lfloor w_s \rfloor$ is the row vector containing the deflections due to the unit displacements computed previously, and $\{D_m\}$ is the displacements of the floor beams corresponding to the degrees of

freedom at the ends of the panel under consideration. All deflections referred to are computed at the same location on the deck.

In the same manner, the stresses at any particular point can be evaluated from the similar relationship.

$$\sigma = \sigma_f + [\sigma_s] \{D_m\} \tag{3.30}$$

where σ, σ_f and σ_s are all referred to any of the stresses σ_x, σ_y, σ_{xy} and σ_y'.

It should be noted that for each loading component of the series, there is a new matrix [S] and in each case, the displacements D_j are to be evaluated from Eq. (3.28). Therefore, for the final solution, the values of deflection and stresses obtained from each component of the series are to be added algebraically.

3.7 PRACTICAL CONSIDERATIONS

Although the method of analysis presented is capable of evaluating the deflection and stresses at any desired location of the deck, for design purpose, however, only the maximum stresses in the deck plate and the ribs are of practical importance and use. These occur at the midspan of the rib between floor beams, which correspond to the maximum positive moment, and at the rib support corresponding to the maximum negative moment. For a single wheel load, the maximum

stress at the middle of the rib-span is produced when the load is placed at the same location, and the maximum stress at the support occurs when the load acts at a particular distance on either side of the support under consideration. For design purposes, this distance can be taken as that given in References (6) and (7). Again, the maximum deflection of the rib will occur at the middle of the rib span when the load is placed at the midspan. Therefore, it is sufficient to consider only these two sections, namely, the middle of the rib span and the rib support, to evaluate the maximum stresses and deflection for a particular moving wheel load.

The actual bridge structure consists of a large number of floor beams and as such, it would be impractical to consider all of these in the analysis. The continuity effect can be adequately taken into account, if only a number of panels, at least four, are considered on either side of the section being investigated. The effect of a load acting on a remote panel is negligible at the section under consideration.

3.8. COMPUTER PROGRAM

A computer program was developed incorporating the proposed method to readily analyze an orthotropic bridge deck. The program was written in FORTRAN and run on CDC 6600.

For the sake of brevity, the essential feature of the entire program is only presented in Figure 3.6. The

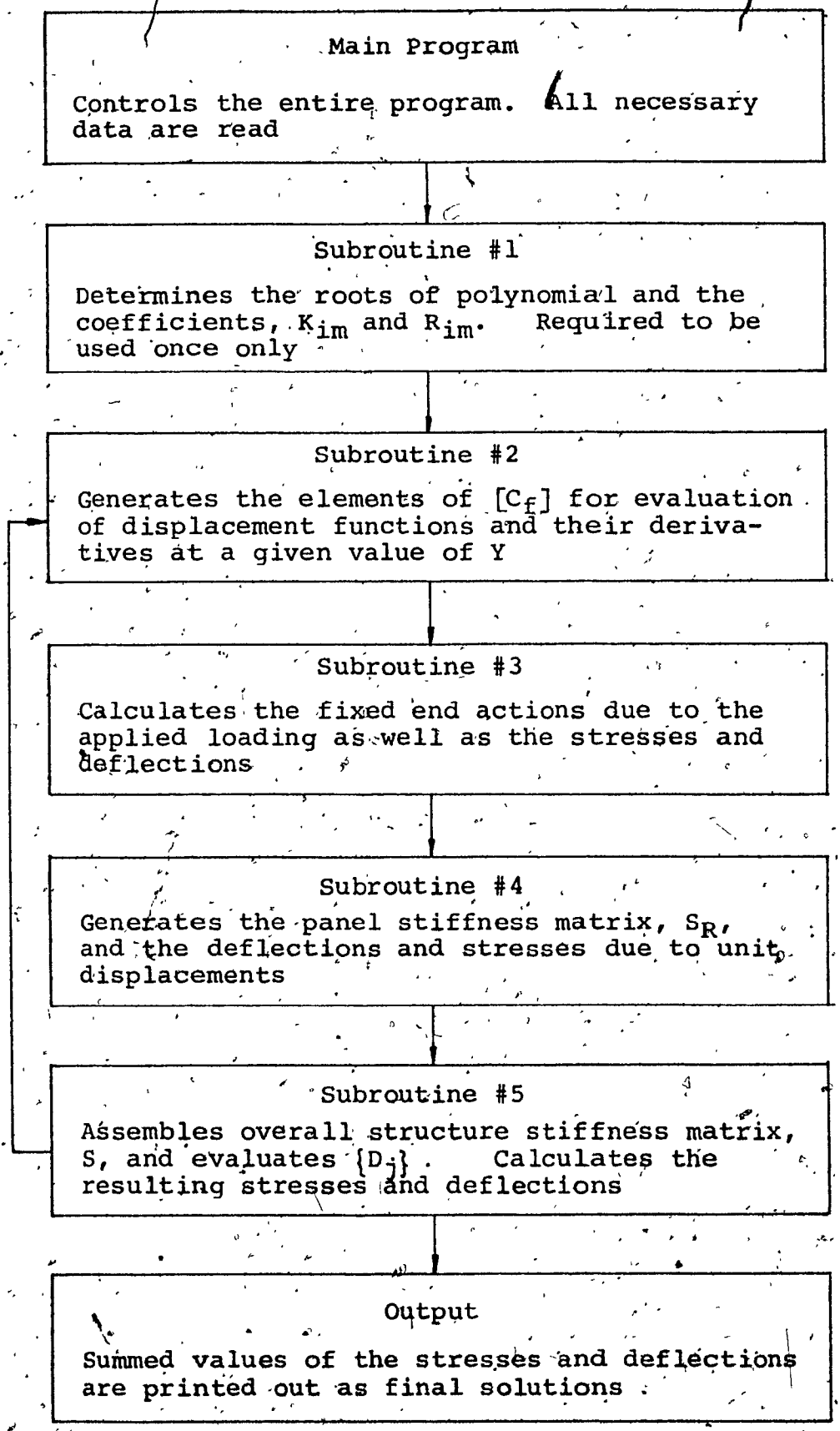

FIG.3.6 - BLOCK DIAGRAM FOR COMPUTER PROGRAM

required input data includes the structural dimensions of the plate and ribs, elastic constants, loadings and also the structural characteristics of the floor beams (values of A_w, I_b and J_b). For a long structure, the number of spans to be considered for a satisfactory account of the continuity effect is also needed.

Subroutine 1 determines the roots of the eighth order polynomial and allocates the values of necessary parameters s_1, s_2, s_3, s_4, α and β. Using them, the values of k_i and R_i are also determined. Subroutine 2 generates the elements of $[C_f]$ for the evaluation of displacement functions and their derivatives at a given value of y. Subroutine 3 calculates the fixed end actions corresponding to a component loading of the series and evaluates the desired stresses and displacements.

Subroutine 4 determines the elements of a typical panel stiffness matrix, as well as the deflection and stresses due to the unit displacements. Subroutine 5 assembles the overall structure stiffness matrix and gives the unknown displacements at supports. It also evaluates the resulting stresses and deflections corresponding to a particular component loading. The program prints out some important data in the stages of computation, in addition to the final values of the deflection and stresses at the desired locations on the deck.

CHAPTER 4

APPLICATION OF THE PROPOSED METHOD AND COMPARISON WITH PELIKAN-ESSLINGER

4.1 INTRODUCTION

In this Chapter, the proposed method and the design method of Pelikan-Esslinger are both applied to solve several hypothetical decks of various proportions. At first, as an example, a deck structure stiffened with open ribs is selected to demonstrate the application of the proposed method, following which the two sets of theoretical results from the analyses of several decks, stiffened by both open and closed ribs, are presented and compared.

For the shape of stiffeners, flat sections and the commercially available sections[57] are considered, respectively as the open type and the closed type. The readily available sectional properties of the closed ribs[57] helped to reduce the computational work and was mainly the reason for the choice of this type.

For simplicity, a single wheel load is assumed to act at the midspan of a rib of a typical deck under consideration. In order to have a favourable comparison with Pelikan-Esslinger's method, the flexibility of the floor beams due to shear and torsional deformations are both neglected in the proposed refined analysis.

The solutions from the proposed method are readily obtained using the computer program as developed. For the application of the design method of Pelikan-Esslinger, the design charts and procedures as given in References (6-7) are used to analyse decks stiffened by open ribs. However, for decks having closed ribs, a computer program incorporating the design method is used. The program, written in Fortran, is developed primarily to use it in the theoretical analysis of the model bridge deck undertaken in the experimental program. Whithout the convenient use of such a program, it would have been difficult and laborious to use the design method appropriately, because of the geometric limitations imposed upon the model.

4.2 EXAMPLE BRIDGE DECK

A hypothetical bridge structure as shown in Figure 4.1 is selected to demonstrate the application of the proposed method. The deck plate is $\frac{1}{2}$ in. thick, stiffened by longitudinal open ribs of size 8 in. x $\frac{1}{2}$ in. thick which are spaced 12 in. centres. The floor beams are located at every 6 ft. centre and are arbitrarily assumed of having moment of inertia $I_b = 200.0$ in^4. The flexibility of the beams due to shear deflection is ignored in this particular example in order to have a favourable comparison with the results from Pelikan-Esslinger's method.

The main carrying girders are not dimensioned as

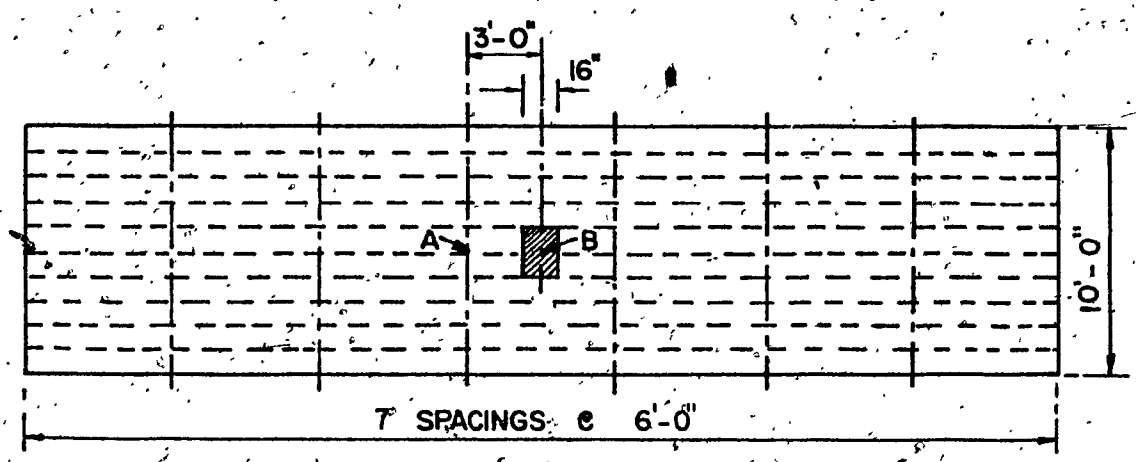

A. TOP PLAN

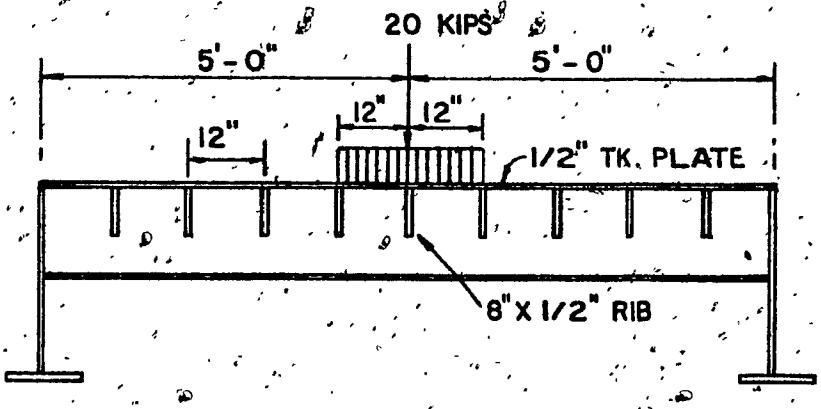

B. CROSS SECTION THROUGH LOADED AREA

FIG. 4.1 - EXAMPLE BRIDGE DECK

they are assumed to provide only the simple supports to the deck. A single load of 20 kips, distributed on an area of 24 in. x 16 in. is placed symmetrically on the central panel of the seven-span continuous deck structure, as shown in Figure 4.1.

From the computer solution, the roots of the polynomial are determined as

$$S_1 = 1.23665$$

$$S_2 = 0.75836$$

$$S_3 = 0.14384 + 0.13252i$$

and

$$S_4 = 0.14384 - 0.13252i$$

which gives

$$\alpha = 0.14384$$

and

$$\beta = 0.13252i$$

The coefficients K_{jm} and R_{jm} are then evaluated as

$$K_1 = 11.76583 \ \bar{m}$$

$$K_2 = 2.57240 \ \bar{m}$$

$$K_{3_r} = 0.00703 \ \bar{m}$$

and

$$K_{3_i} = 0.00015 \ \bar{m}$$

$$R_1 = 6.80271 \ \bar{m}$$

$$R_2 = 4.16811 \ \bar{m}$$

$$R_{3_r} = 0.03935 \ \bar{m}$$

$$R_{3_i} = 0.03881 \ \bar{m}$$

With the completed data on structural characteristics, the desired stresses and deflections are obtained from the computer solutions. These values corresponding to the two

locations, A and B, on the deck, Figure 4.1, represent the maximum stresses and deflections of the deck for the given loading, and are shown in Table 4.1. The satisfactory convergence in stresses, assumed when the stress change is less than 0.1 ksi, was obtained at cycle m = 25. The convergence in deflection is very rapid and, after only a few cycles, the change becomes negligible. The values of elastic constants, E and μ are taken as equal to 29×10^3 and 0.3 respectively.

The results from the proposed analysis are shown in Table 4.1. A second run with assumed torsional constant, J_b, of the floor beam is 1.0 in^4, produced hardly any change in results, indicating that torsional rigidity of open type floor beams has small influence. The results obtained from the design method of Pelikan-Esslinger are also shown in Table 4.1 to compare them with those from the proposed method. It is seen that the longitudinal stresses at the bottom of the rib at both locations A and B, and those at top of the deck plate at location B are in good agreement. However, those at top of the deck plate at location A show some difference.

4.3 DECK STIFFENED BY OPEN RIBS

The general arrangement of the decks under consideration is shown in Figure 4.2, which is similar to the one previously chosen as an example bridge deck. The

Table 4.1

DEFLECTIONS AND STRESSES AT LOCATIONS A AND B FOR EXAMPLE DECK

Method of analysis	At Support of Rib - Location A				At Midspan of Rib - Location B			
	Deflection, in inch	Stress at top of plate in ksi		Stress σ_y at bottom of rib, in ksi	Deflection in inch	Stress at top of plate in ksi		Stress σ_y at bottom of rib, in ksi
		σ_x	σ_y			σ_x	σ_y	
Refined analysis (J_b=0)	.0465	-0.53	0.61	-3.25	.0526	-5.60	-3.60	12.92
Pelikan - Esslinger			1.00	-3.85			-3.52	13.60

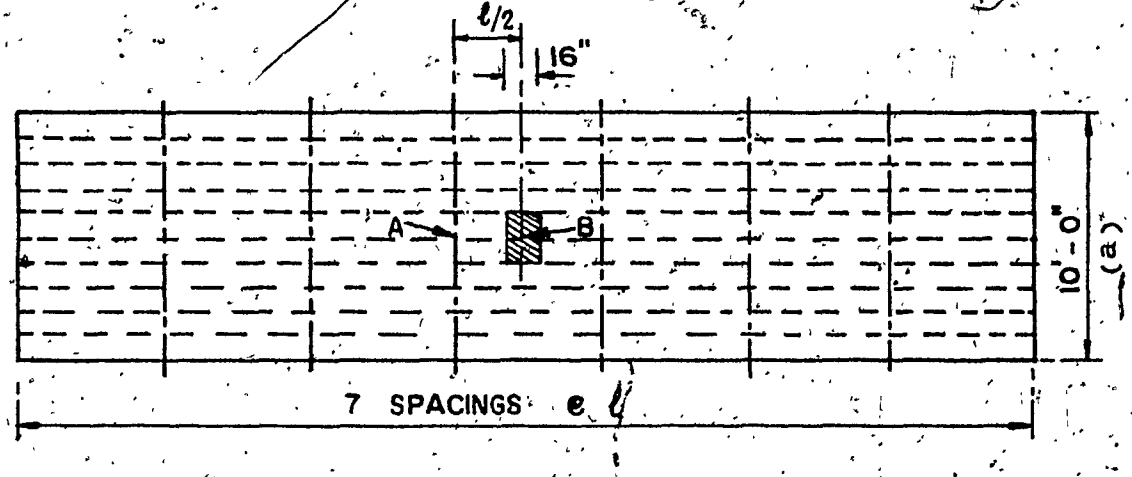

A . TOP PLAN

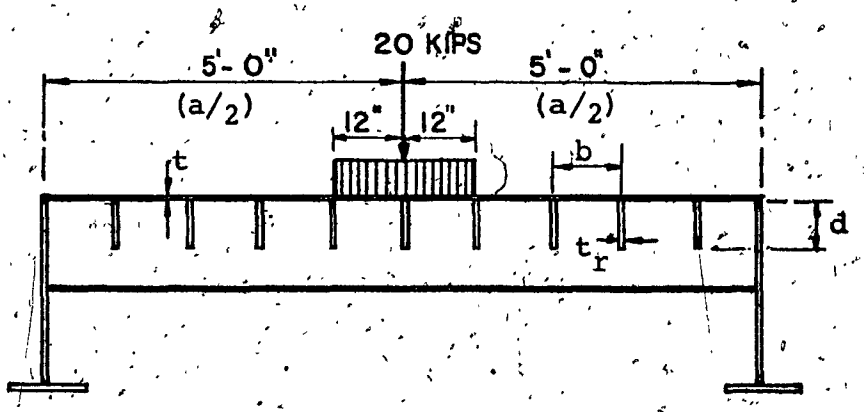

B . CROSS SECTION THROUGH LOADED AREA

FIG. 4.2 - ARRANGEMENT OF HYPOTHETICAL DECKS WITH OPEN RIBS

dimensions t and b as well as the rib size and rib span are varied. Table 4.2 contains the dimensions of decks which are also numbered for an easy reference to a particular deck structure.

A single wheel load of 20 kips, distributed on an area of 24 in. x 16 in., is assumed to act at midspan of the central rib of the seven span continuous deck structure, as indicated in Figure 4.2. The floor beams are assumed to have moment of inertia of 200.0 in^4 . The proposed method and Pelikan-Esslinger's method are both applied to solve these decks and the results are presented in Figures 4.3 - 4.14. As the maximum stresses are of concern to the designers, those corresponding to the locations A and B, Figure 4.2, are evaluated only. They are presented in Figures 4.3 - 4.8, which show the variation of stress at top and bottom of the loaded rib with the change in the rib span. For the rib size, 8 in. x $\frac{1}{2}$ in. the maximum rib span considered is 10 ft, whereas for larger rib sizes, the span is increased up to 12 ft.

Figures 4.3 - 4.6 show the stresses at bottom of the rib at both locations A and B. An examination of the plots shows that in general there is a good agreement between the two sets of results. The design method indicates higher rib stresses and in the case of shorter rib spans, the results are close to those obtained from the proposed analysis. However, with longer rib spans, the design method becomes

TABLE 4.2

DIMENSIONS OF HYPOTHETICAL DECKS WITH OPEN RIBS

Deck No.	Deck plate thickness t, in inch	Rib size d x t_r in inch	Spacing of ribs b, in inch	Rib span ℓ in feet
1	3/8	8 x 1/2	12	4 - 10
2	1/2	8 x 1/2	12	4 - 10
3	5/8	8 x 1/2	12	4 - 10
4	3/4	8 x 1/2	12	4 - 10
5	3/8	8¾ x 9/16	12	6 - 12
6	3/4	8¾ x 9/16	12	6 - 12
7	3/8	9½ x 5/8	12	6 - 12
8	3/4	8 x 1/2	15	4 - 10
9	3/8	8 x 1/2	10	4 - 10
10	3/4	8¾ x 9/16	15	6 - 12

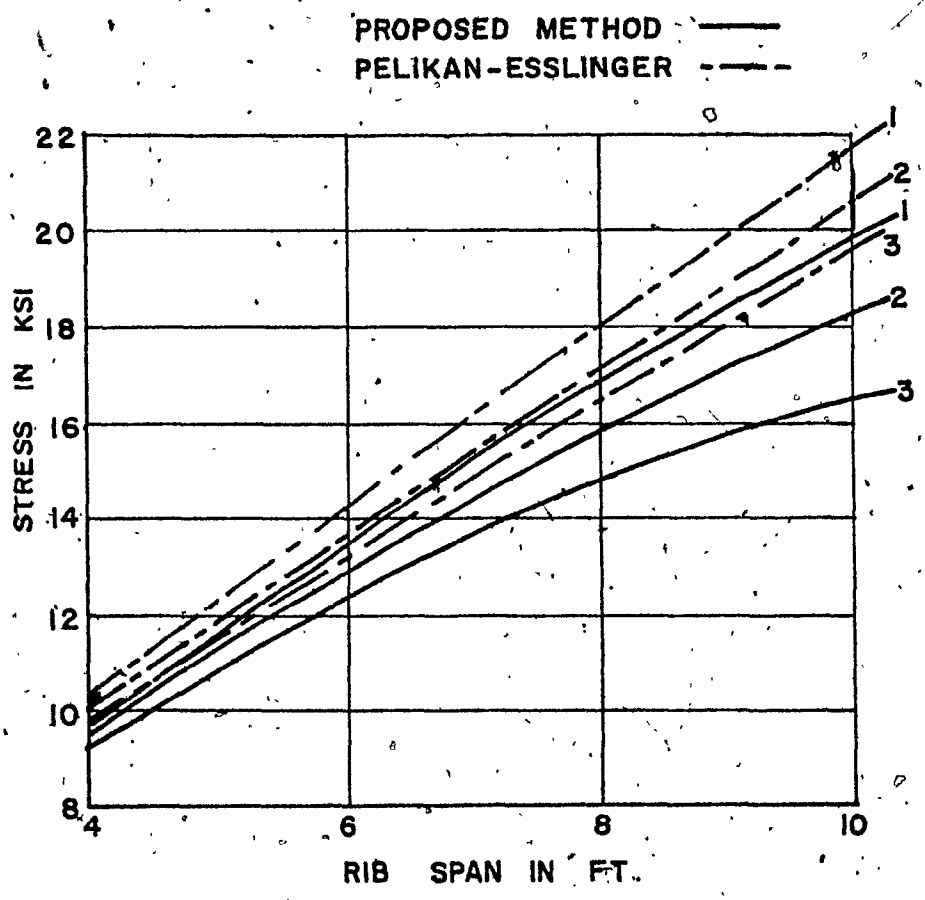

A. AT LOCATION B

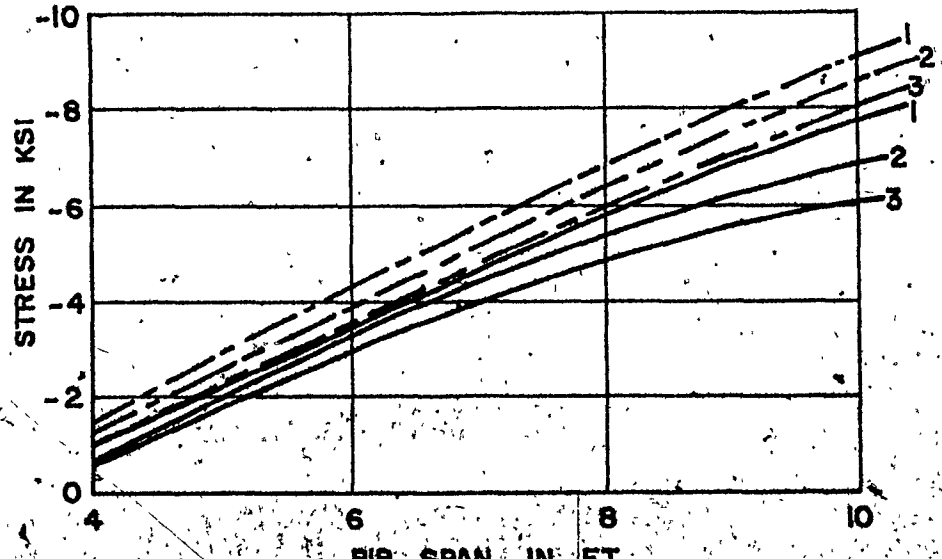

B. AT LOCATION A

FIG. 4.3 - VARIATION OF STRESS AT BOTTOM OF RIB WITH SPAN

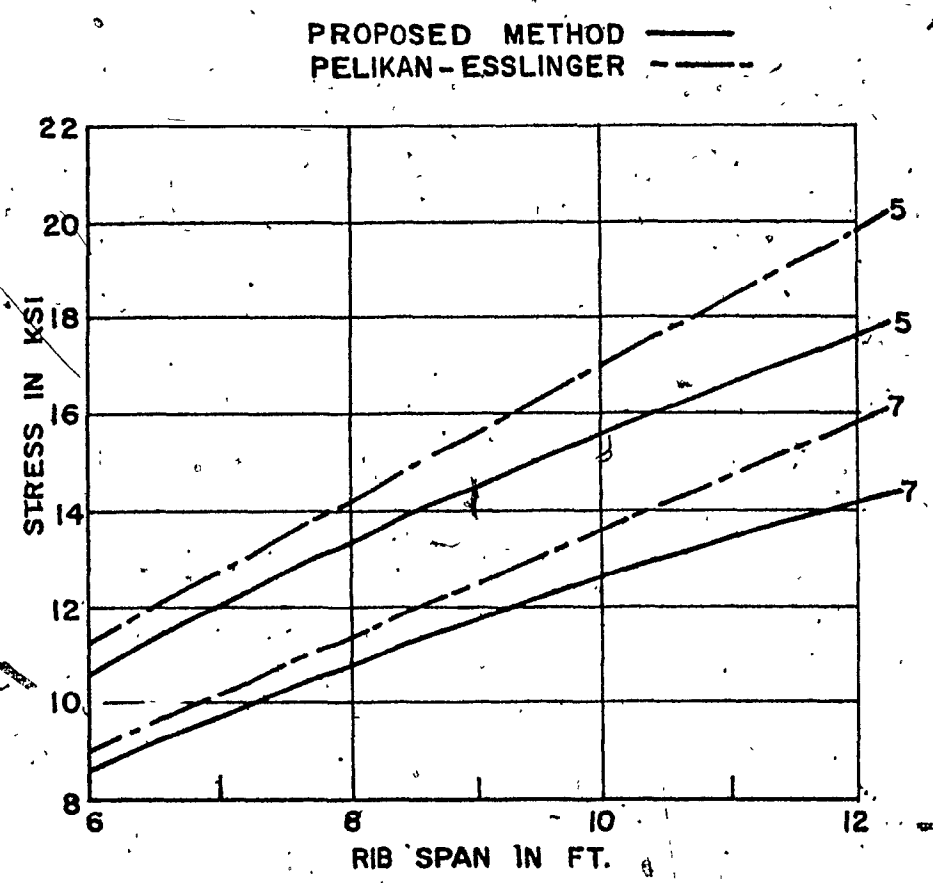

A. AT LOCATION B

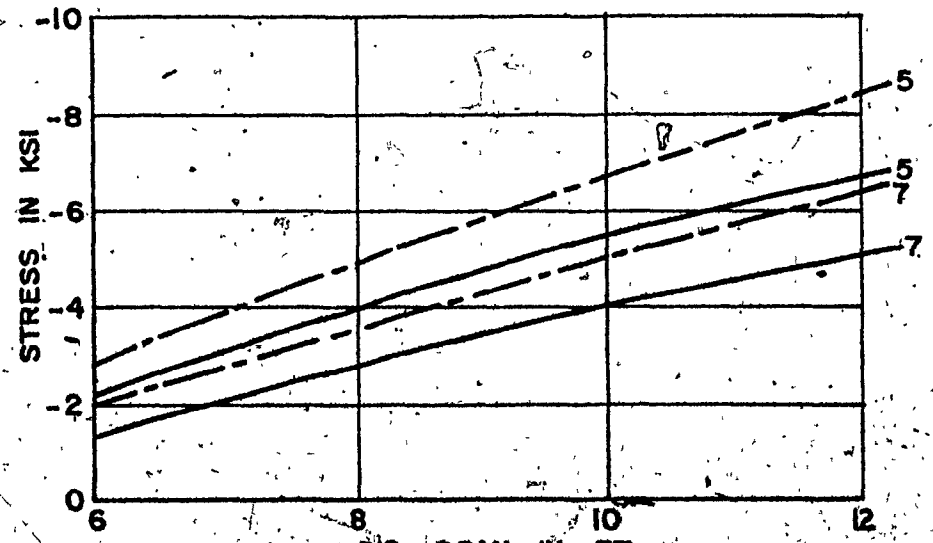

B. AT LOCATION A

FIG. 4.4 - VARIATION OF STRESS AT BOTTOM OF RIB WITH SPAN

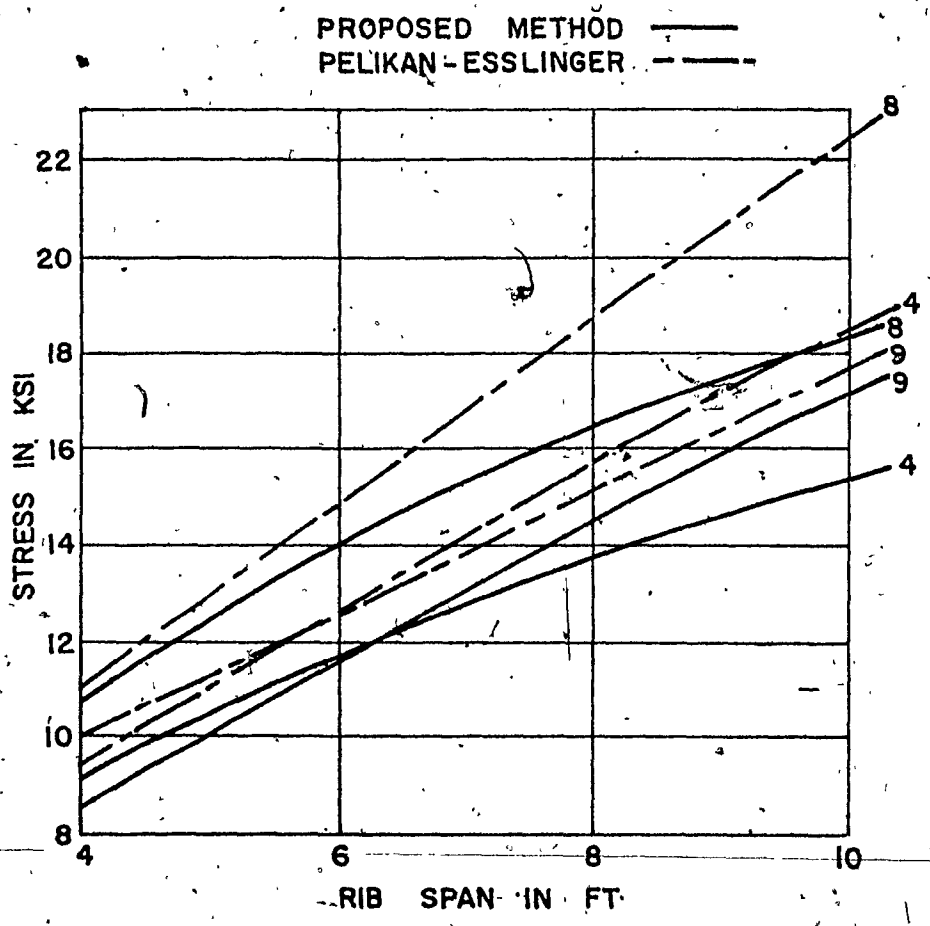

A. AT LOCATION B

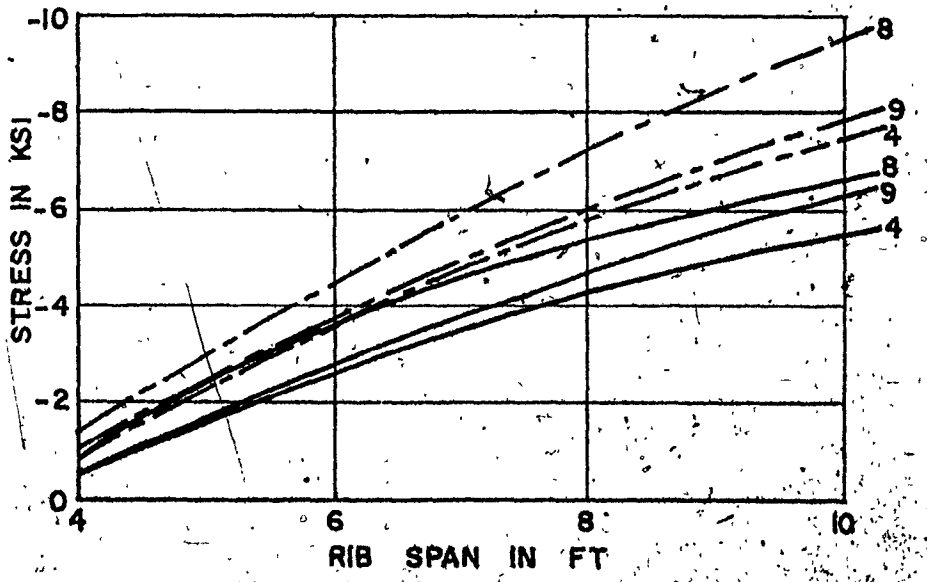

B. AT LOCATION A

FIG. 4.5- VARIATION OF STRESS AT BOTTOM OF RIB WITH SPAN

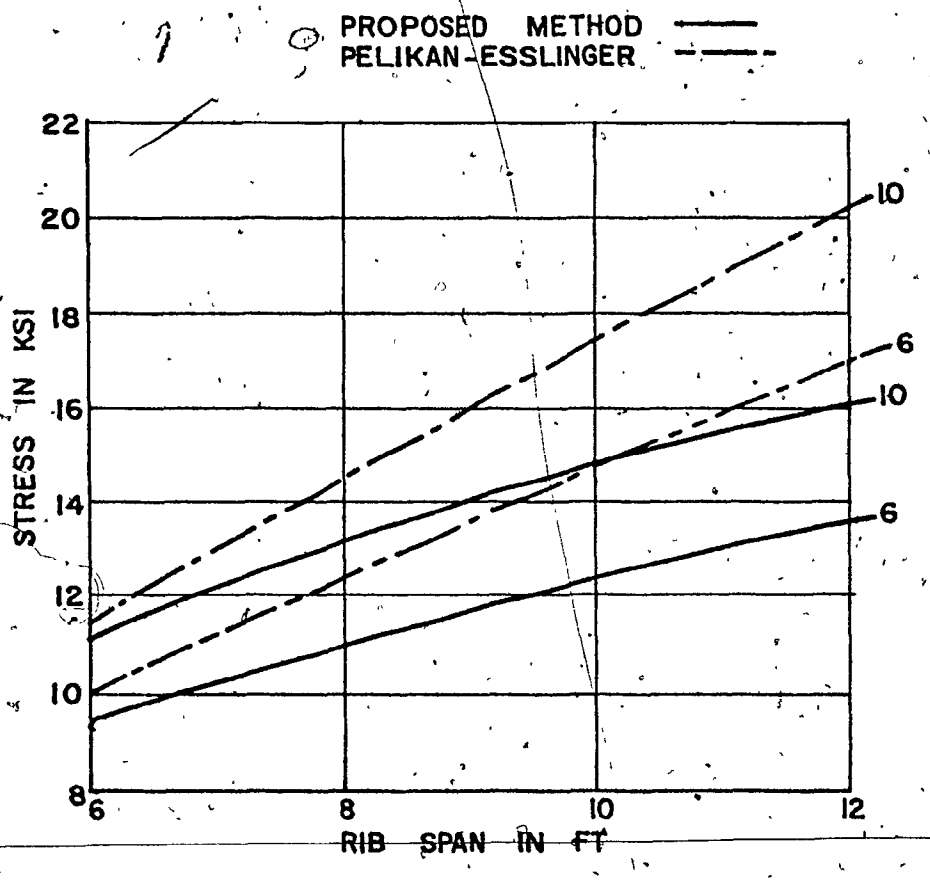

A. AT LOCATION B.

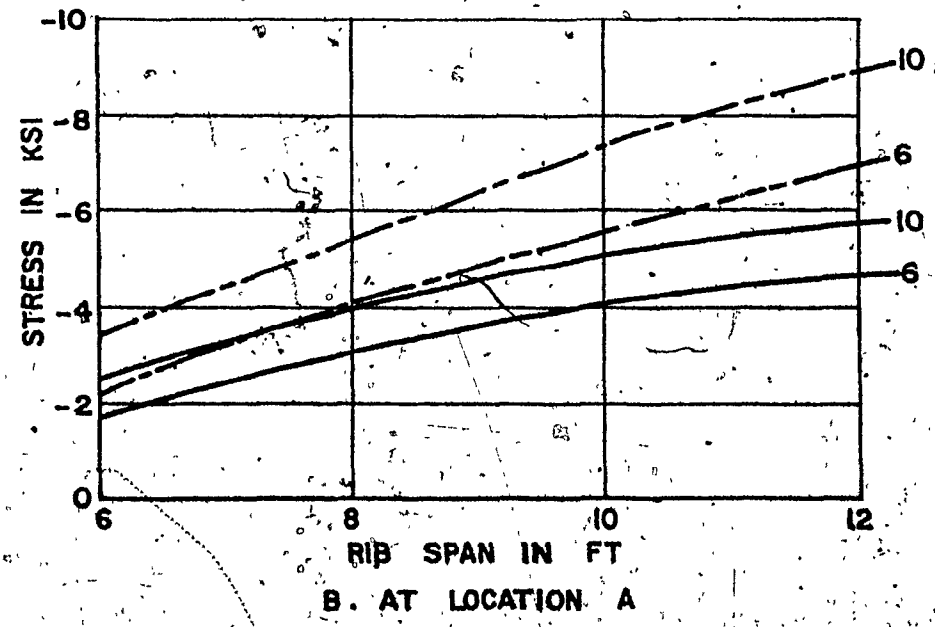

B. AT LOCATION A

FIG. 4.6 - VARIATION OF STRESS AT BOTTOM OF RIB WITH SPAN

increasingly conservative with higher estimate of the maximum rib stresses. For the range considered, the stresses obtained from the design method are generally about 6% to 30% higher, depending upon the deck proportions. Such increasing deviations with longer spans are not however unexpected and can be attributed to the fact that the design method ignores the continuity of the deck in the x-direction. In this procedure, the rib with a certain portion of the deck plate is assumed to act as an independent beam.

Regarding the longitudinal stress, σ_y, at top of the deck plate, those at midspan of the loaded rib, i.e. at location B, show a good agreement, as seen from Figures 4.7a and 4.8a. Depending on the deck plate thickness, the results from the design method are either slightly higher or lower than those from the proposed method, higher values are being for relatively thin deck plates. It is also observed that the two sets of results are usually close for all rib sizes and spans, unlike those at bottom of the rib.

The longitudinal deck plate stress at location A, as determined from the two methods, show some differences as seen from Figures 4.7b and 4.8b. Both methods, however, indicate low values of stresses, with results from Pelikan-Esslinger's method being higher in magnitude.

In order to find the distribution of longitudinal stresses across the width of deck, Figures 4.9 and 4.10 are

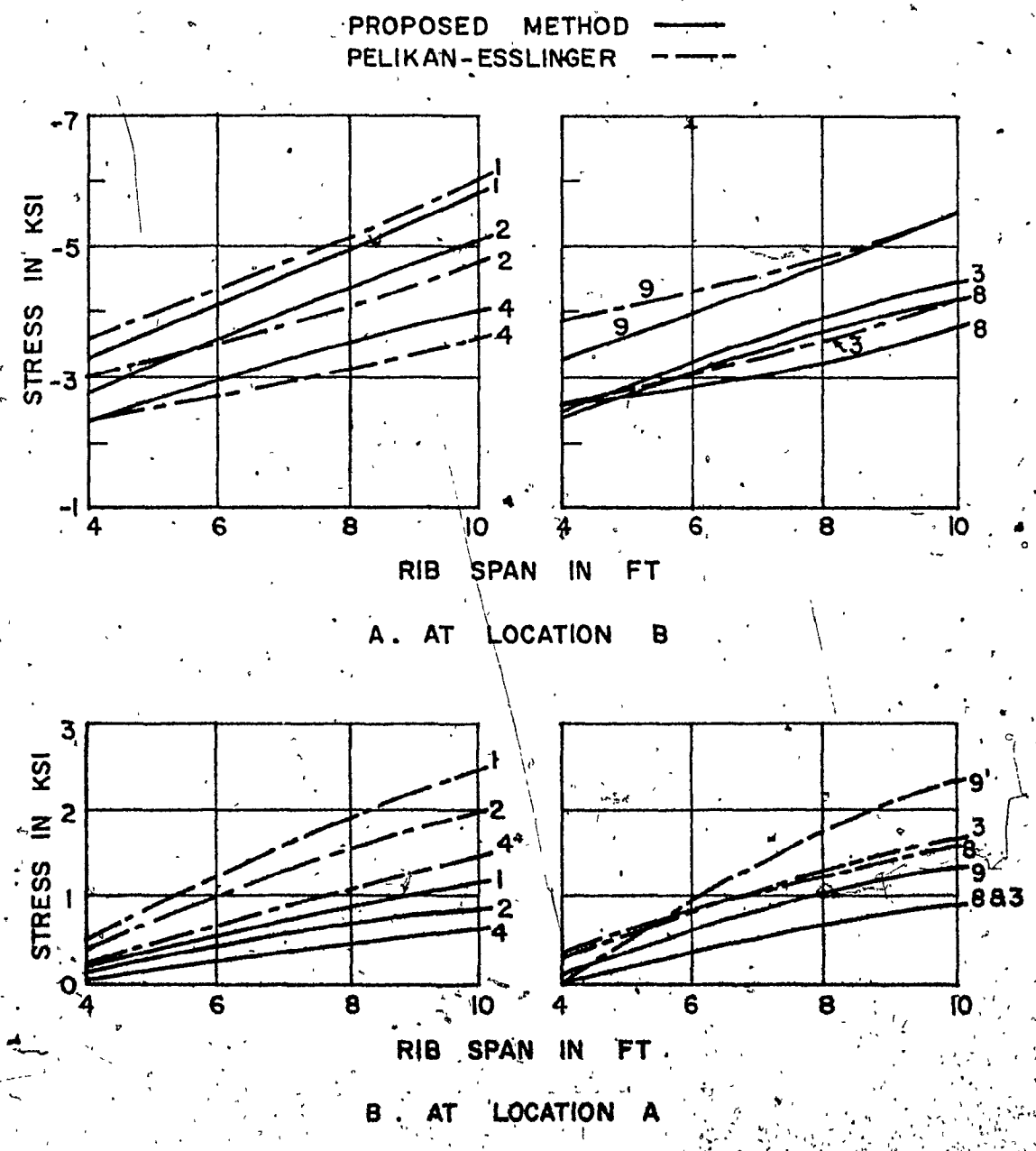

FIG. 4.7 - VARIATION OF LONGITUDINAL STRESS AT TOP OF DECK PLATE WITH RIB SPAN

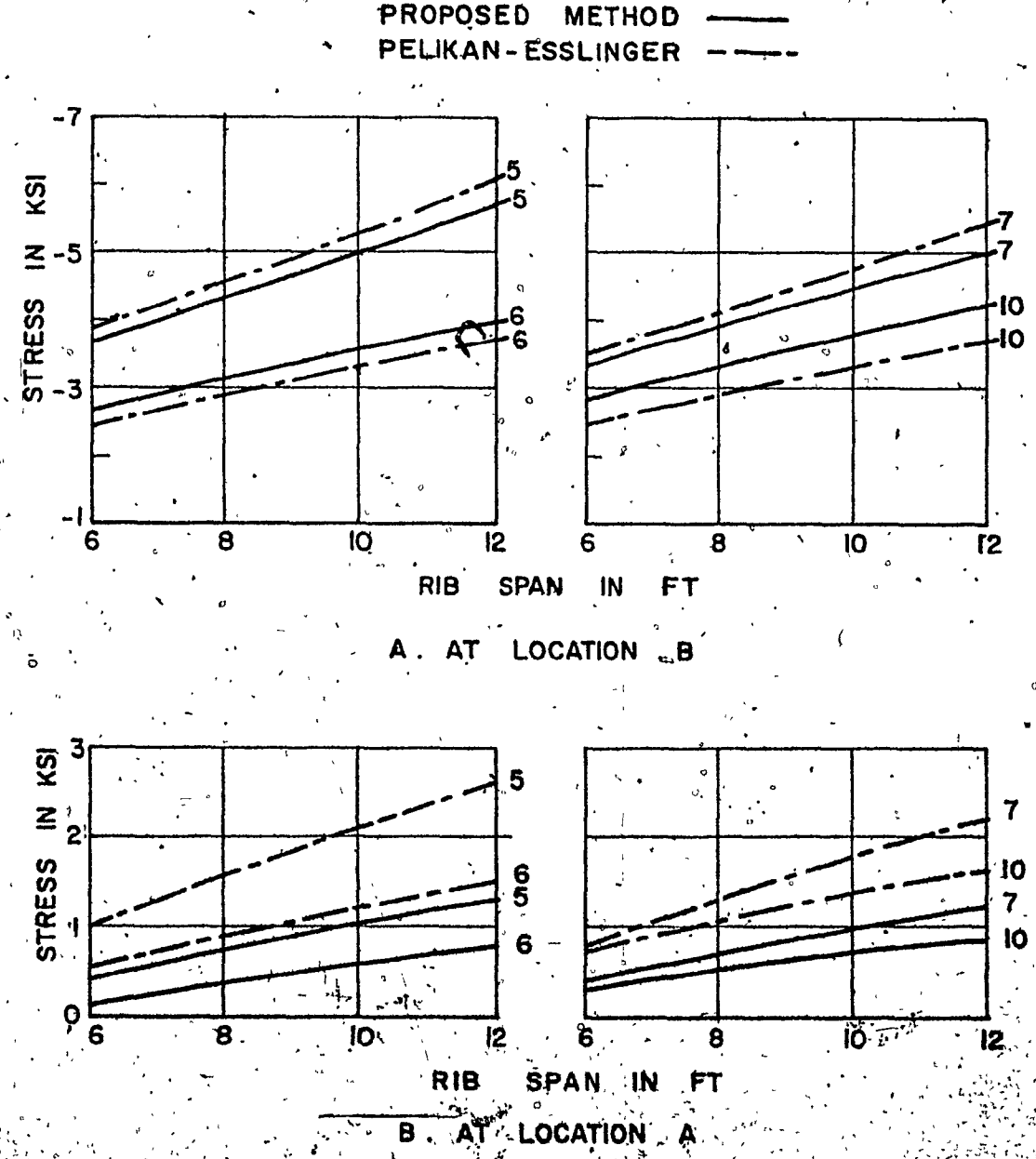

FIG. 4.8 - VARIATION OF LONGITUDINAL STRESS AT TOP OF DECK PLATE WITH RIB SPAN

plotted with stresses at top and bottom of the ribs located on either side of the loaded central rib. It is clearly seen that the longitudinal stress decreases rapidly with the increase in transverse distance, indicating that the directly loaded rib carries a major part of the load and that the load distribution in the lateral direction is restricted only to a small part of the deck.

The effect of the deck width, a, on the stresses of the centrally loaded rib or in its load carrying capacity is also examined by comparing the stresses when the deck width is increased to 15 ft. from 10 ft, keeping the floor beam flexibility constant. This is done by simply increasing the moment of inertia of the floor beams to 1012.0 in^4. in proportion to the fourth power of the ratio of the spans. The results, entered in Table 4.3 for two rib sizes, indicate that there is no significant change in the stresses obtained by the proposed method. This can be explained by observing that the stiffness of the deck in the transverse or the X-direction, which depends upon the plate thickness, is very small compared with that in the longitudinal or the Y-direction. Therefore, the width of deck has small influence upon the load transfer in the transvers- direction.

In order to check further the above conclusion, the rib next to the central rib is loaded at midspan with identical loading for the decks marked 1 and 6. The maximum stresses at top and bottom of the rib are almost similar with

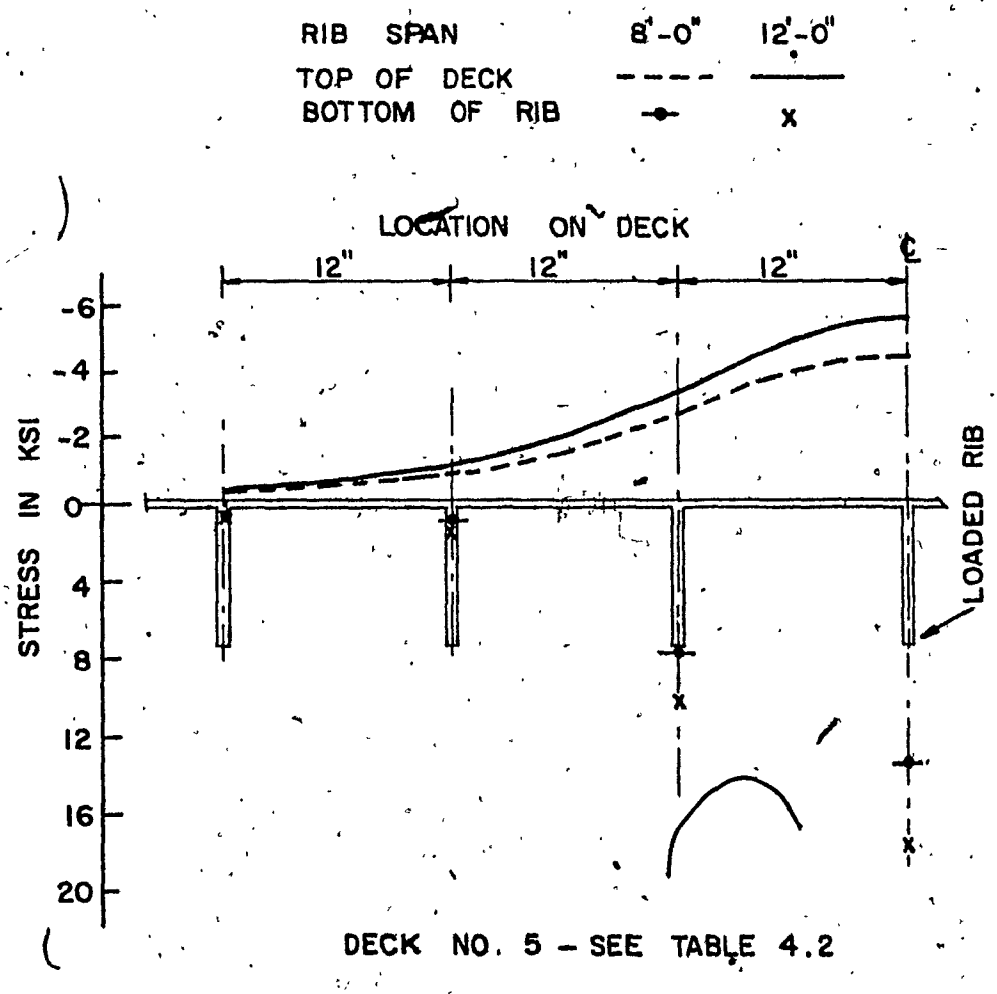

FIG. 4.9 - LONGITUDINAL STRESS ACROSS THE WIDTH OF DECK AT LOCATION B

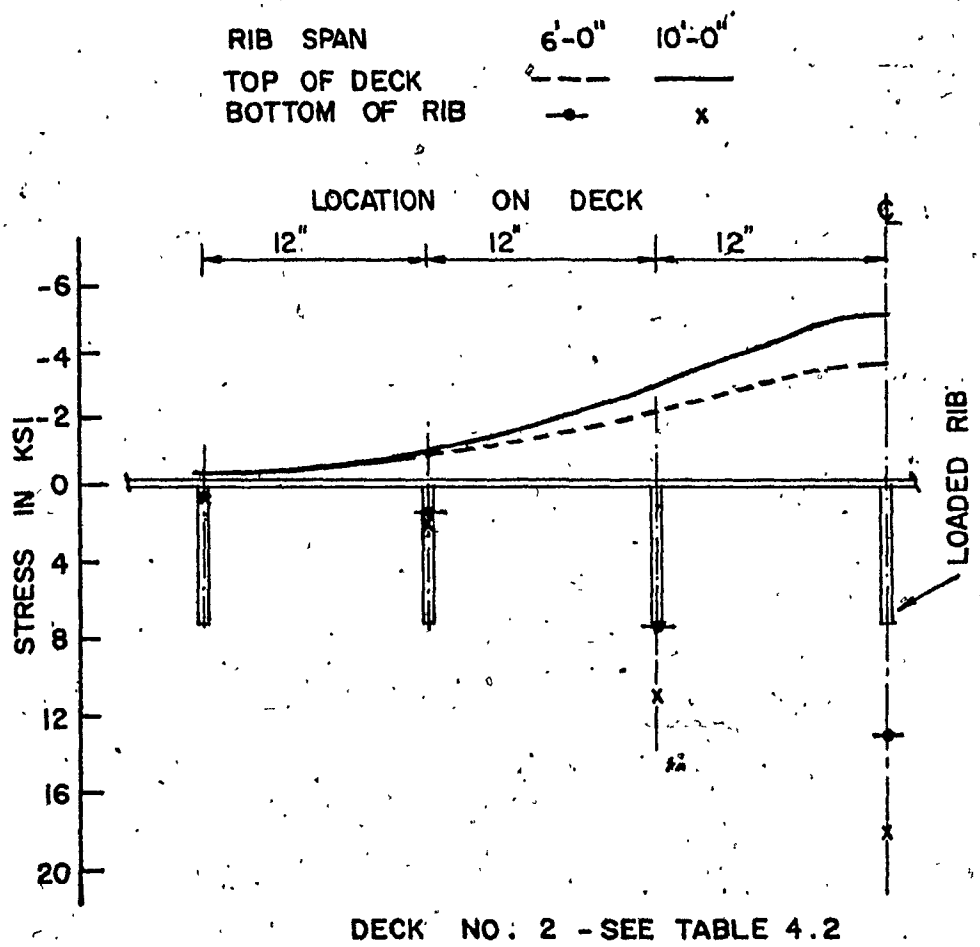

FIG. 4.10 - LONGITUDINAL STRESS ACROSS THE WIDTH OF DECK AT LOCATION B

TABLE 4.3

STRESSES AND DEFLECTION FROM THE PROPOSED METHOD FOR TWO WIDTHS OF DECK

Deck No.	Width of deck, a in feet	Rib span, in feet	At location A			At location B		
			Longitudinal stress, in ksi		Deflection, in inch	Longitudinal stress, in ksi		Deflection, in inch
			At top of deck	At bottom of rib		At top of deck	At bottom of rib	
4	10	6	0.28	-2.76	.0521	-3.04	11.73	.0571
		10	0.64	-5.33	.0609	-4.15	15.25	.0685
	15	6	0.25	-2.81	.0523	-3.00	11.76	.0575
		10	0.61	-5.23	.0612	-4.19	15.44	.0688
10	10	8	0.53	-3.95	.0568	-3.35	13.18	.0625
		12	0.86	-5.67	.0630	-4.23	15.91	.0718
	15	8	0.51	-3.90	.0569	-3.40	13.29	.0629
		12	0.82	-5.59	.0633	-4.31	16.18	.0720

little change to those obtained for the central rib when it is loaded. This confirms the above conclusion, and more important, it validates the assumption of the design method to a certain degree, where the load distribution among the ribs is independent of the width of the deck as long as there are sufficient number of ribs on either side of the loaded area.

To find the effect of floor beam flexibility on the stresses, Figures 4.11 and 4.12 are plotted using different values of the relative rigidity ratio of the rib to the floor beam as defined in References (6-7). It is seen that the two sets of curves for stresses σ_y at top of the deck plate at B are in good agreement for all values of γ. However, those at A show closer agreement only with stiffer floor beams (smaller γ) and show relatively longer differences with increasing γ. Observing more or less a constant difference between the stresses at bottom of the rib for all values of γ it may be concluded that the procedure outlined in References (6-7) for computation of floor beam flexibility for Pelikan-Esslinger's method is satisfactory concerning the rib stresses and the deck plate stress at midspan of the rib.

The deflections of the rib determined at locations A and B by the proposed method are shown in Figures 4.13 and 4.14. From the nature of the curves, it is seen that they are not directly proportional to the span of the rib.

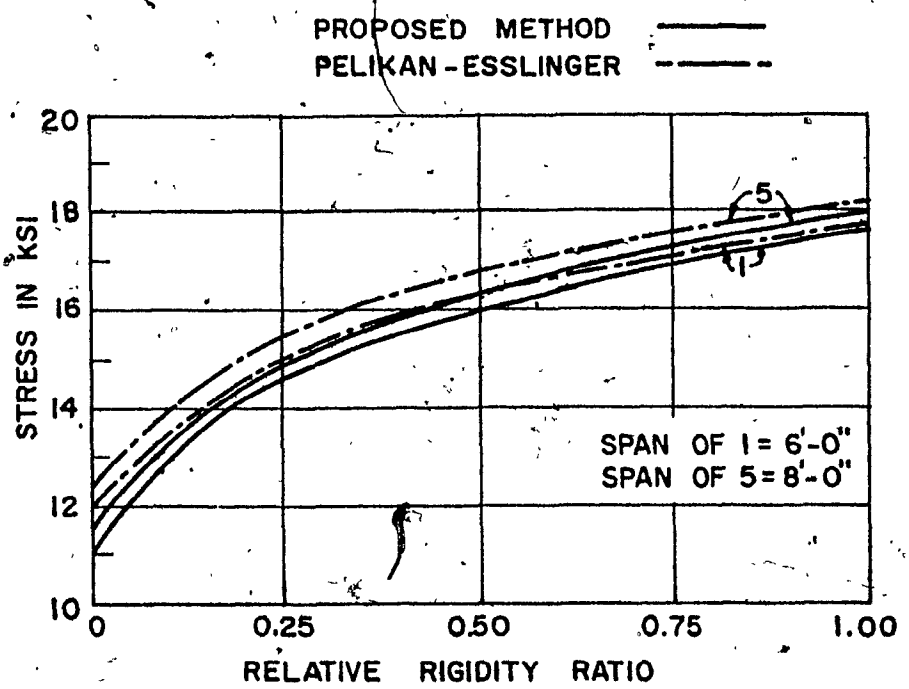

A. AT LOCATION B

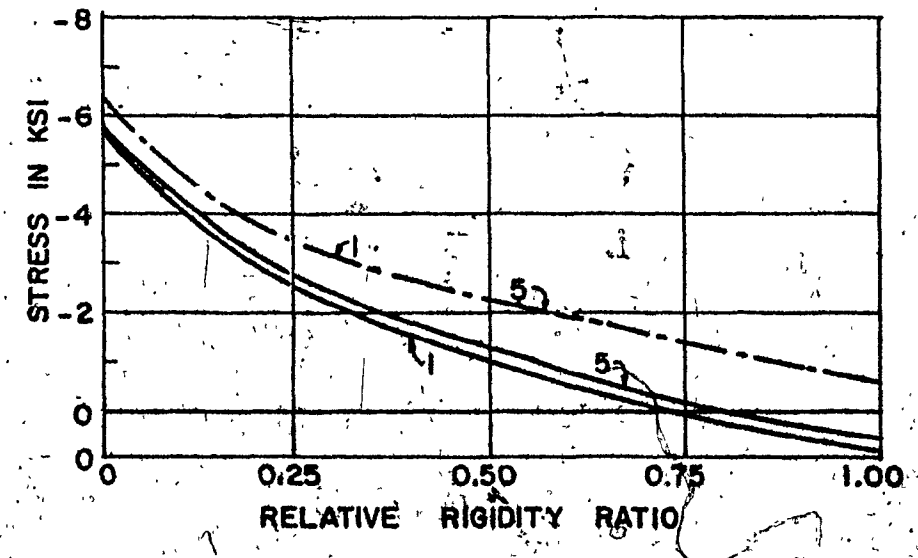

B. AT LOCATION A

FIG. 4.11 - STRESS AT BOTTOM OF RIB VERSUS RELATIVE RIGIDITY RATIO

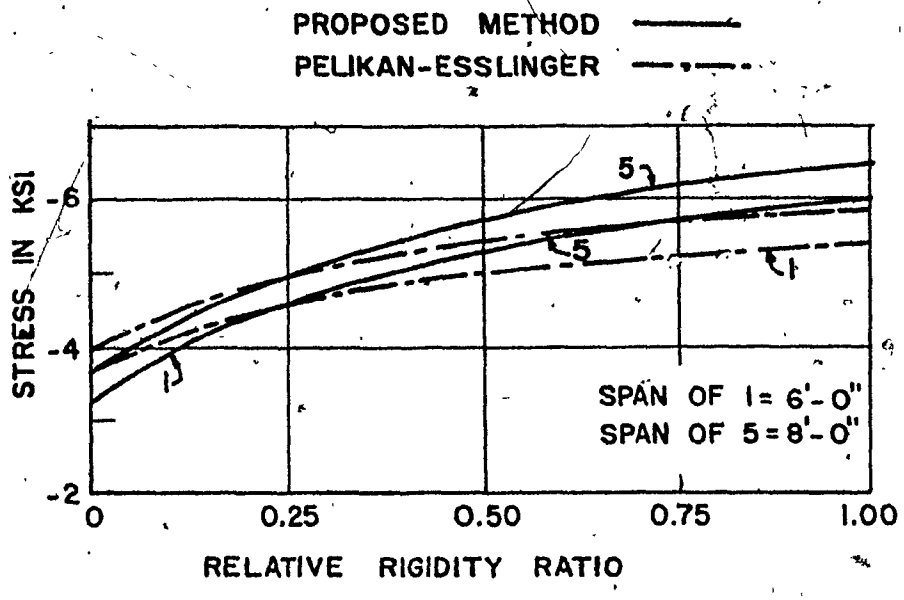

A. AT LOCATION B

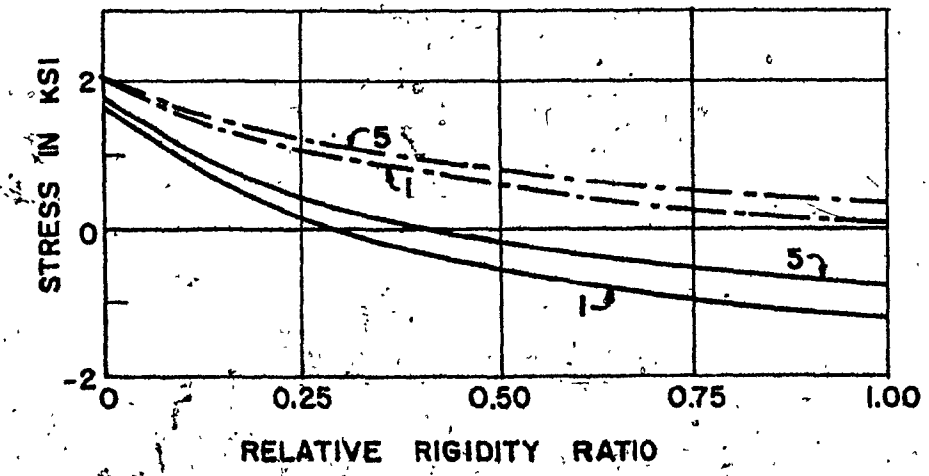

B. AT LOCATION A

FIG. 4.12 – LONGITUDINAL STRESS AT TOP OF DECK PLATE VERSUS RELATIVE RIGIDITY RATIO

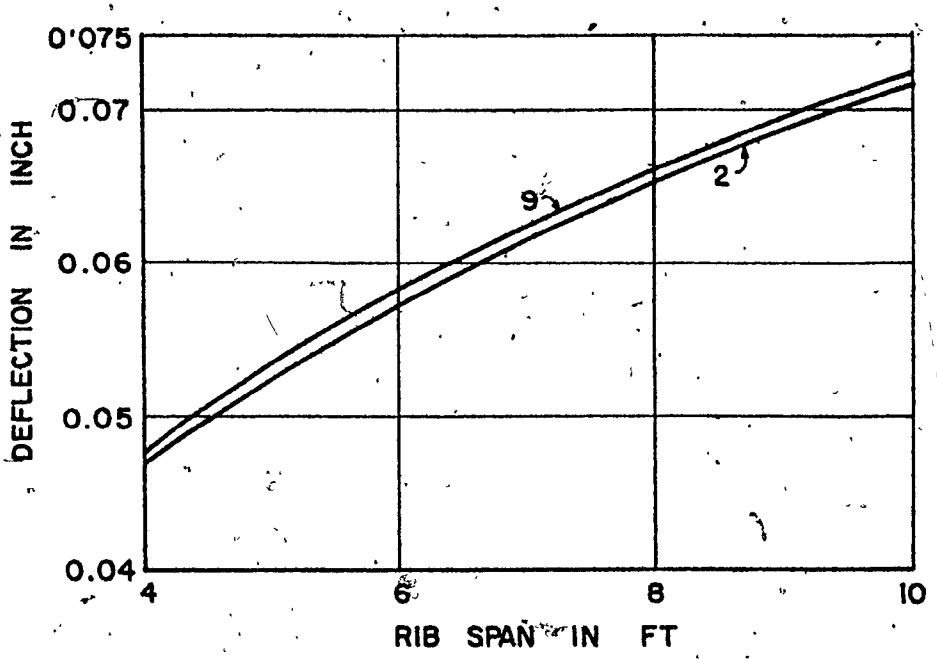

A. AT LOCATION B

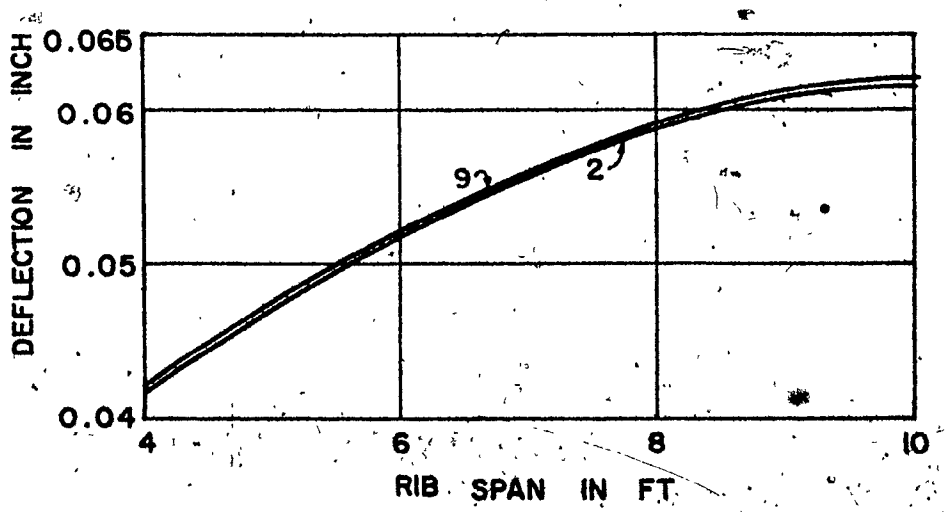

B. AT LOCATION A

FIG. 4.13 - DEFLECTION OF LOADED RIB

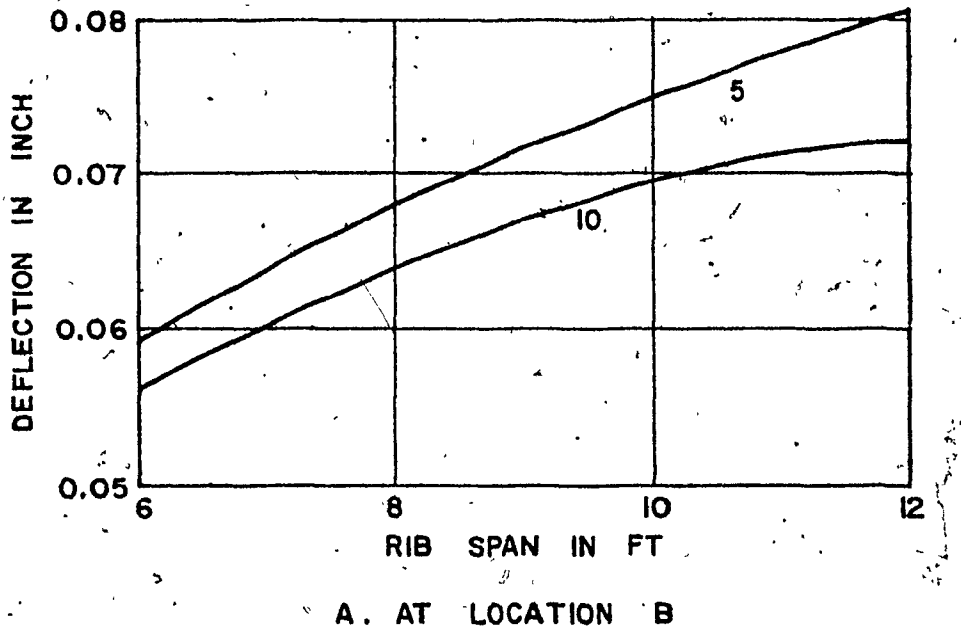

A. AT LOCATION B

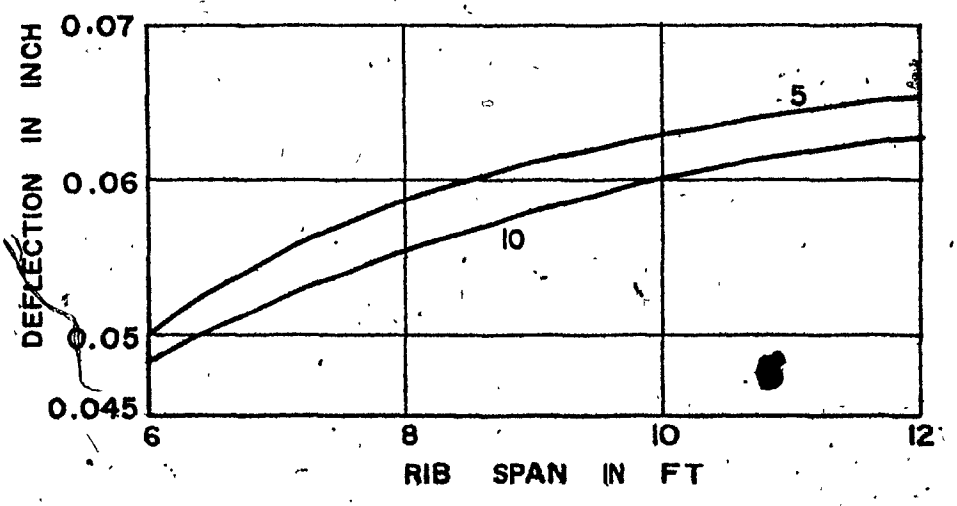

B. AT LOCATION A

FIG. 4.14 - DEFLECTION OF LOADED RIB

4.4 DECKS STIFFENED WITH CLOSED RIBS

The general arrangement of the decks stiffened by closed ribs is shown in Figure 4.15. The types of the closed rib are chosen arbitrarily from the commercially available section as listed in Reference (57). The rib sizes, their centre to centre spacings and spans, and the deck plate thickness are varied. Table 4.4 contains the dimensions of these decks together with their designations.

All decks are assumed again to consist of seven panels and are subjected to a single wheel load of 20 kips at middle of the central rib, as indicated in Figure 4.15. The floor beams have moment of inertia being equal to 200.0 in^4 .

Two sets of values of stresses at top and bottom of the loaded rib at locations A and B are presented in Figures 4.16 - 4.21. The stresses at bottom of the rib obtained from two methods are in good agreement with all rib spans, with the design method indicating higher stresses in all cases. Looking into the stress curves in Figures 4.16 - 4.18, an interesting feature of the closed ribs is quickly observed. With the increase in the rib span, the stresses in the rib increases first but after a certain span, the stress increment becomes relatively small. Both analytical methods indicate identical behaviour of the closed ribs. This shows that the load distribution in the transverse direction of the

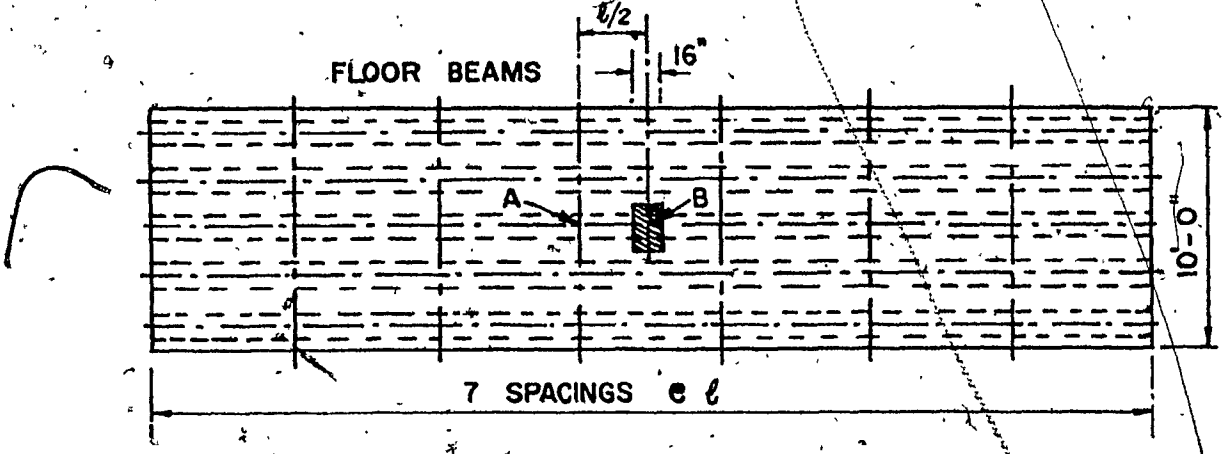

A. TOP PLAN

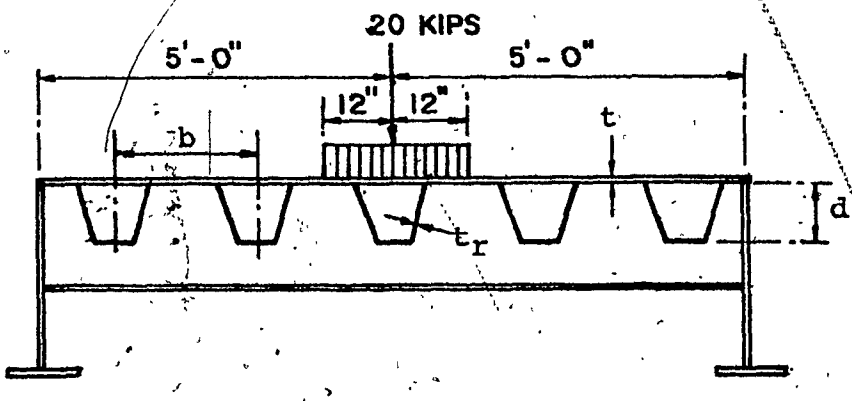

B. SECTION THROUGH LOADED AREA

FIG. 4.15 - ARRANGEMENT OF HYPOTHETICAL DECKS WITH CLOSED RIBS

TABLE 4.4

DIMENSIONS OF HYPOTHETICAL DECKS WITH CLOSED RIBS

Deck identification No.	Deck plate thickness t, in inch	Rib particulars			Rib span ℓ in feet
		d x t_r in inch	b in inch	Designation*	
1C	3/8	8 x 5/16	24	85	7-15
2C	5/8	8 x 5/16	24	85	7-15
3C	3/8	11 x 5/16	24	115	7-15
4C	3/8	10 x 5/16	24	105	7-15
5C	1/2	10 x 5/16	24	105	7-15
6C	1/2	10 x 5/16	22	105	7-15
7C	1/2	10 x 5/16	28	105	7-15
8C	3/4	10 x 5/16	24	105	7-15

* Designation in accordance with Reference 57

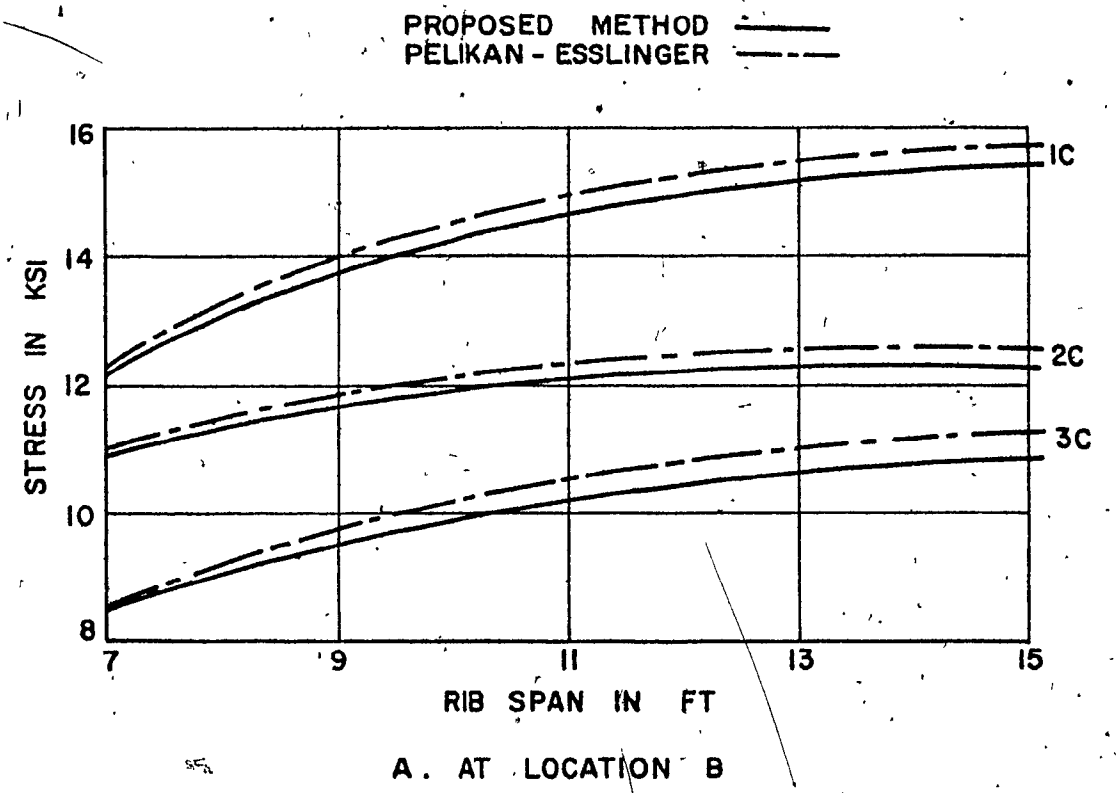

A. AT LOCATION B

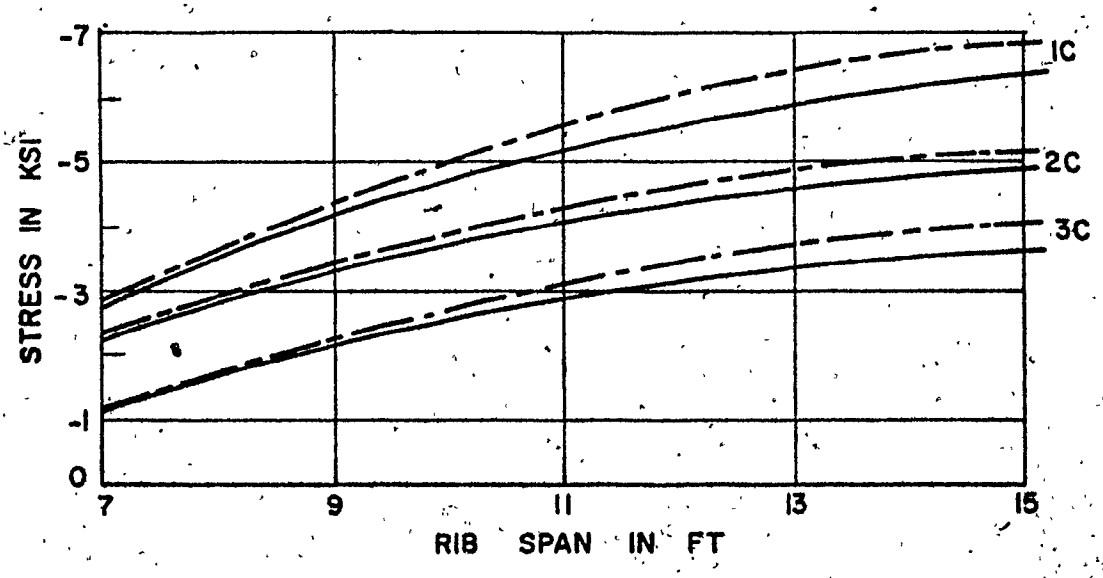

B. AT LOCATION A

FIG. 4.16 - VARIATION OF LONGITUDINAL STRESS AT BOTTOM OF RIB WITH SPAN

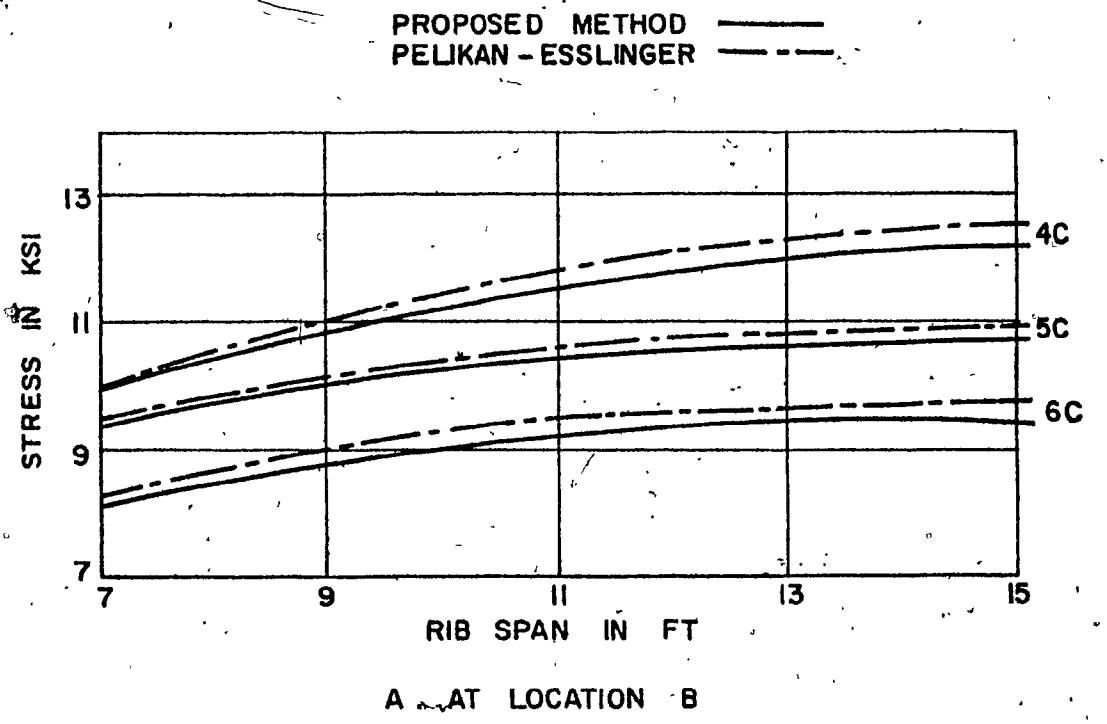

A . AT LOCATION B

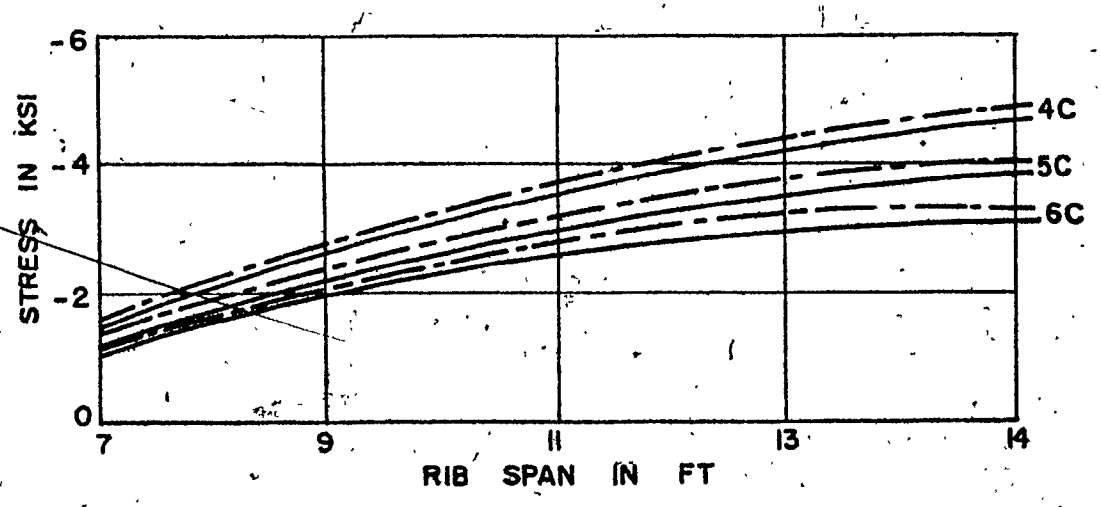

B . AT LOCATION A

FIG. 4.17 - VARIATION OF LONGITUDINAL STRESS AT BOTTOM OF RIB WITH SPAN

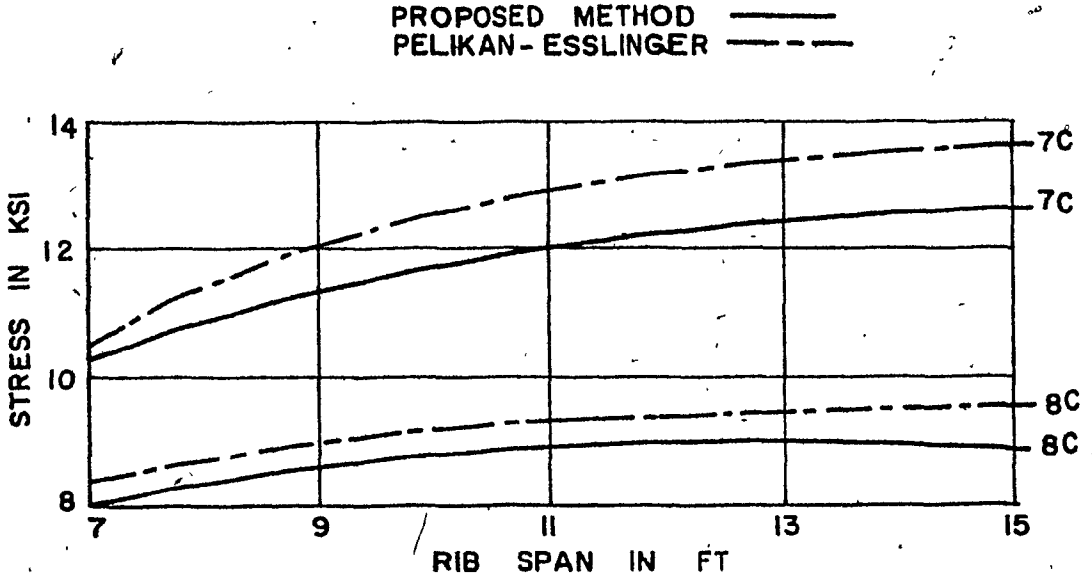

A. AT LOCATION B

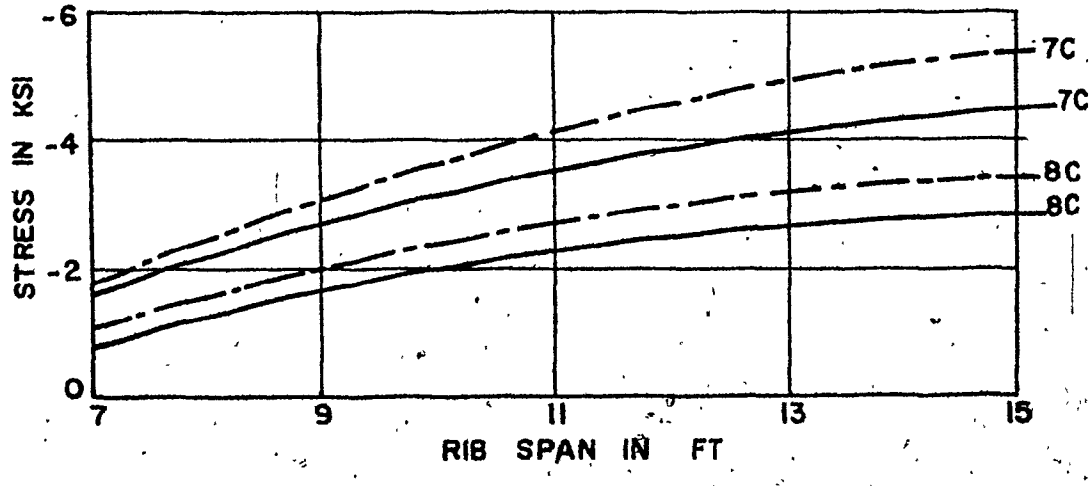

B. AT LOCATION A

FIG. 4.18 - VARIATION OF LONGITUDINAL STRESS AT BOTTOM OF RIB WITH SPAN

deck, which depends upon the effective torsional rigidity, increases with the increase in the rib span. In other words, the directly loaded rib carries lesser load with the increase in its span.

The longitudinal stresses at top of the plate are shown in Figures 4.19 - 4.21, and they indicate more or less the similar findings as in the case of open ribs. Better agreement between two sets of results is observed at location B, compared with that at location A.

The distribution of longitudinal stresses across the width of deck at section B is shown in Figures 4.22 and 4.23. It is seen that the stress decreases rapidly from a peak value at the load position with the increase of the transverse distance from the loaded rib. The effective participation of the deck in carrying the load increases with the increase in rib span, but still is restricted to a smaller part of the deck width which is, however, greater than that in the case of open ribs.

The deflections of the deck at locations A and B are shown in Figures 4.24 and 4.25, which indicate that the deflection curves flatten somewhat with the increase in the rib span. In other words, the rate of increase of the deflection quickly reduces with larger spans.

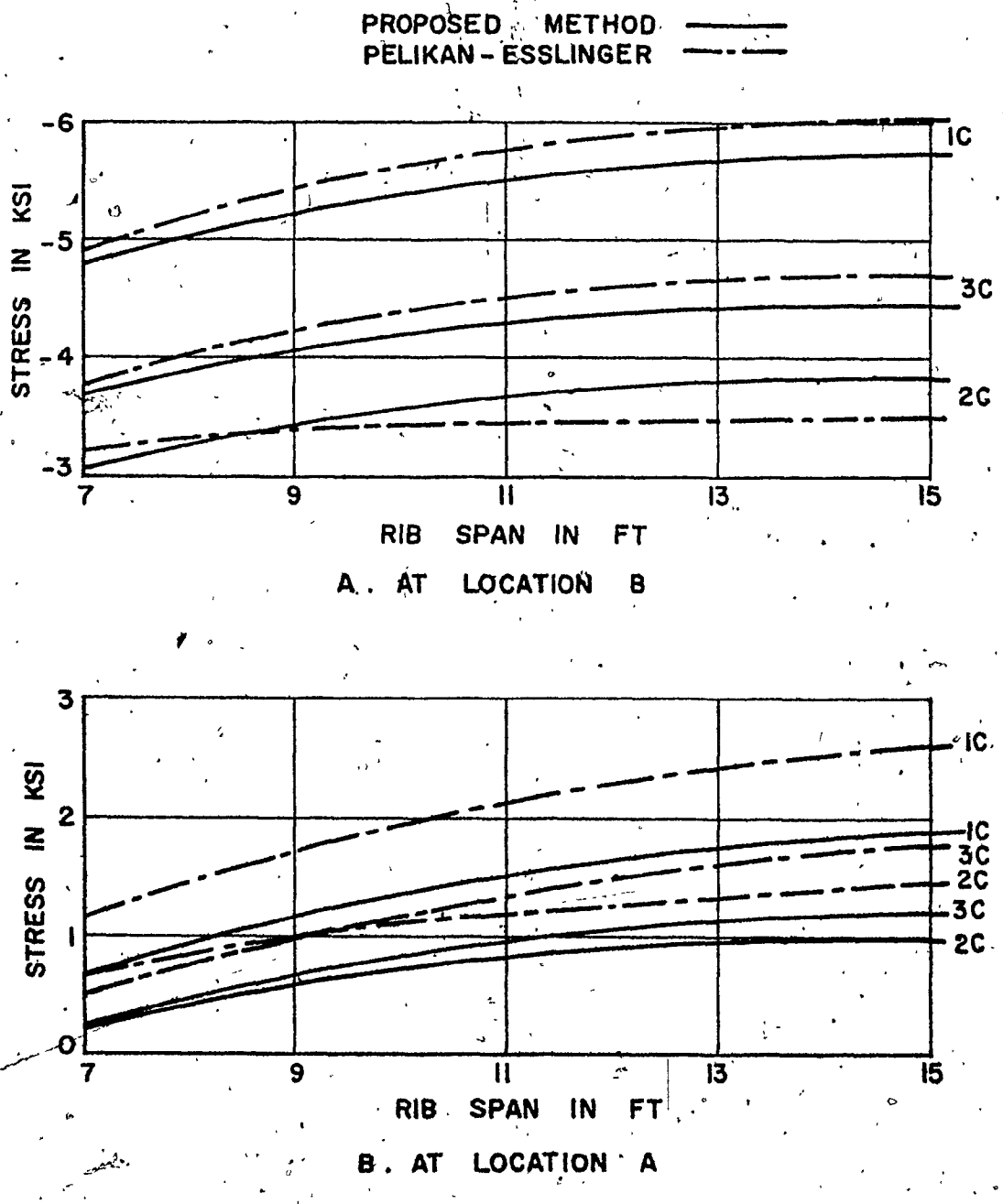

FIG. 4.19 - VARIATION OF LONGITUDINAL STRESS AT TOP OF DECK PLATE WITH RIB SPAN

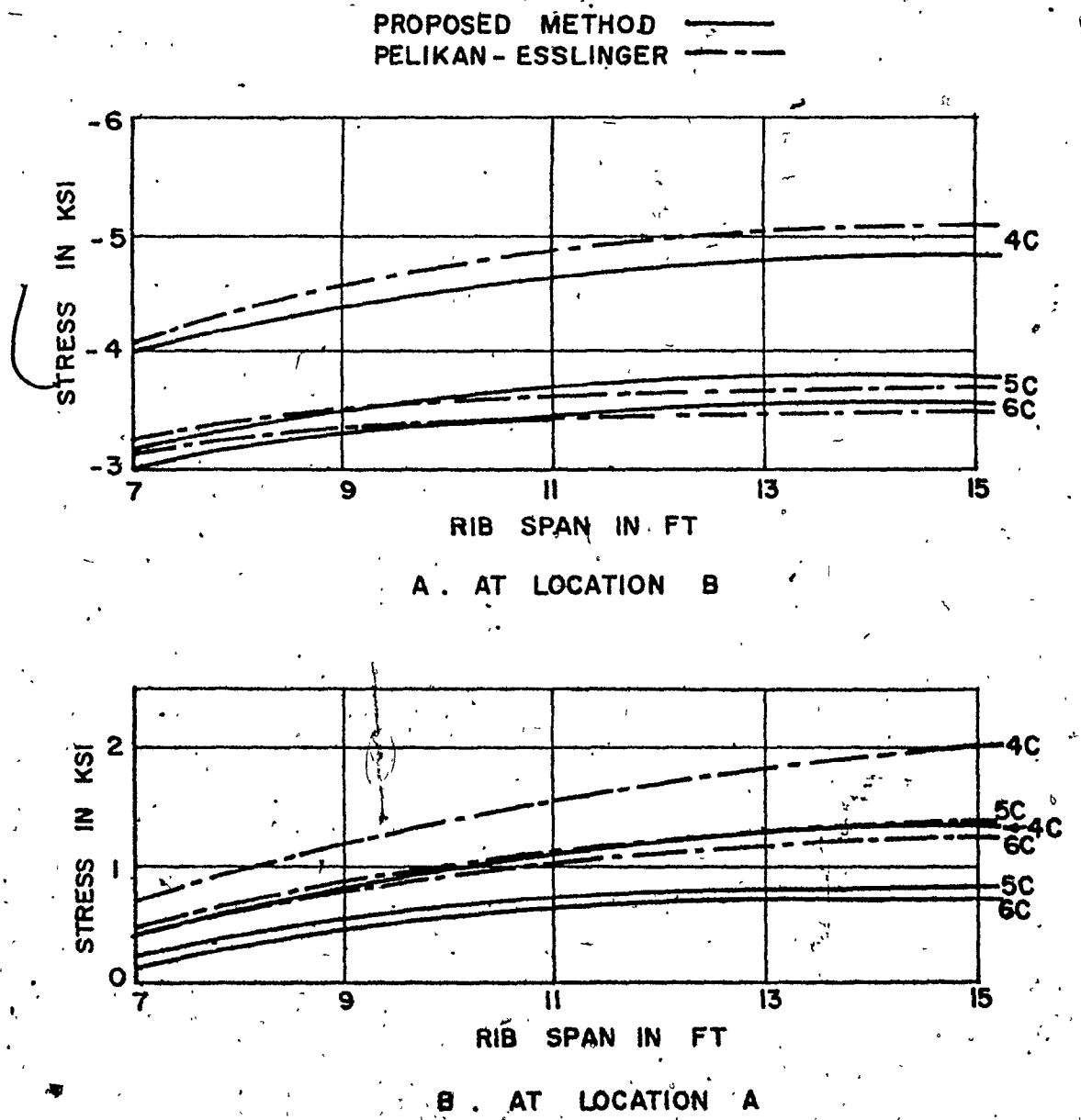

FIG. 4.20 - VARIATION OF LONGITUDINAL STRESS AT TOP OF DECK PLATE WITH RIB SPAN

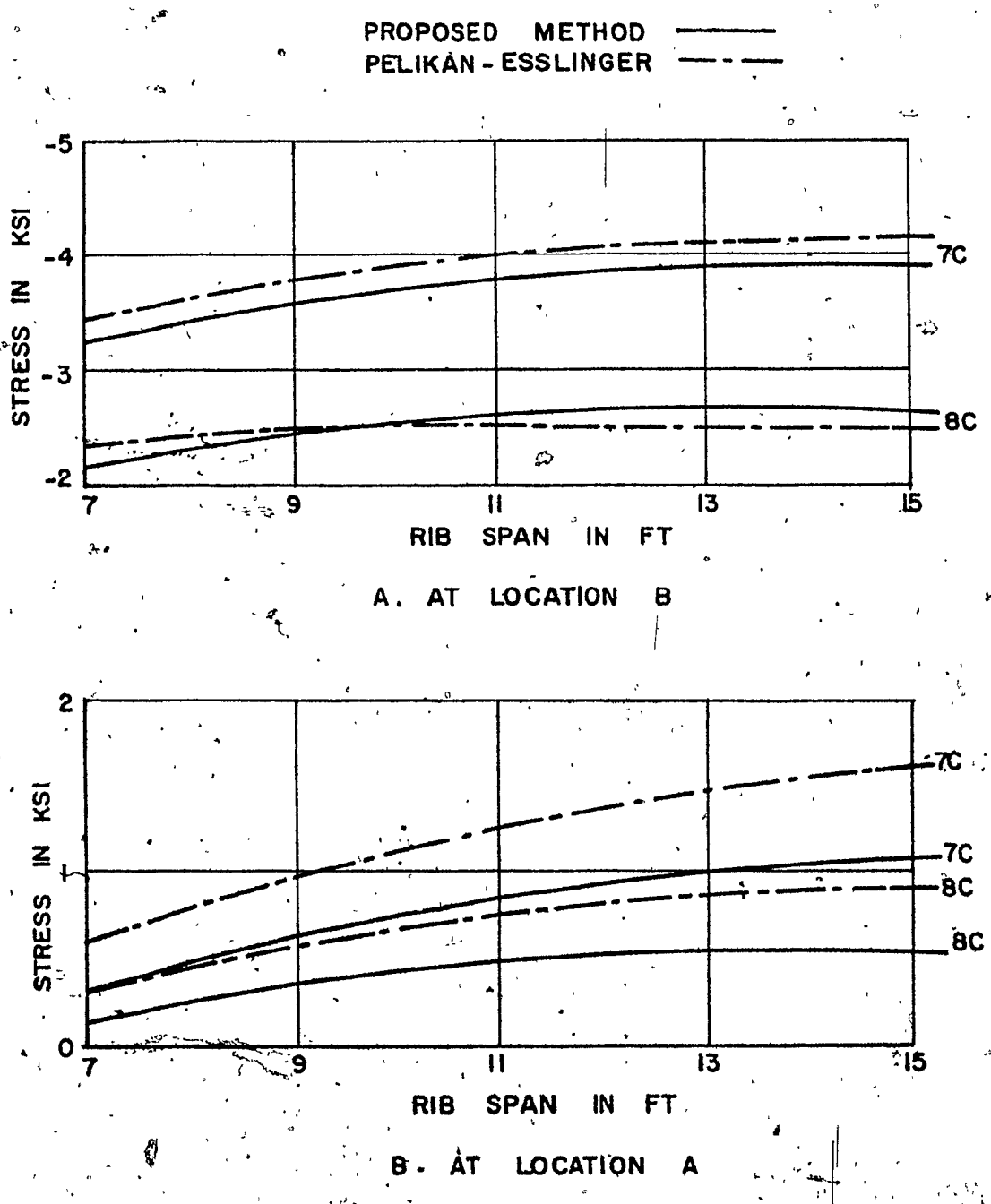

FIG. 4.21 - VARIATION OF LONGITUDINAL STRESS AT TOP OF DECK PLATE WITH RIB SPAN

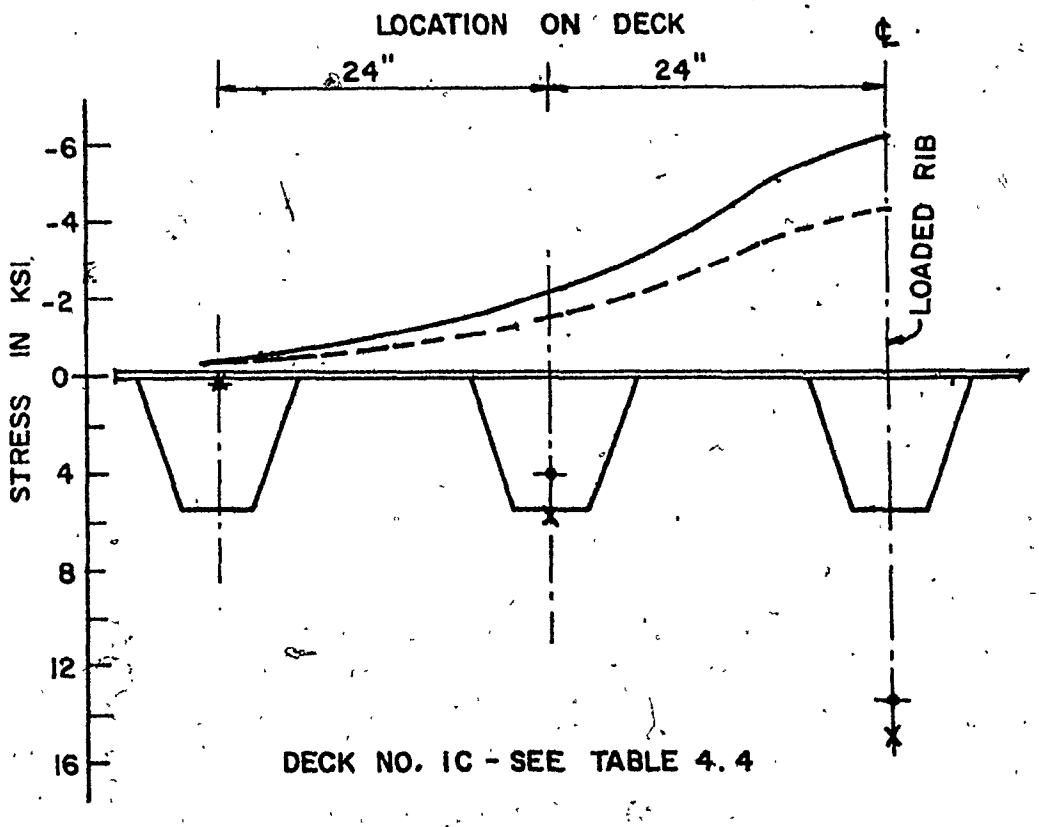

FIG. 4.22 - LONGITUDINAL STRESS ACROSS THE WIDTH OF DECK AT LOCATION B

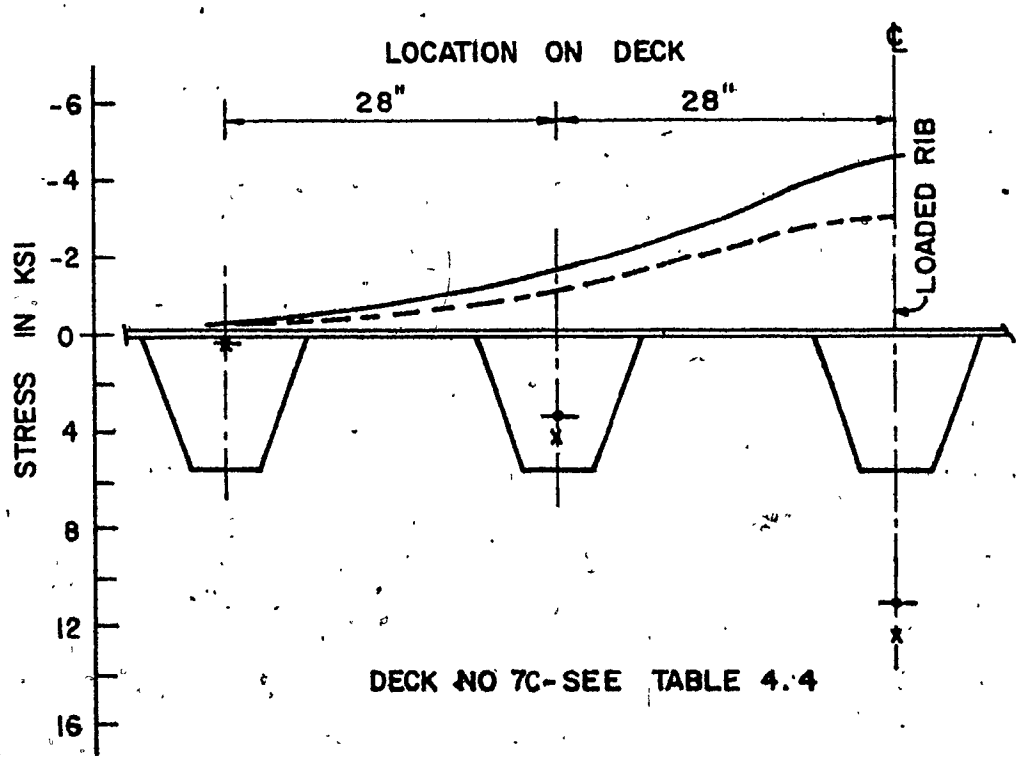

FIG. 4.23 - LONGITUDINAL STRESS ACROSS THE WIDTH OF DECK AT LOCATION B

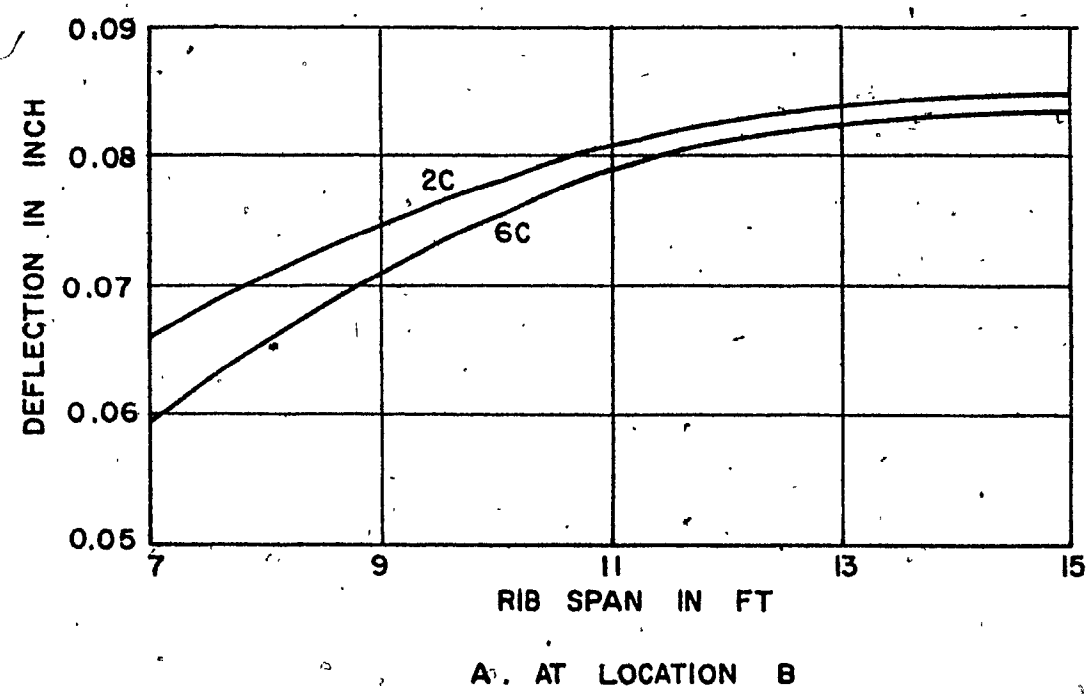

A. AT LOCATION B

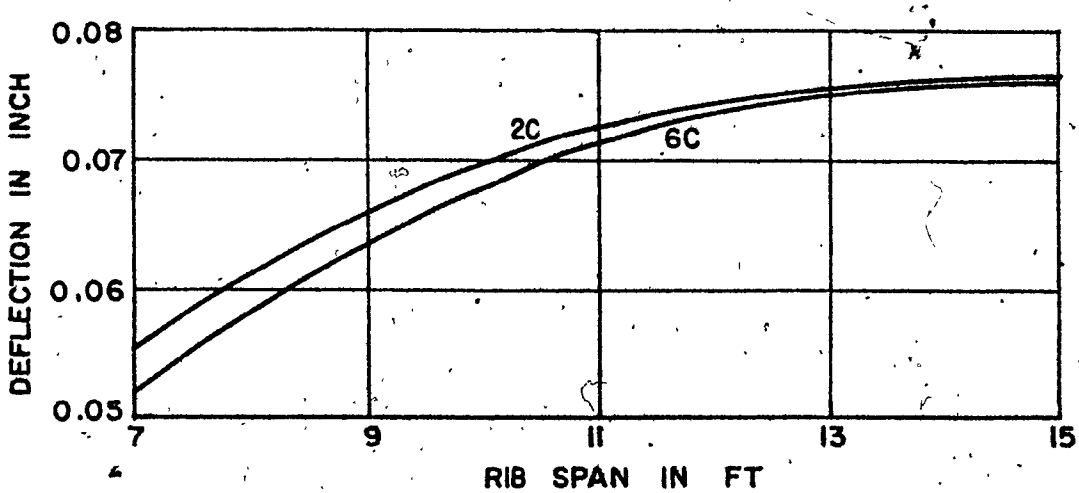

B. AT LOCATION A.

FIG. 4.24 - DEFLECTION OF LOADED RIB

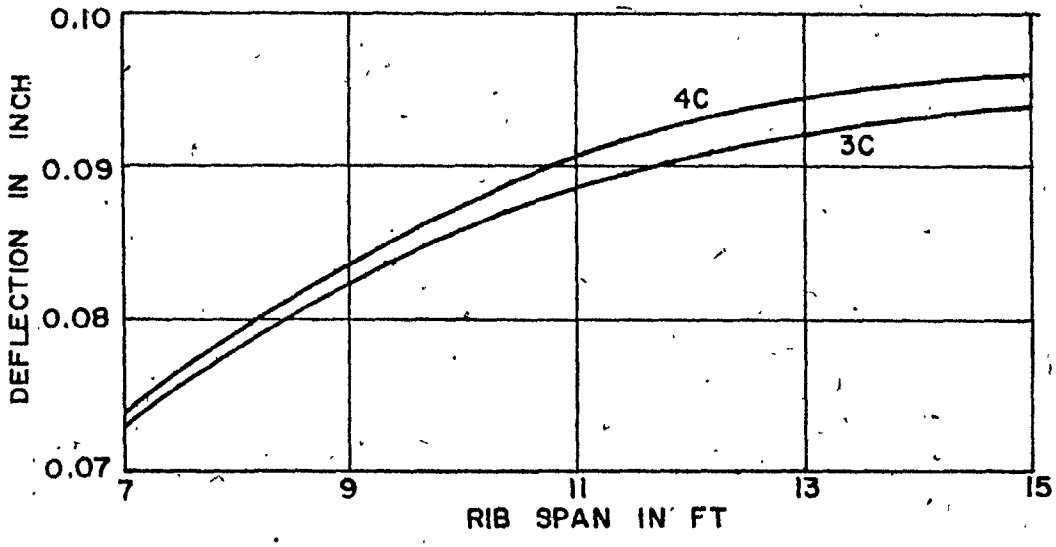

A. AT LOCATION B

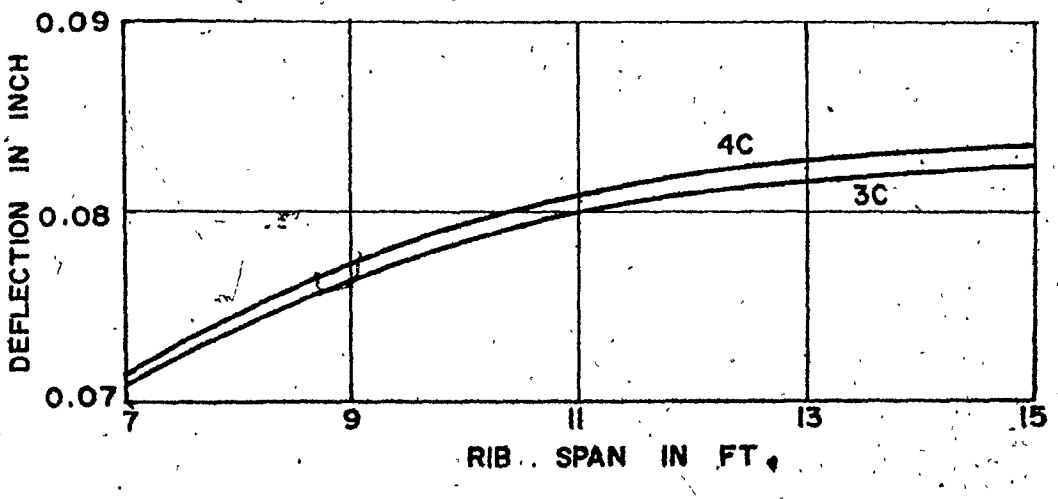

B. AT LOCATION A

FIG. 4.25 - DEFLECTION OF LOADED RIB

4.5 CONCLUSIONS

The presentation and discussion of the results lead to the following conclusions.

1. The proposed analytical method can be used to determine adequately the stresses and deflections of the deck.

2. The design method of Pelikan-Esslinger provides satisfactory estimate of the magnitude of stresses in the deck. The results are usually higher and thus, can be used for a safe design of a deck structure.

3. Pelikan-Esslinger's method becomes increasingly conservative with longer span of open type ribs.

4. The closed ribs can span a longer distance without significantly increasing the maximum or critical stresses obtained with commonly used span lengths.

5. The width of deck has insignificant effect on the stresses in the ribs located near the centre of the deck, provided that the flexibility of the floor beams remain constant and that there are sufficient number of ribs on either side of the loaded rib.

6. The effective participation of the deck in transverse direction in carrying load is restricted to a small

width of the deck. However, the effective width of the deck in transverse direction is relatively larger for decks with closed ribs than those having open ribs.

CHAPTER 5

EXPERIMENTAL PROGRAM

5.1 INTRODUCTION

An experimental program was planned in this research to examine the structural behaviour of an orthotropic bridge deck and to check the analytical predictions more meaningfully. The behaviour of an orthotropic deck having open ribs was investigated by Troitsky and Azad [52] in an earlier study. For this test program, therefore, an orthotropic steel bridge deck model with closed ribs was selected. The primary objectives of the experimental program were:

(i) To examine the stress distribution and the elastic behaviour of the deck.

(ii) To compare the test results with those predicted by the analytical methods.

(iii) To check the conventional method of superposition of stresses due to bending of the orthotropic deck and the main girder.

It is expected that the experimental information obtained on the above items would add to the available test data in this area and be useful to check the reliability of an analytical method.

The experimental tests were performed on a simple span plate girder bridge model with a four-panel orthotropic steel bridge deck on top. The longitudinal ribs or stiffeners used were of box-type, with rounded bottom. The static loads distributed on small areas to simulate the actions of wheel loads were restricted to be within the elastic range of the steel used.

For theoretical analysis of the model, the proposed refined analytical method and the design method of Pelikan-Esslinger were used. This Chapter describes in detail, the experimental program, which includes the model design, fabrication, instrumentations and the test procedures.

5.2 MODEL SIZE AND MATERIAL

For an experimental investigation of this type, the prime consideration is the proper size and material for the model to be used. This is usually dictated by the cost of construction, the available laboratory facilities for testing and the usefulness of the model in obtaining the desired degree of performance. After comparing several alternatives and proposals, it was finally decided to use steel as the model material and to restrict the size of the model to a maximum of 26' - 0" in length and 5' - 6" in width. These dimensions were the permissible limits, taking into consideration the facilities and the available space under the existing testing frame.

The use of steel as model material offered the greatest leverage in claiming the model behaviour to be directly comparable with an actual orthotropic steel bridge deck, essentially due to the involvement of the same material and similar details of construction in both cases.

5.3 MODEL DESIGN AND FABRICATION

The model for the test was 24' - 0" long between the centres of the end bearings and 24' - 6" in overall length. Five torsionally stiff trapezoidal ribs with round bottom were welded at 12" centres to a 3/16" thick deck plate. The width of the deck was 5' - 0" between the main girders. The floor beams, spaced 6' - 0" centres, and the girders were of inverted T-sections. The model dimensions and details are shown in Figure 5.1.

In proportioning the model, a thickness less than 3/16" was not considered for the deck plate and the rib to avoid any problem in welding and fabrication. The model dimensions used in this test were not obtained by the scaling down of a particular prototype. This was virtually impossible due to so many restrictions. However, this did not pose any problem in this investigation, since the same model was tested and analyzed like a bridge, itself.

The model was designed initially, following the method outlined in References (6) and (7), to indicate a maximum stress in the model below the elastic limit of the

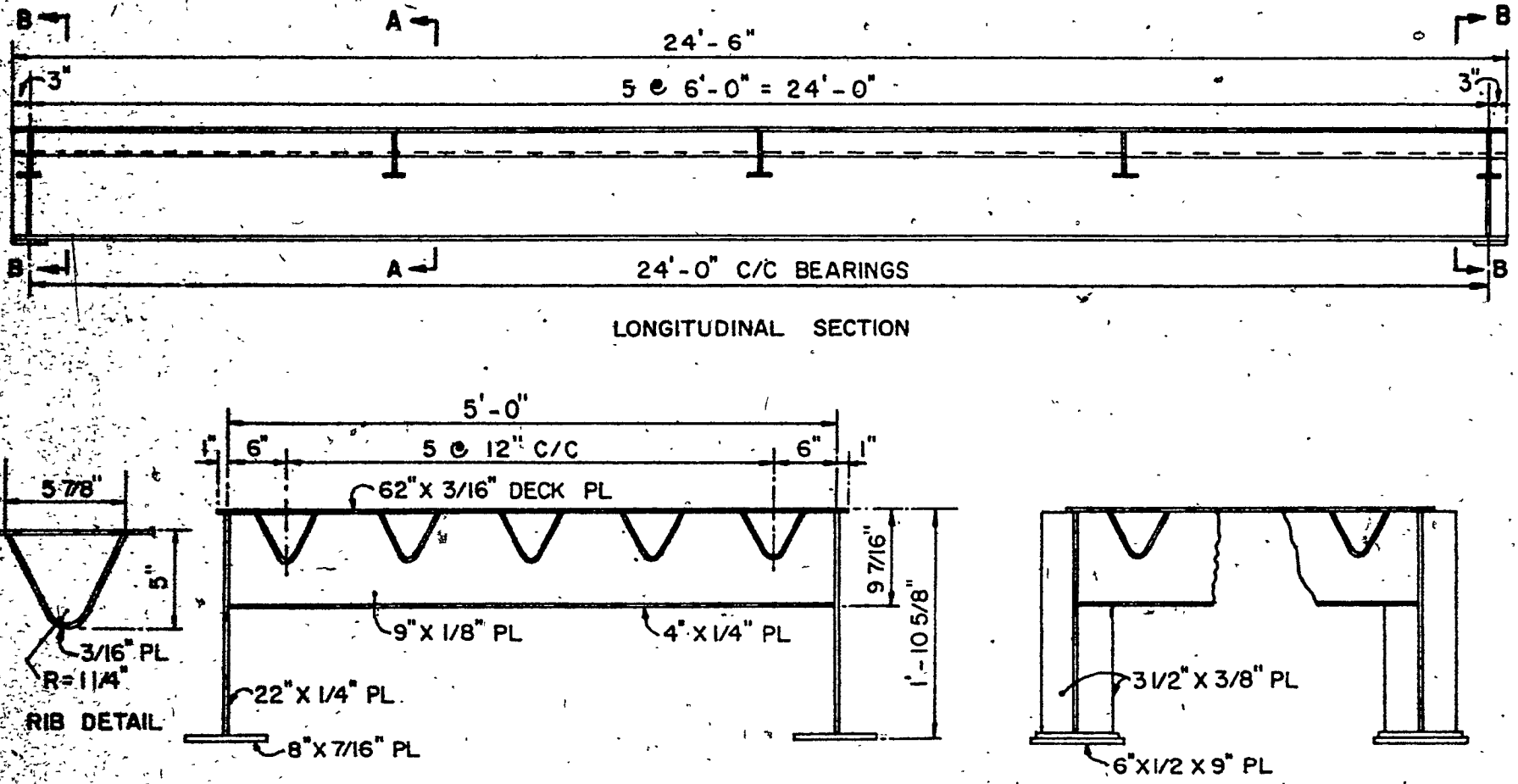

FIG. 5.1 - MODEL DETAILS AND DIMENSIONS

steel used, when a chosen load of 10 kips was assumed to act at the midspan of the central rib. The load was taken as distributed, on an assumed area of 8" x 12", simulating the action of a wheel load.

The model was fabricated from steel conforming to ASTM A36 and standard Canadian fabrication and welding procedures. All welding was done by manual stick electrodes. While welding the cold-formed troughs or ribs to the deck plate, care was taken to avoid undesirable distortion and the building up of excessive residual stress. The ribs were run continuously through the floor beam web cut-outs, which were shaped to conform with the rib geometry and were welded to them. The fabricated model was delivered and fixed to its position for testing, as one piece.

5.4 TEST SET-UP

For all tests, the model was supported under a testing frame. In the first phase of the testing, the girders were provided with intermediate supports in addition to the end supports, as shown in Figure 5.2, to eliminate the girder bending under a load. Although a continuous support along the length of the girders would have been more desirable for this purpose, the structural arrangement of the test frame made such a set-up impractical. However, the support arrangement used was satisfactory, in the sense that the small girder bending for the short span was negligible. In the second phase

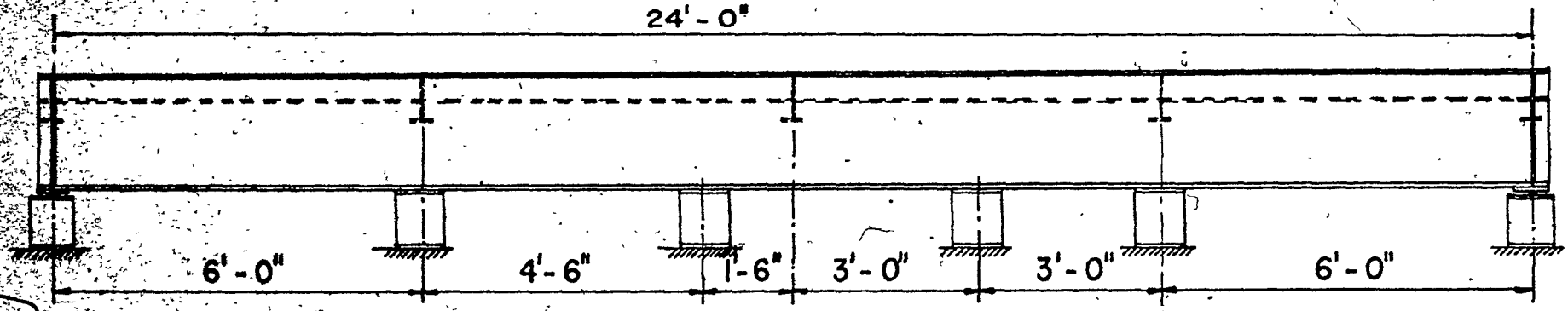

A/ FIRST PHASE OF TEST

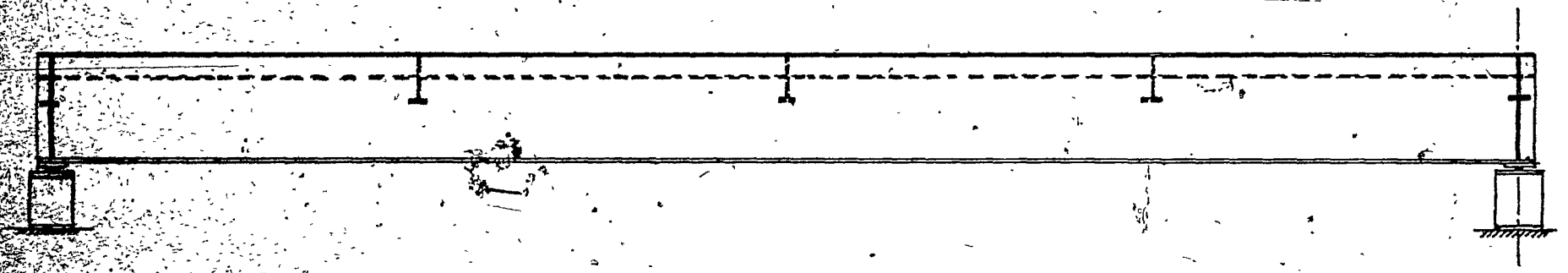

B. SECOND PHASE OF TEST

FIG. 5.2 - GIRDER SUPPORTS

of the testing, the girders were simply supported at the end supports, which permitted the girders to rotate freely at the ends. The weight of the model itself, was ample to hold it firmly in its position, during the whole experiment.

Three sections of the model were chosen for testing, Section P being near the rib support and Sections Q and R corresponding to the midspans of the rib, as indicated in Figure 5.3. Electrical strain gages were used at these sections to measure the strains. Since the strain gages at the underside of a rib could only be placed just outside the floor beam web, Section P was chosen 1 in. away from the centre of the floor beam web.

Three-element rosettes were fixed at the top of the deck to find the strain field. Single gages were used both in the longitudinal and transverse directions for the ribs to measure the strains in the respective directions. It was necessary only to instrument the half width of the model, as the results can be predicted by the use of the principle of symmetry. Dial gages with graduations of 0.001 in. were used to record the deflections. They were firmly held on stands and connected to the locations where the deflection measurements were sought. Figures 5.3 and 5.4 show respectively, the locations of the strain gages and dial gages used in testing the model. To identify the ribs, they were marked as indicated in Figure 5.4. Ribs 1, 2L and 3L were instrumented only, which constituted the half-width of the model.

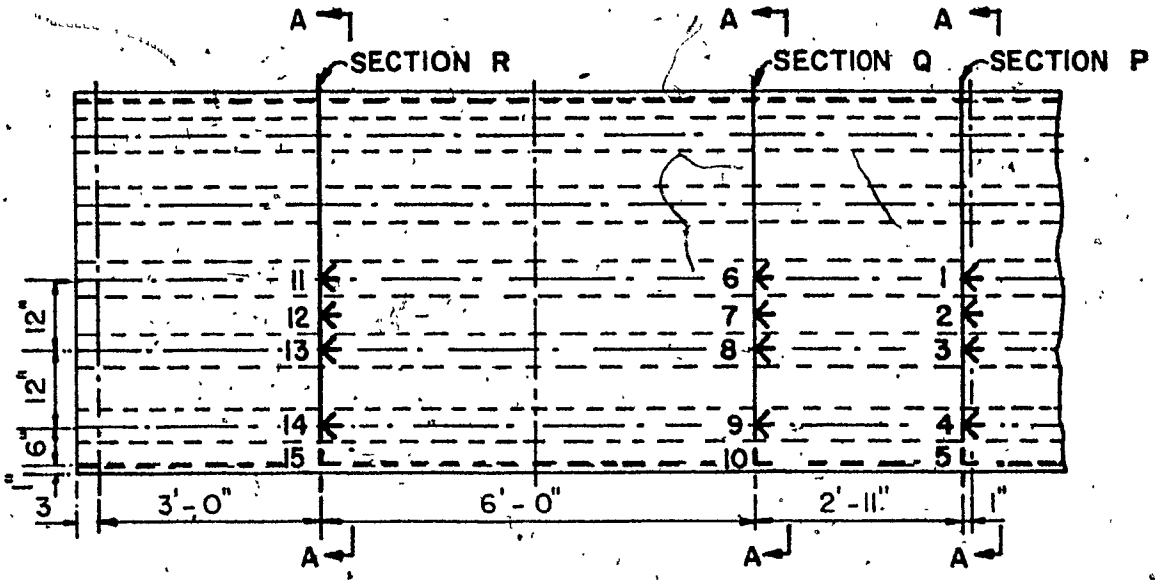

A. DECK PLAN

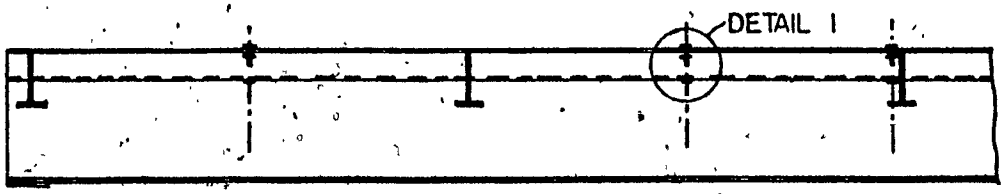

B. LONGITUDINAL SECTION SHOWING GAGES ON RIB

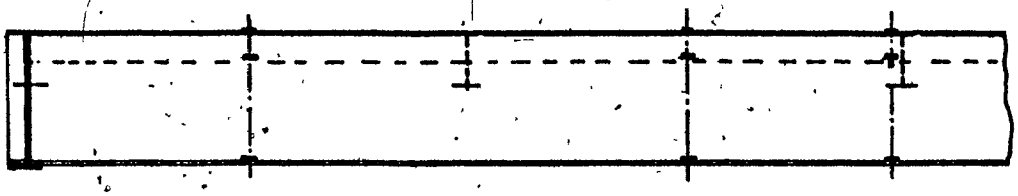

C. FRONT ELEVATION SHOWING GAGES ON GIRDER

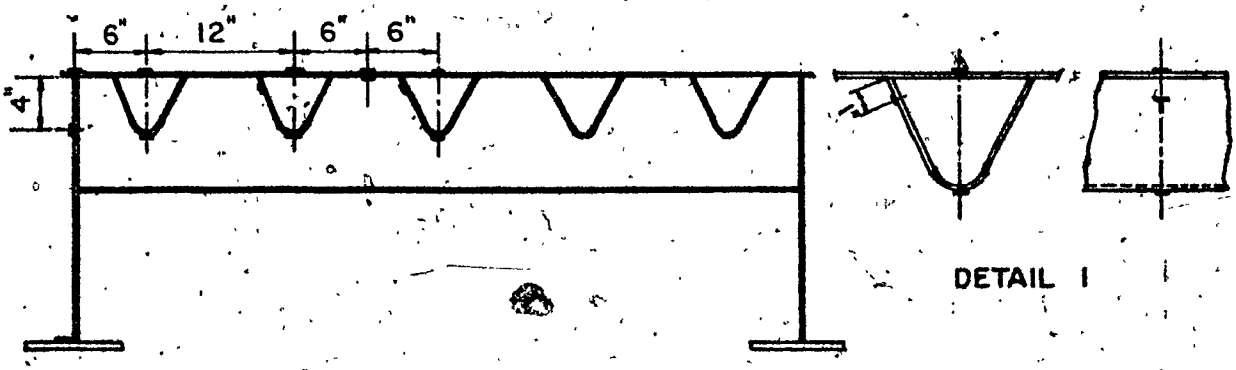

D. SECTION A-A

FIG. 5.3 - LOCATION OF SECTIONS AND STRAIN GAGES

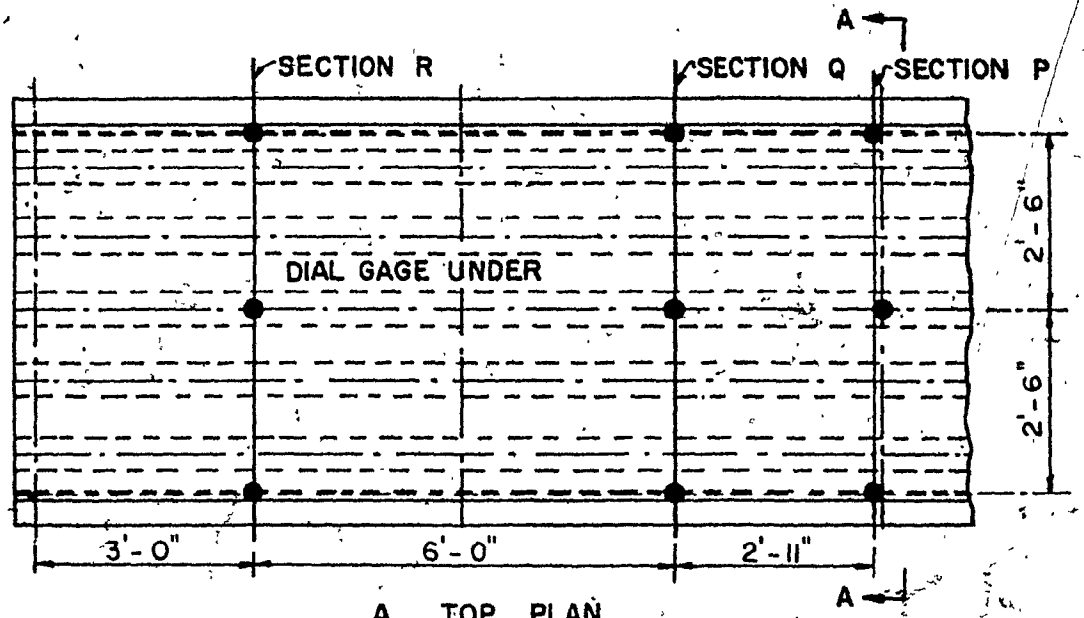

A. TOP PLAN

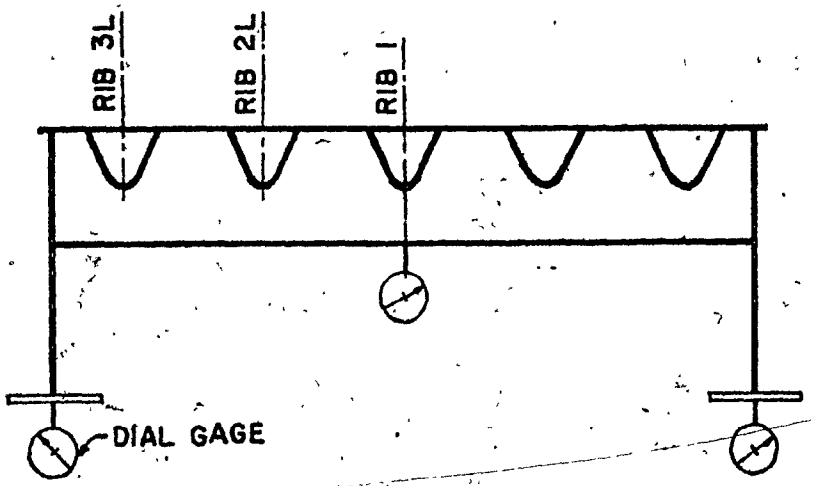

B. SECTION A-A

FIG. 5.4 -RIB MARKINGS AND LOCATIONS OF DIAL GAGES

Two 8" x 12" x 1/2" thick rubber pads, together with a steel plate of 8" x 12" x 3/4" thick on top, were used as a unit under each loading to distribute the load on an area of 8" x 12", simulating the action of a wheel load. The bottom pad had the necessary cut-outs to clear the strain gages on top of the deck. The loss of contact area of the pad with the deck plate was small.

The loads were applied to the deck by means of a hydraulic jack of 20 kips capacity, operated by a Structural Loading System of Gilmore type. The jack was fastened to a movable support block hung under the bottom flange of a cross-beam of the testing frame, Figure 5.5. The cross-beam, supported by the main beams, can be moved to any position along the frame, thus permitting the jack to be fixed at any desired location for loading. For a single load on the model, the bearing end of the jack was directly placed on the top of the pad. However, for two of the loads acting on a line parallel to the ribs, the jack was held against the top flange of a simply supported beam on the deck. The support actions of the beam provided the desired loading.

A Data Acquisition System for strain analysis was available to record all strains automatically on a magnetic tape at any instant of loading. All the strain gage leads were connected to the channels of this recorder. Figure 5.6 shows the Data Acquisition System and the Gilmore

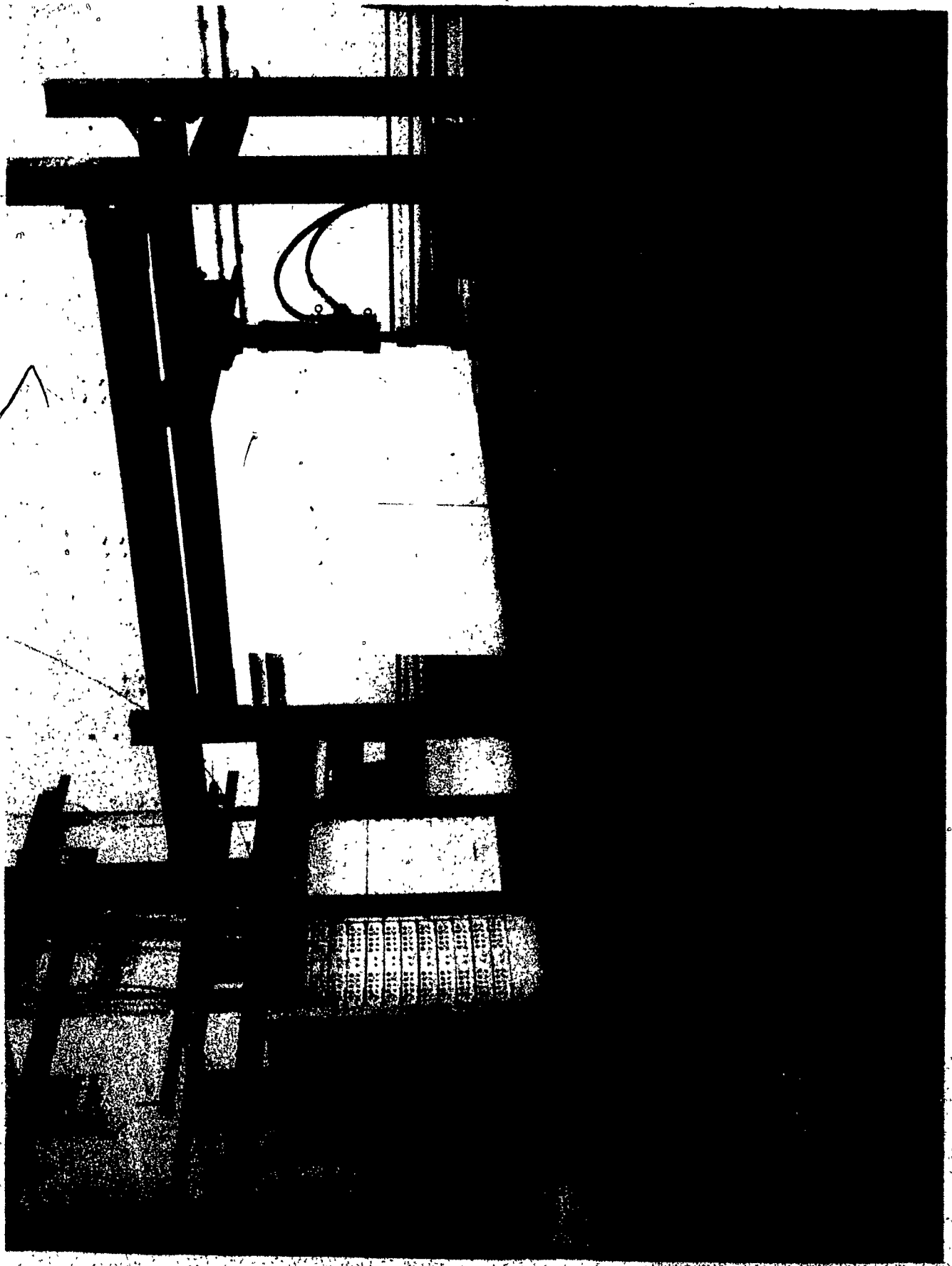

FIG. 5.5 – TESTING FRAME

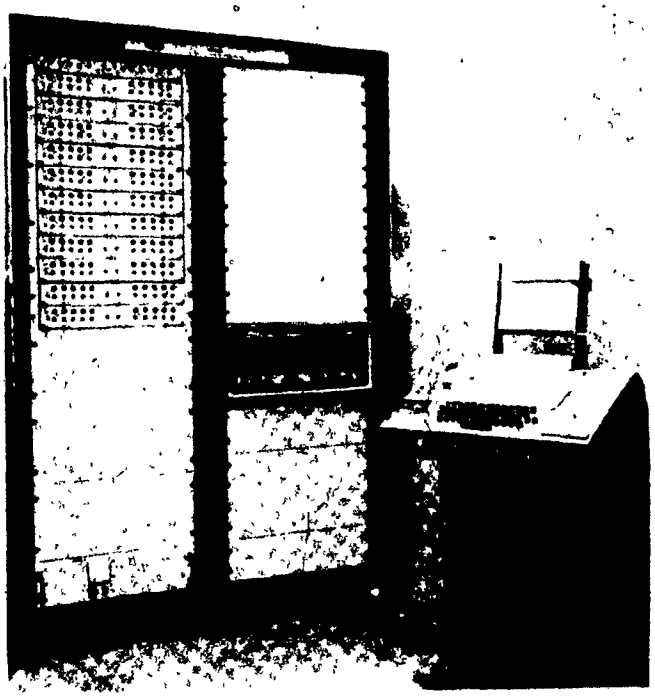

A. DATA ACQUISITION SYSTEM

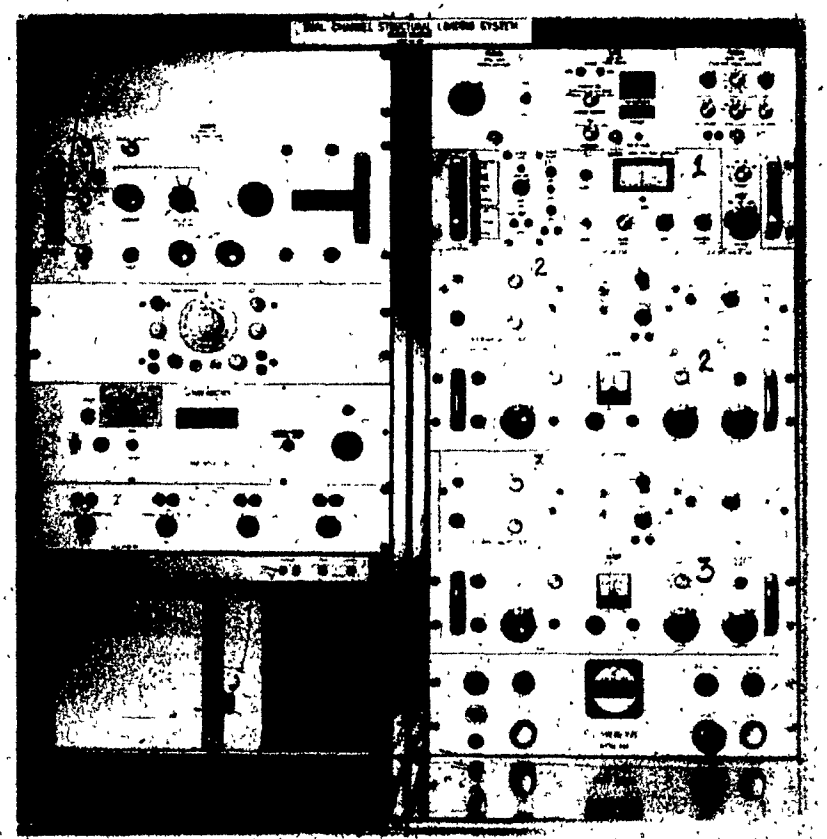

B. GILMORE STRUCTURAL LOADING SYSTEM

FIG. 5.6 - DATA ACQUISITION SYSTEM AND GILMORE STRUCTURAL LOADING SYSTEM

Structural Loading System used in the test. A model view and test set-up are shown in Figure 5.7.

5.5 EXPERIMENTAL PROCEDURE

Before any load was applied to the deck, all strain gage channels in the Data Acquisition System were set to indicate zero readings and the initial dial gage readings were taken. The jack was fixed to the right position and an initial load of 4 kips was applied slowly by operating the Gilmore Structural Loading System. With a brief pause to stabilize the whole system, all the strain gage and dial gage readings were recorded. The loading was then increased in steps of 2 kips, and in each case, measurements were taken. When the load reached the maximum value, as indicated in the "Test Sequence" for the particular load position, the jack was then moved to a new location and the whole procedure was repeated.

5.6 TEST SEQUENCE

The whole testing was performed in two phases. In the first phase, the girders were supported with additional intermediate supports to prevent them from an appreciable amount of bending under a load. Test data from this phase produced the results corresponding to the bending of the orthotropic deck alone. In the second phase of the testing, the girders were allowed to deflect freely between the end

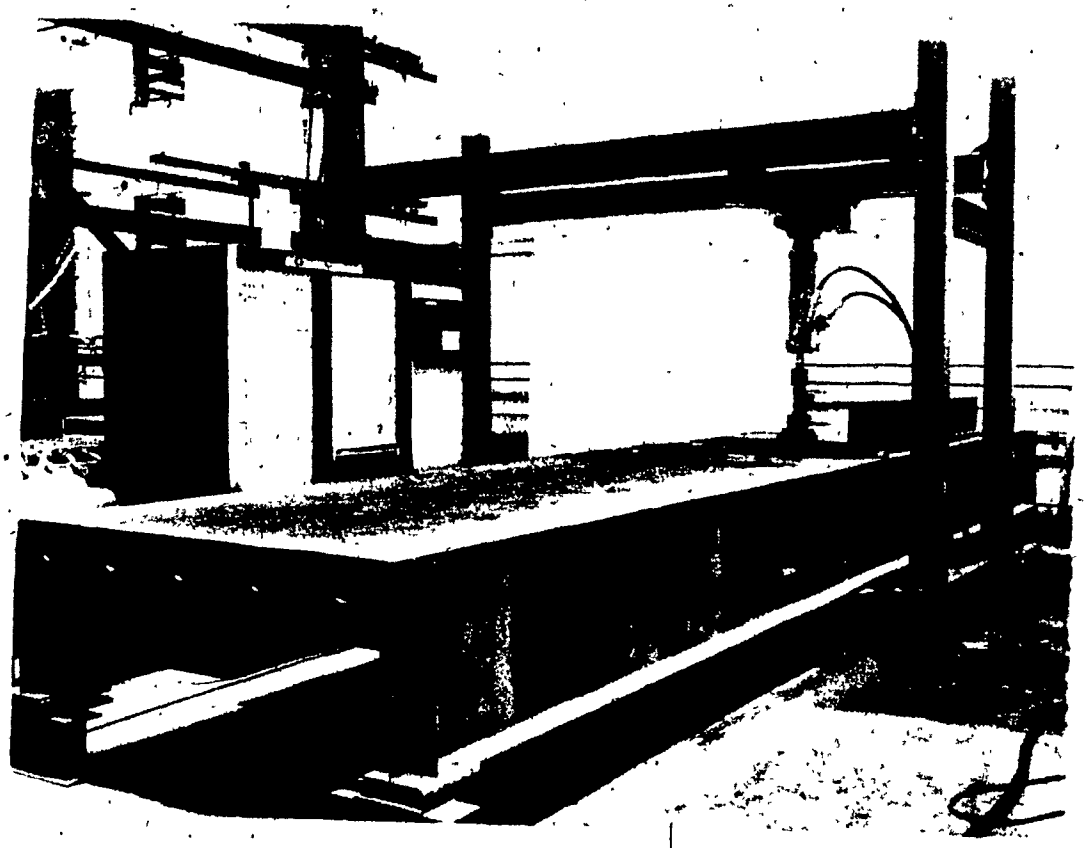

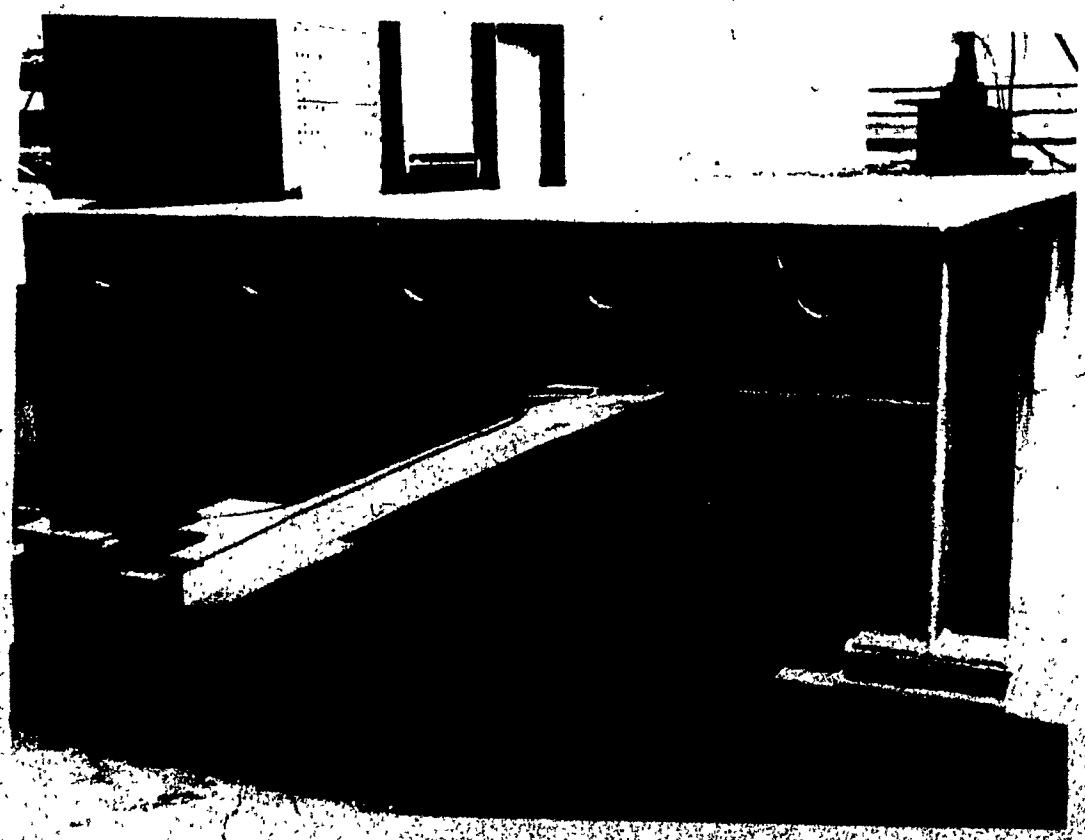

FIG. 5.7 - MODEL VIEW AND TEST SETUP

supports under the application of a load. This case corresponded to an actual bridge behaviour, where the girders and the deck are subjected to a combined bending.

For both phases of the testing, three general loading cases were used: loading case A corresponded to a single load and loading cases B and C were comprised of two loads. Figure 5.8 shows the loading cases and their positions on the deck.

All the five ribs were loaded in sequence, starting from one side and moving the load on the deck across the width, as indicated in Figure 5.9. For each position of a loading case, the load W in Figure 5.8, applied by the hydraulic jack, was increased in steps of 2 kips, starting with an initial value of 4 kips. The maximum magnitude was 10 kips, when Ribs 1, 2R and 2 L were loaded. However, for Ribs 3L and 3R, the maximum magnitude of W was increased to 12 kips. For all loading cases, the strains and deflections were recorded.

5.7 TEST MEASUREMENTS

All experimental data were recorded, following the test sequence and procedure, as stipulated earlier. In the first phase of the test, when the girders were held against the deflection, all the test data corresponded to the bending of the orthotropic deck, alone.

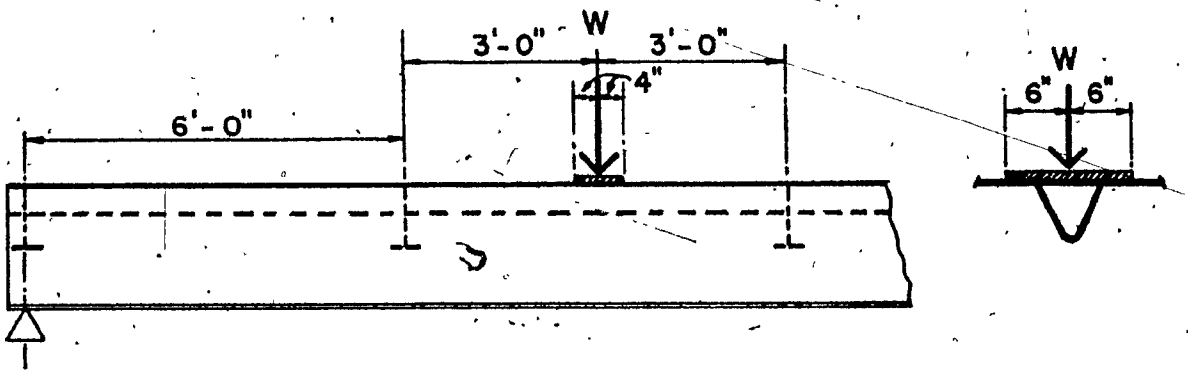

A. LOADING CASE A

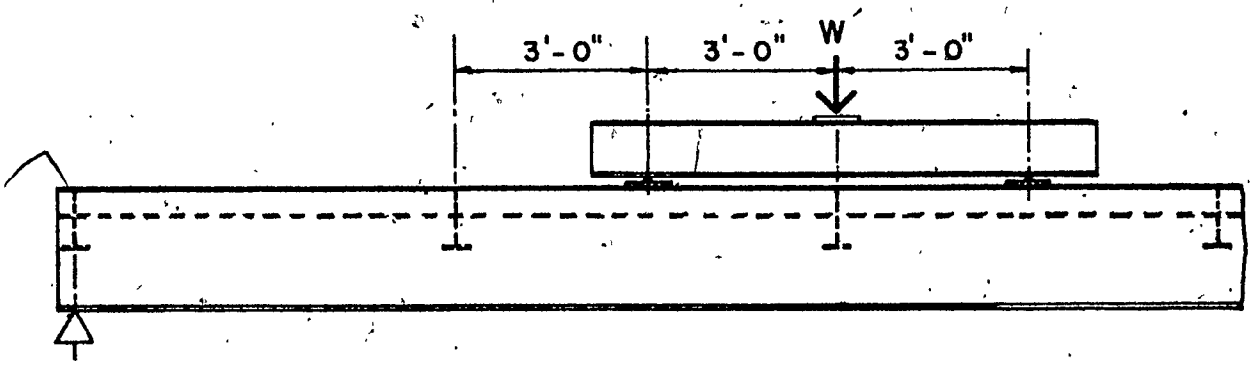

B. LOADING CASE B

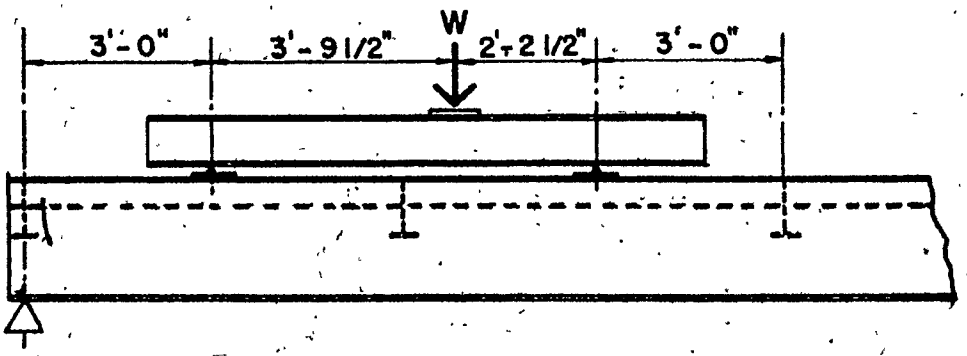

C. LOADING CASE C

FIG. 5.8 - LOADING CASES AND THEIR LOCATIONS ON DECK

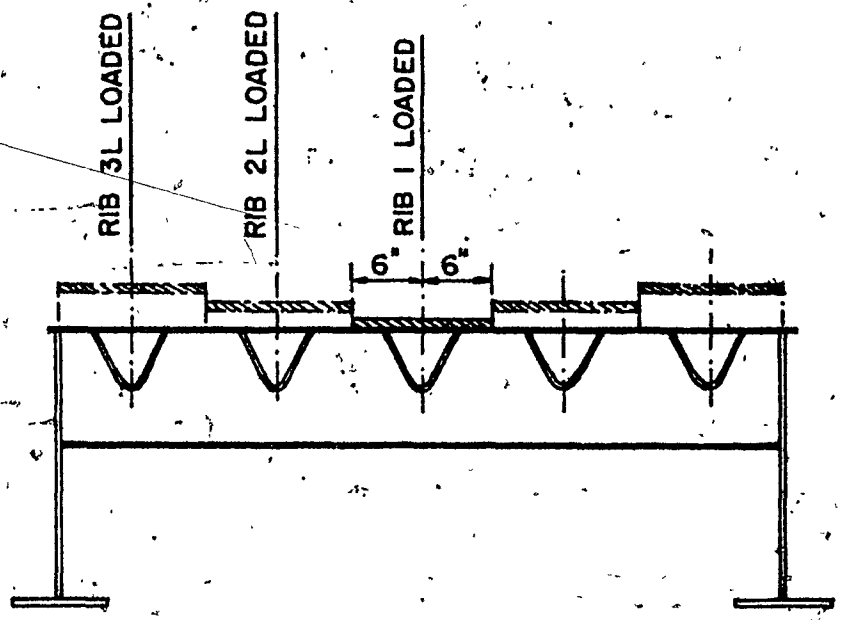

FIG. 5.9 - LOADING POSITIONS ACROSS THE WIDTH OF DECK

In the second phase of the test, when the girders were simply supported at their ends, the strains measured corresponded to the combined bending of the girder and the orthotropic deck. The rib deflections obtained would give the total deflection of the rib and the girders. Thus, the difference in the values obtained in the two phases of testing, would present the effect of the girder bending.

For each loading, the Data Acquisition System recorded three sets of readings. The average of these readings, which was usually close, was accepted as the final measured strain for the loading. In order to verify the experimental procedure and consistency of the strain gage readings, some of the loading cases were repeated. The two sets of readings corresponding to the same loading agreed closely, thus indicating the test measurements were satisfactory. The strains were converted to stresses applying Hooke's law with the modulus of elasticity and Poisson's ratio, as being equal to 29,000 ksi, and 0.30, respectively.

The dial gage readings indicating the measured deflections were also recorded for all loading cases. With a concentric loading on the deck, the similar readings registered by the dial gages fixed underneath the girders indicated an equal share of the load carried by the girders. However, under an eccentric load on the deck, these dial gage readings were different, as expected, and the measured values could be used

to predict the possible magnitude of the load carried by each girder.

CHAPTER 6

TEST RESULTS AND DISCUSSION

6.1 INTRODUCTION

Test data obtained in this experiment and the results from the theoretical analyses of the model are presented in Figures 6.1-6.24, of which Figures 6.1-6.20 are related to stresses and strains at various locations on the model and the remaining figures to the load-deflection behaviour. For a better presentation, the results, together with their discussion and interpretation are grouped into separate headings of

(i) Stress and strain

(ii) Deflection.

6.2 STRESS AND STRAIN

The two sets of results corresponding to the two phases of experiment are presented separately under each phase to distinctly identify the structural actions and the deck behaviour.

6.2.1 First Phase of Test

The test results obtained from this phase of the experiment in which girders were held against bending, represented the values of deck bending and thus, were compared

directly with the analytical solutions. The theoretical values obtained were based on the assumption that the deck was simply supported longitudinally along the main girder supports. The support conditions were approximately satisfied in this test by having the main girders of the open type with relatively small torsional rigidity.

Figures 6.1-6.5 show the measured and calculated longitudinal stresses at locations 1, 6 and 11, on the top of the deck plate and at the bottom of Rib 1, at Sections P, Q and R, when Rib 1 was subjected to loading cases A, B and C. An examination of plots indicates that the experimental stresses were almost linear with loads in the range considered and those at the bottom of the rib agreed closely with the theoretical values obtained from both the proposed refined analysis and the design method of Pelikan-Esslinger (P-E method). The latter values at the bottom of the rib were, however, the largest of all in magnitude. It was also observed by both measurements and analyses that the stresses in the deck at Section P, due to the loading case A, were almost similar to those due to the loading case B. In general, the stresses at the bottom of the rib indicated by the proposed method were found to be higher, in the order of 4-10% than those measured. In comparison with this, those from Pelikan-Esslinger's method were 6-20% higher.

Regarding the stresses at the top of the deck plate, those measured at locations 6 and 11 (midspans of the rib)

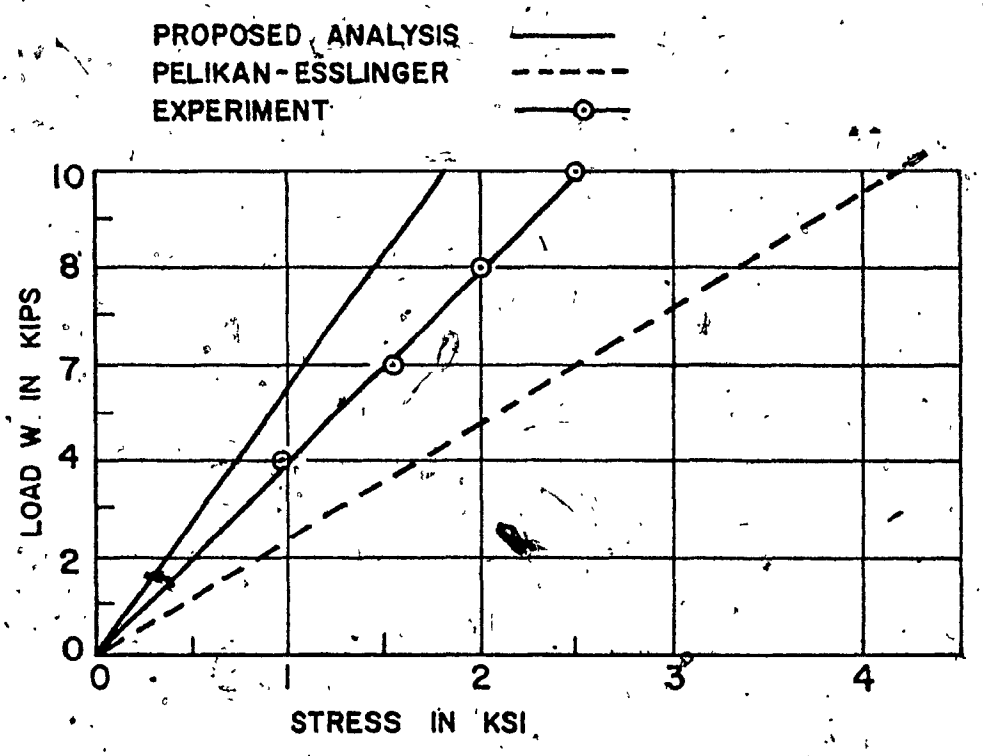

A. AT TOP OF PLATE - LOCATION I

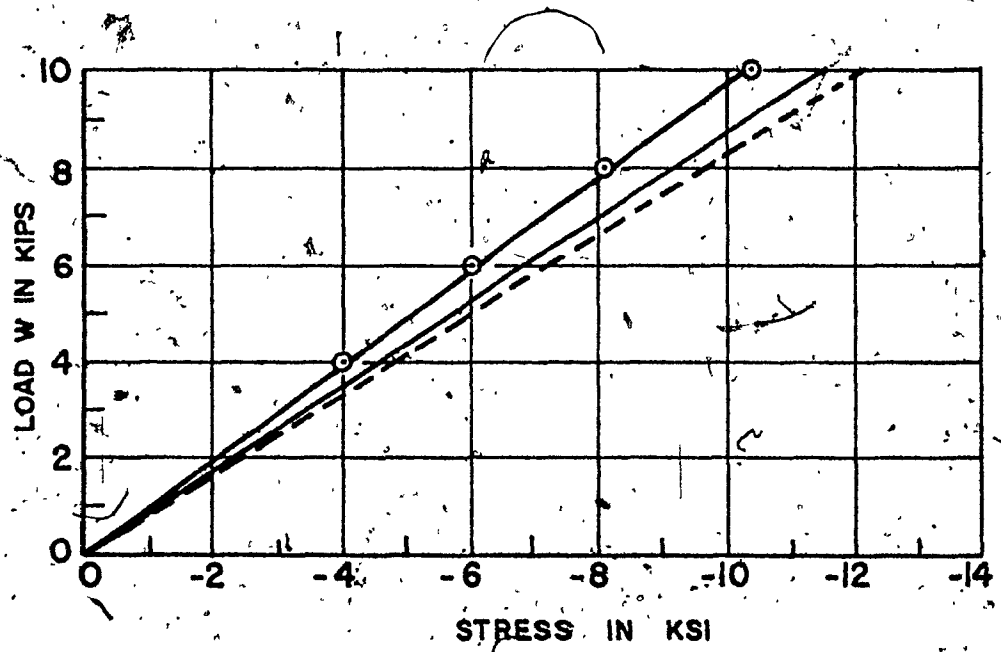

B. AT BOTTOM OF RIB

FIG. 6.1 - LONGITUDINAL STRESSES AT TOP AND BOTTOM OF RIB I AT SECTION P WITH RIB I LOADED (LOADING CASE A)

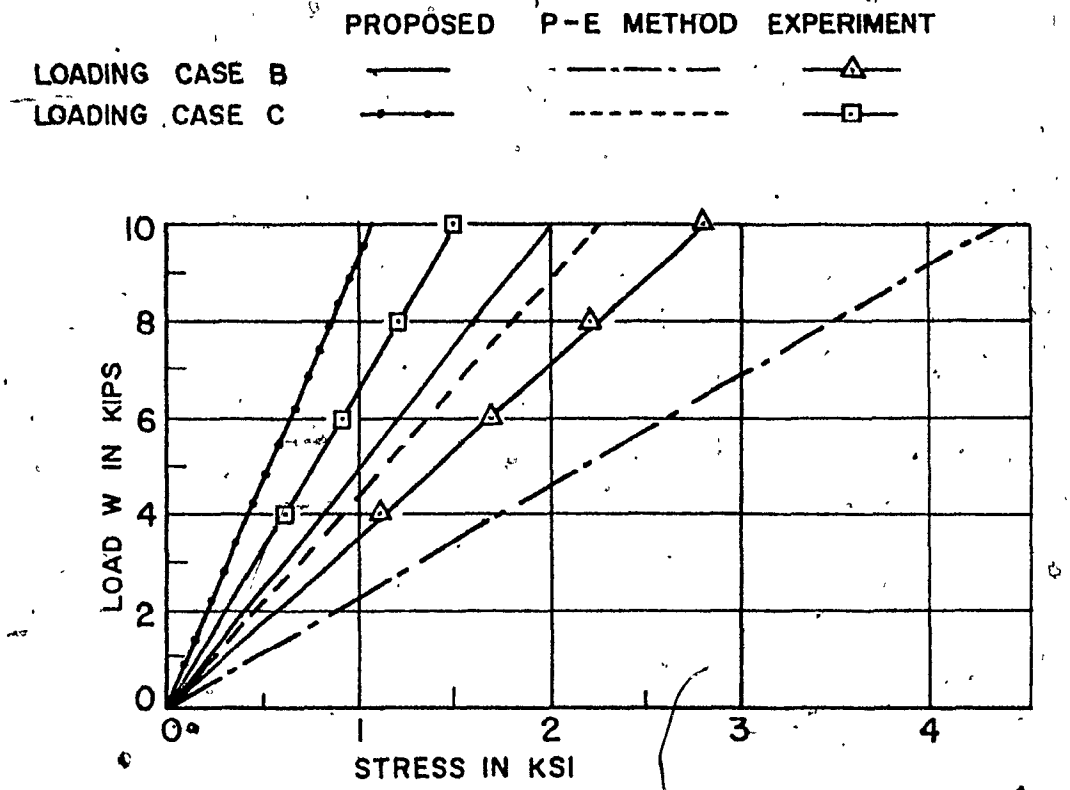

A. AT TOP OF PLATE - LOCATION 1

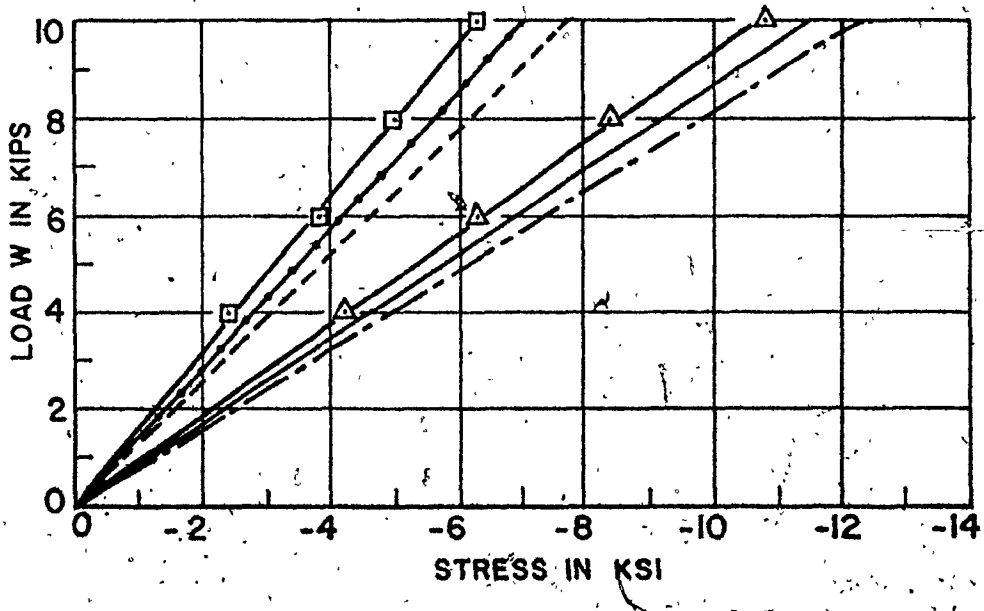

B. AT BOTTOM OF RIB

FIG. 6.2 - LONGITUDINAL STRESSES AT TOP AND BOTTOM OF RIB 1 AT SECTION P WITH RIB 1 LOADED (LOADING CASES B & C).

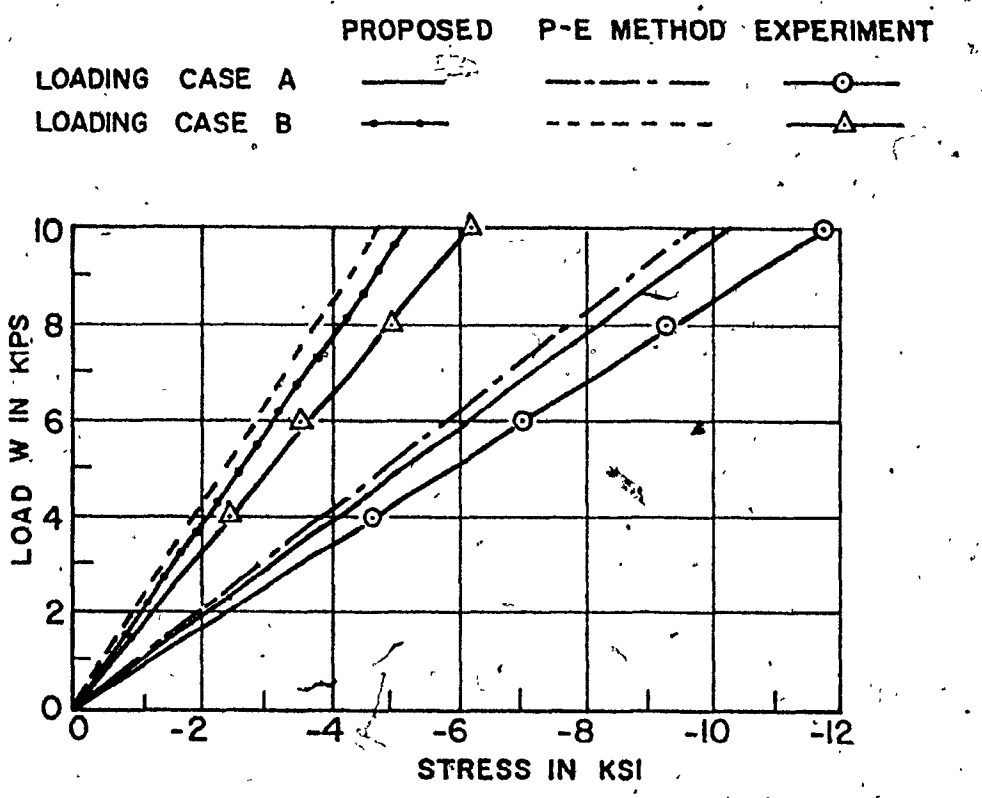

A. AT TOP OF PLATE - LOCATION 6

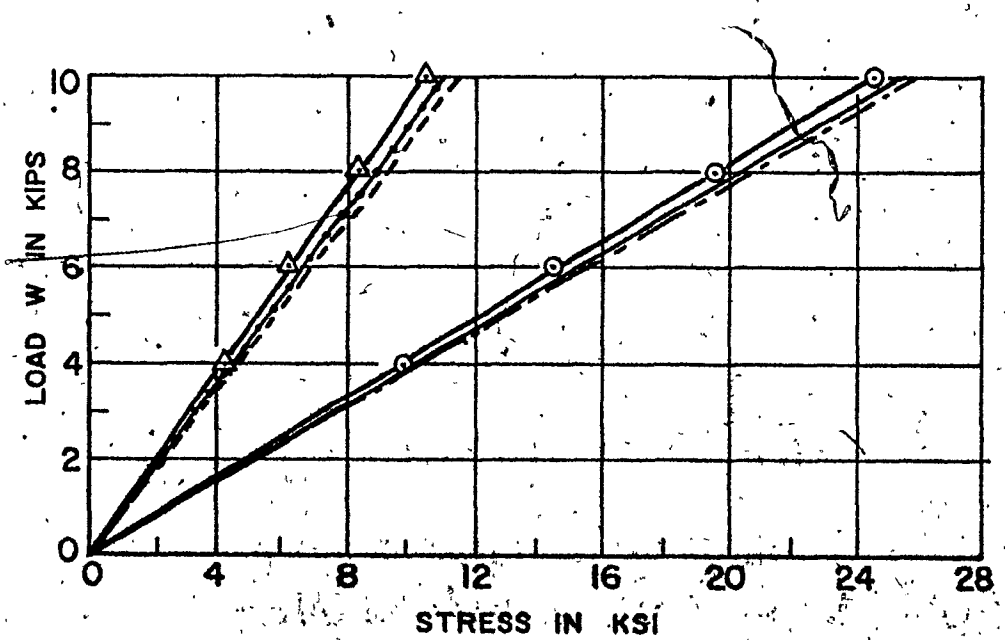

B. AT BOTTOM OF RIB

FIG. 6.3 - LONGITUDINAL STRESSES AT TOP AND BOTTOM OF RIB I AT SECTION Q WITH RIB I LOADED (LOADING CASES A & B)

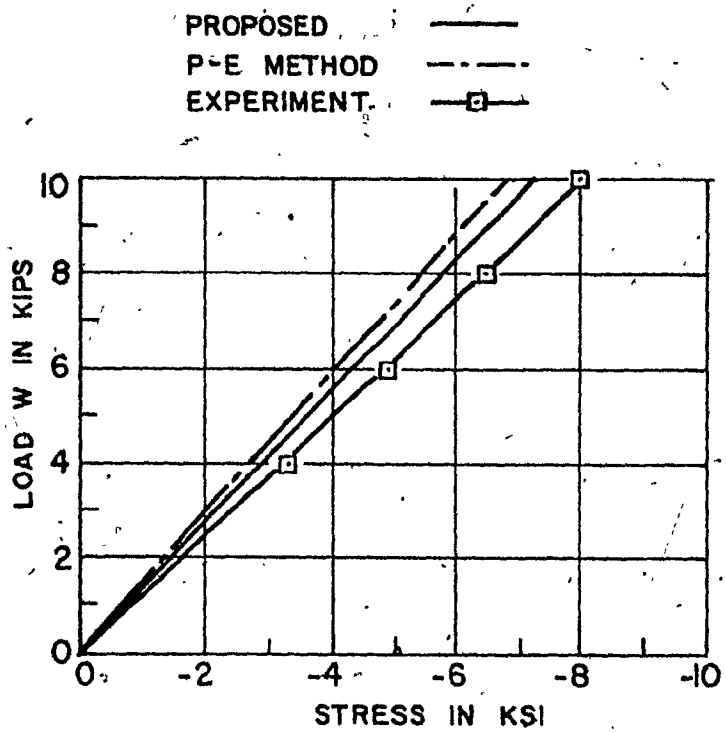

A AT TOP OF PLATE – LOCATION 6

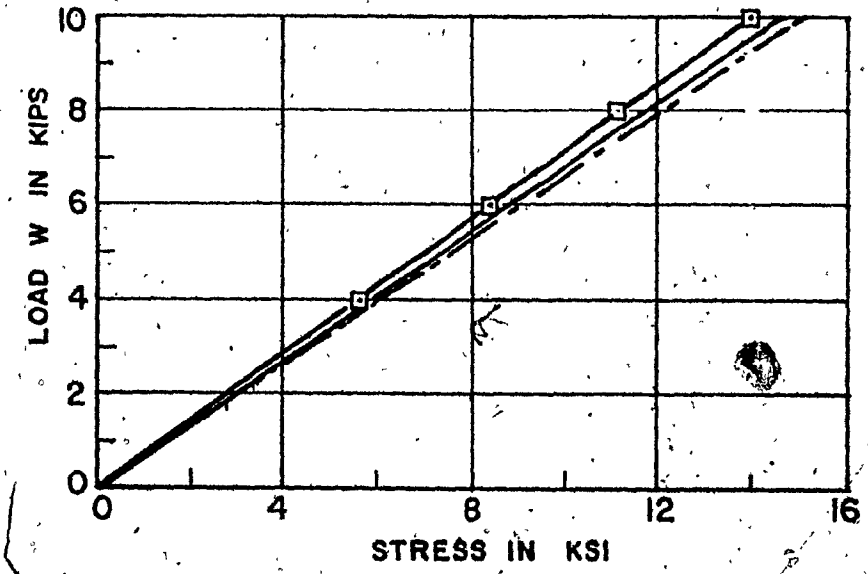

B. AT BOTTOM OF RIB

FIG. 6.4 - LONGITUDINAL STRESSES AT TOP AND BOTTOM OF RIB I AT SECTION Q WITH RIB I LOADED (LOADING CASE C)

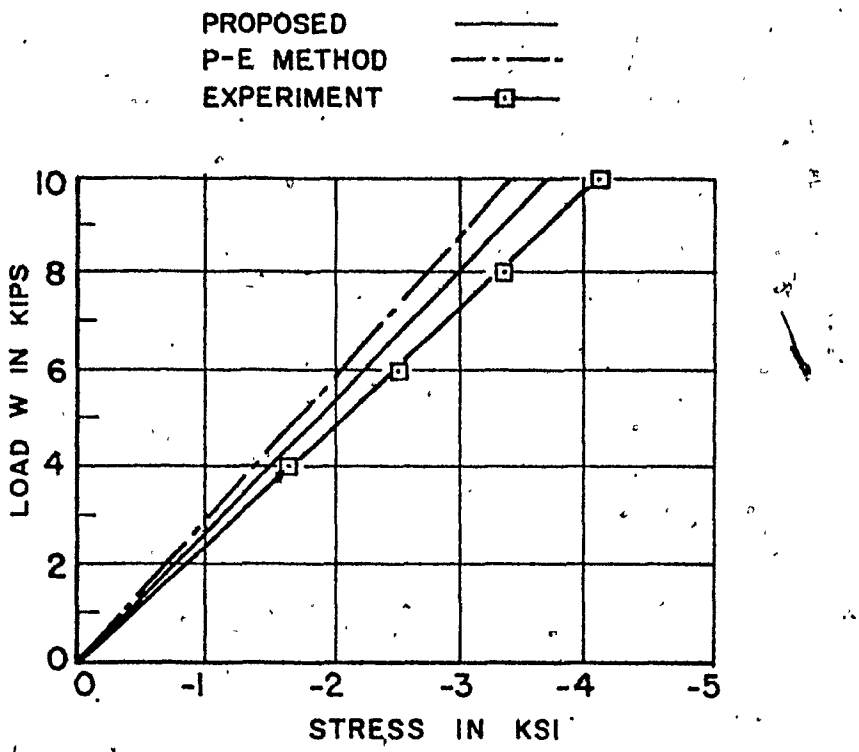

A. AT TOP OF PLATE - LOCATION II

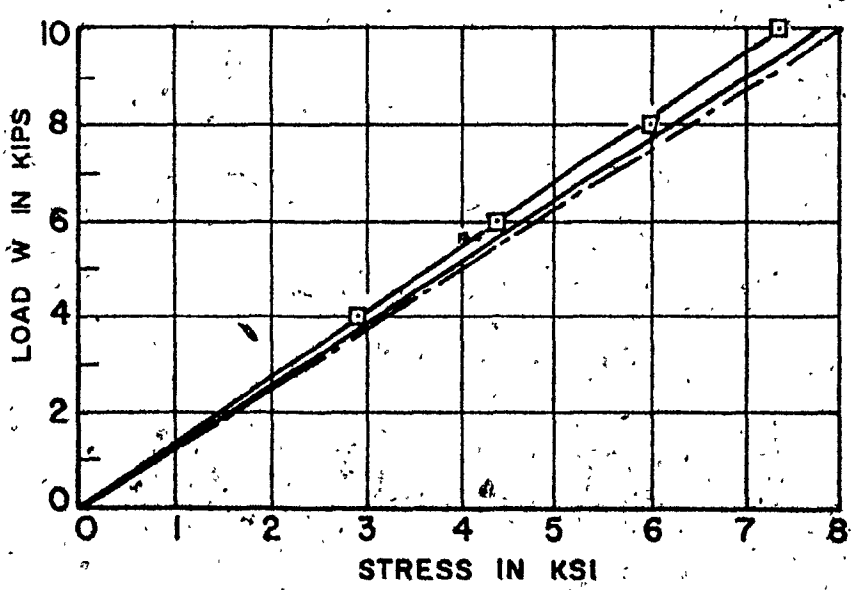

B. AT BOTTOM OF RIB

FIG. 6.5 - LONGITUDINAL STRESSES AT TOP AND BOTTOM OF RIB I AT SECTION R WITH RIB I LOADED (LOADING CASE C)

were in good agreement, being slightly higher in magnitude than those given by both analytical methods. On a percentage basis, the measured stresses were about 11% higher than those given by the proposed method, compared with about 20% higher than those indicated by Pelikan-Esslinger's method. However, at location 1, which was close to the floor beam, the discrepancy between the analytical and experimental results was relatively larger. While the design method indicated stresses about 55% more than those obtained experimentally, the results from the proposed analysis were, in general, 40% lower than those measured. It should be emphasized that the stress magnitudes at location 1 were relatively small for a good comparison and, therefore, the percentage-wise deviations are not too significant. In obtaining the solutions by the analytical methods, the required moment of inertia of the floor beam was calculated, taking into consideration an effective width of the deck plate as a flange of the floor beam, in accordance with References (6) and (7).

Figure 6.6 shows the load versus the longitudinal strains at the top of the deck plate, and at the bottom of Rib 1 at Sections P and Q, when the rib was subjected to loading Cases A and B. The plots again show that a favourable comparison exists between the measured strains and the analytical values from the proposed analysis. The relative magnitudes of the strains at the top of the deck and the bottom of the rib quickly indicated that the neutral axis of the loaded

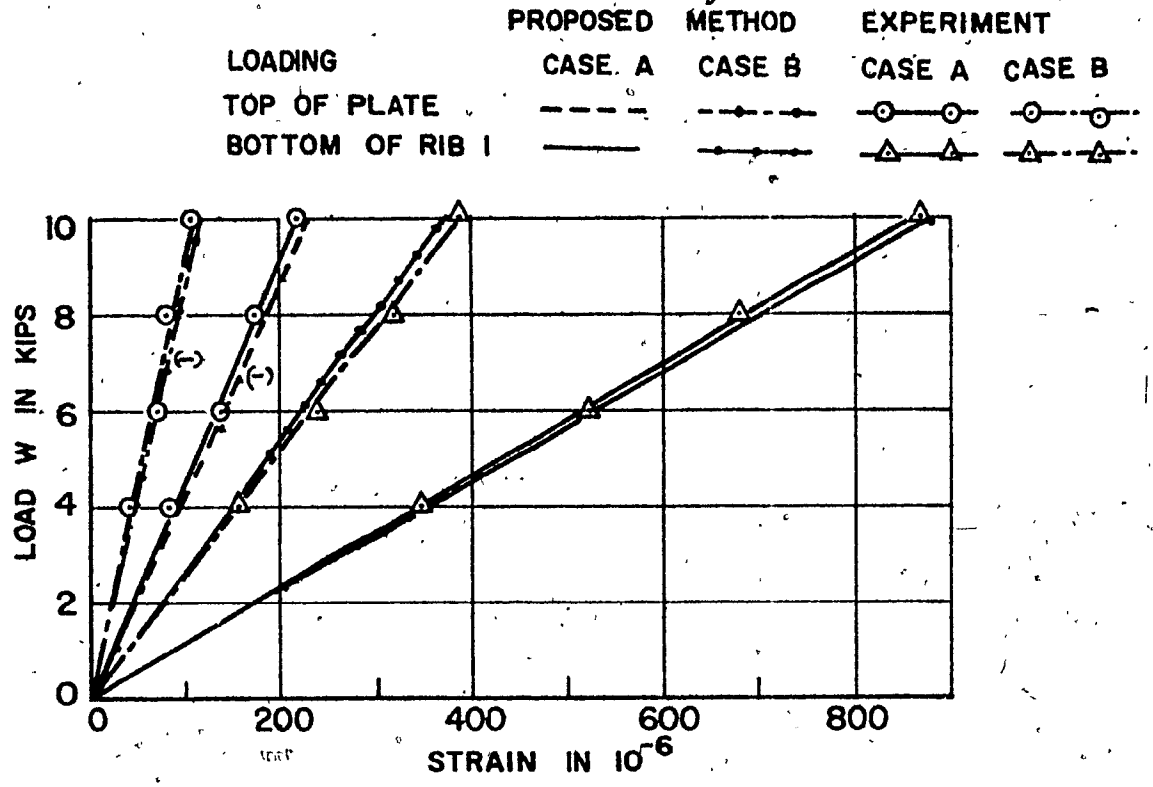

A. AT SECTION Q

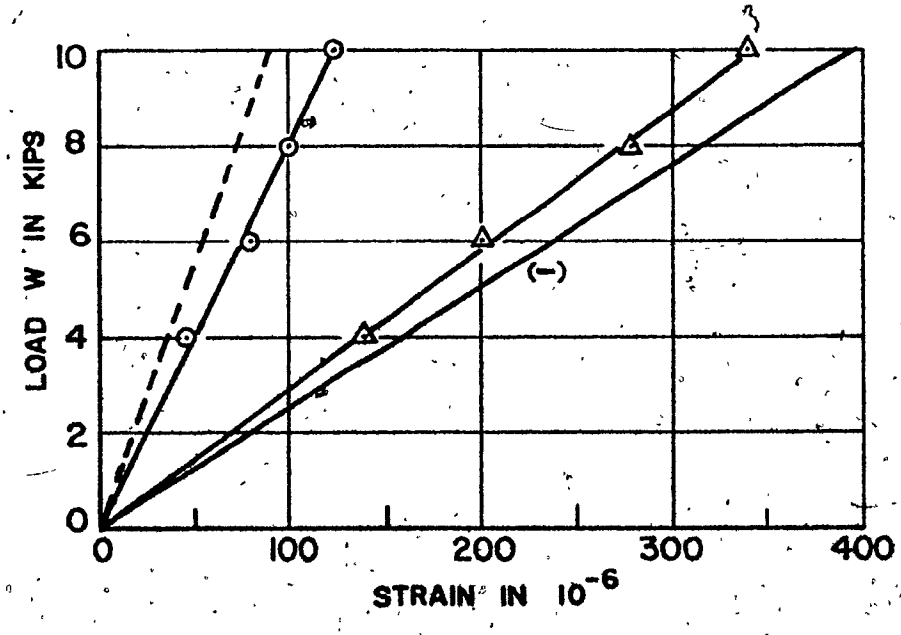

B. AT SECTION P

FIG. 6.6 - LONGITUDINAL STRAINS AT TOP AND BOTTOM OF RIB 1 WITH RIB 1 LOADED

rib was close to the deck plate, as expected. As seen from Figure 6.6, the analytical strains in the longitudinal direction, obtained from the proposed method of analysis, were in better agreement with the measured strains than were the respective stresses.

The longitudinal strain distribution along the depth of loaded Rib 1 is indicated in Figure 6.7, at Sections P and Q, due to the loading Case A, with W = 10 kips. The measured strains corresponded approximately to a linear distribution. The depth of the neutral axis, as indicated by the measured strains varied slightly at Sections P and Q, and were located approximately 1/5 of the overall depth of the rib from the top of the deck plate. The theoretical neutral axis found from Pelikan-Esslinger's method was at a distance of 1.37 in. from the top of the plate.

With Rib 1 being loaded, the values of the longitudinal stress measured at the top and bottom of Rib 2L, are shown in Figure 6.8. For the same loading, the measured stress at the bottom of Rib 3L was negligible. From the relative magnitudes of the rib stresses, it was observed that the major portion of the applied load was carried directly by the loaded rib. The participation of the adjacent ribs in the carrying loads decreased rapidly with the increase in transverse distance from the loaded rib.

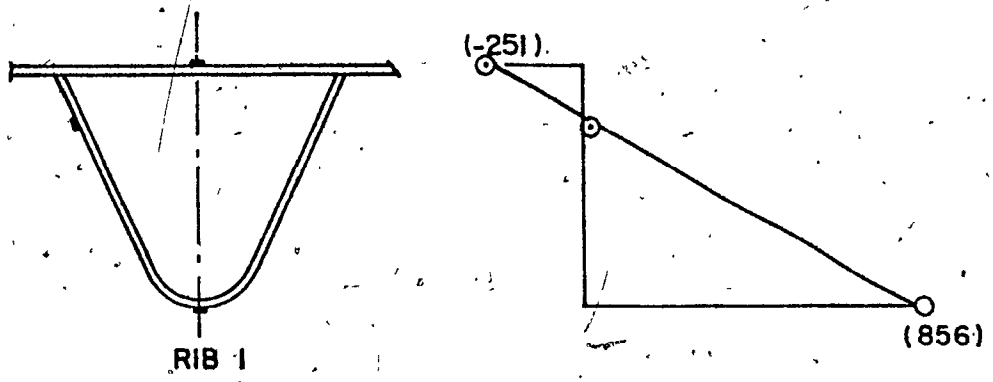

A. AT SECTION Q

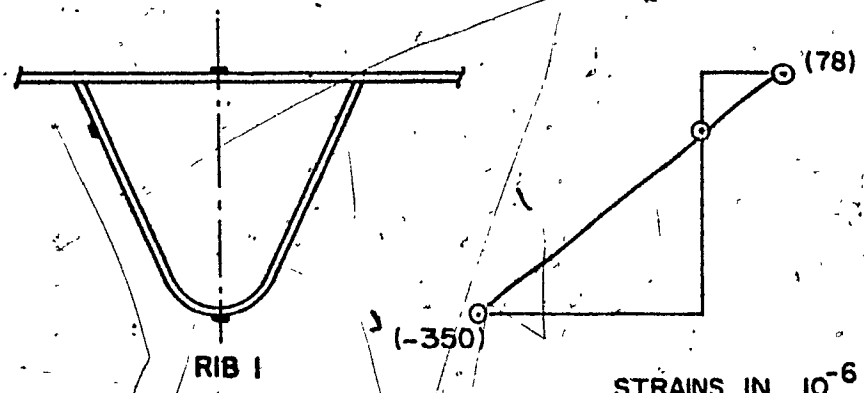

STRAINS IN 10^{-6}

B. AT SECTION P

FIG. 6.7 - MEASURED LONGITUDINAL STRAINS AND NEUTRAL AXES FOR RIB 1 WHEN SUBJECTED TO LOADING CASE A

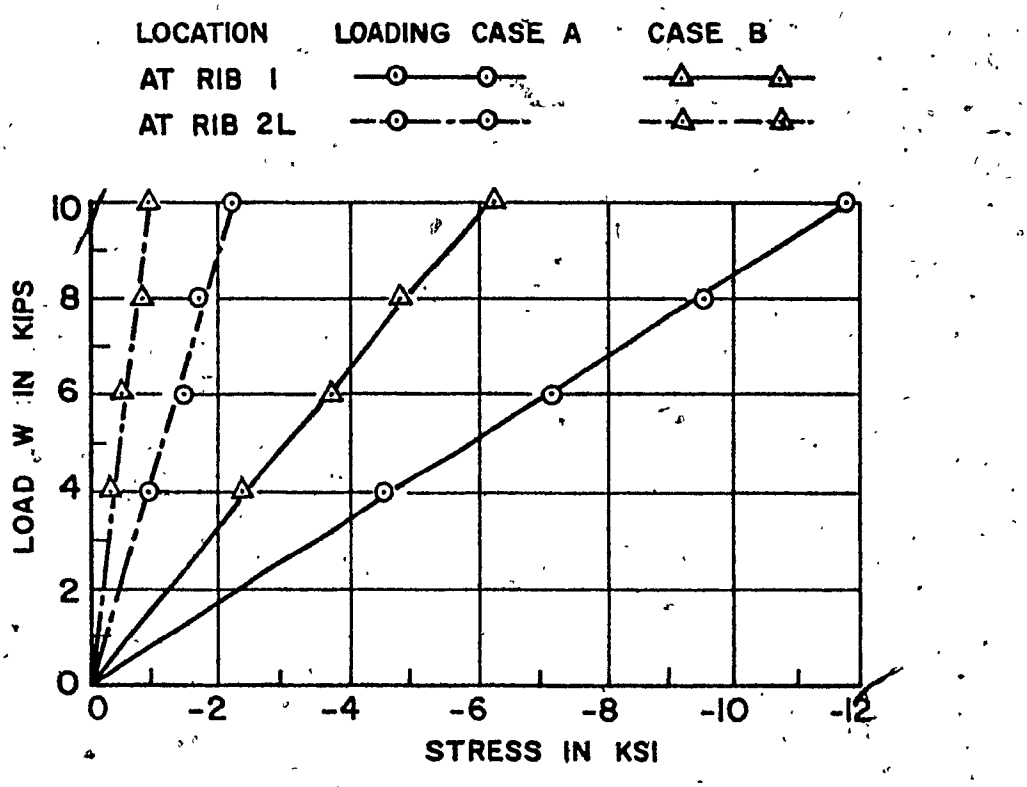

A. AT TOP OF PLATE

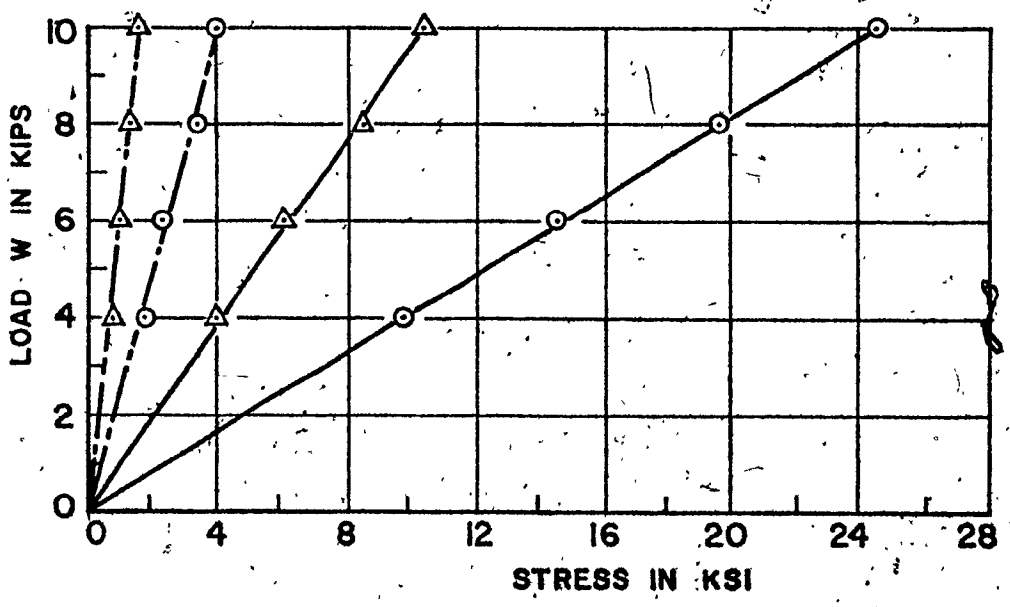

B. AT BOTTOM OF RIB

FIG. 6.8 - MEASURED LONGITUDINAL STRESS IN DECK DUE TO DECK BENDING AT SECTION Q WITH RIB 1 LOADED

The above conclusion was further confirmed by the test results presented in Figure 6.9, where the longitudinal stresses are plotted at the top and bottom of Ribs 1, 2L and 3L, when Rib 2L was subjected to the loading cases A and B. With the change of the load position from Rib 1 to Rib 2L, the stresses at the bottom of Rib 1 were reduced to about 1/5 of the previous values, and those at the bottom of Rib 2L were increased to almost 6 times. The substantial drop of stress at Rib 1 and almost an equal increase of stress at Rib 2L from the values when Rib 1 was loaded confirmed the previous observation that the directly loaded rib contributed greatly to the load carrying action and was subjected to the highest stress in the deck.

Figure 6.10 shows the transverse stress in the deck plate at locations 1 and 6, when Rib 1 was loaded. The magnitude of the measured transverse stress under the loaded area was rather high and even greater than that predicted by the proposed analysis. The significant transverse stress indicated the plate action of the deck in the transverse direction.

The plots of measured and calculated longitudinal stresses across the width of the deck plate at Sections P and Q are shown in Figure 6.11, with the load acting at Rib 1. It demonstrates that the deck plate stress is not uniform over the "effective width of the plate," acting with the loaded rib as assumed in the design method,

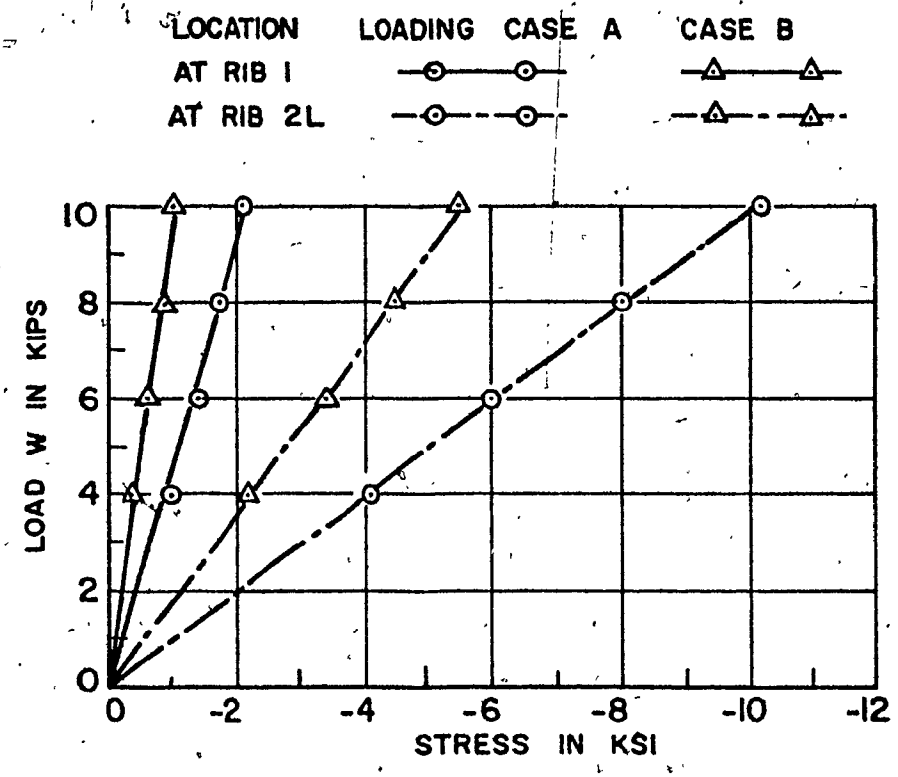

A. AT TOP OF PLATE

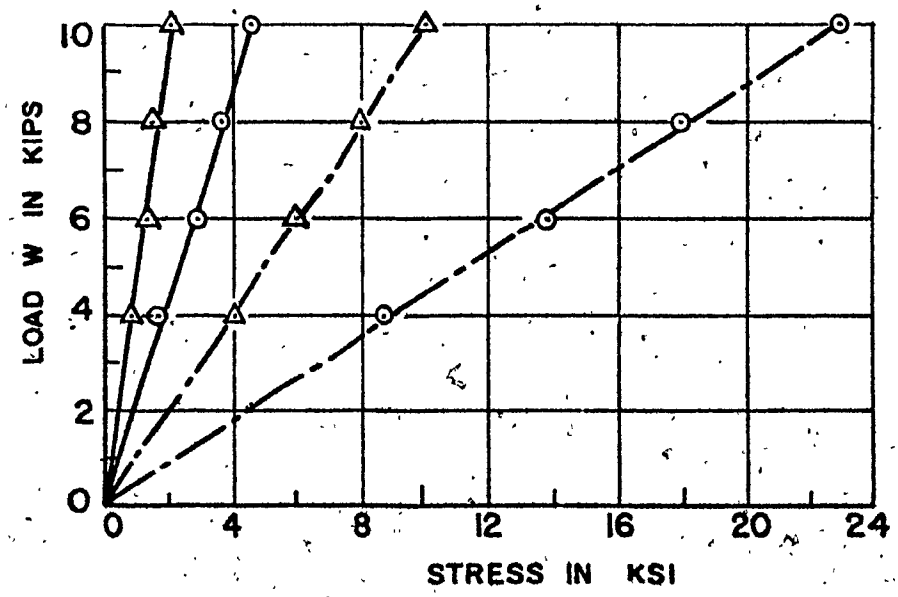

B. AT BOTTOM OF RIB

FIG. 6.9 - MEASURED LONGITUDINAL STRESS IN DECK DUE TO DECK BENDING AT SECTION Q WITH RIB 2L LOADED

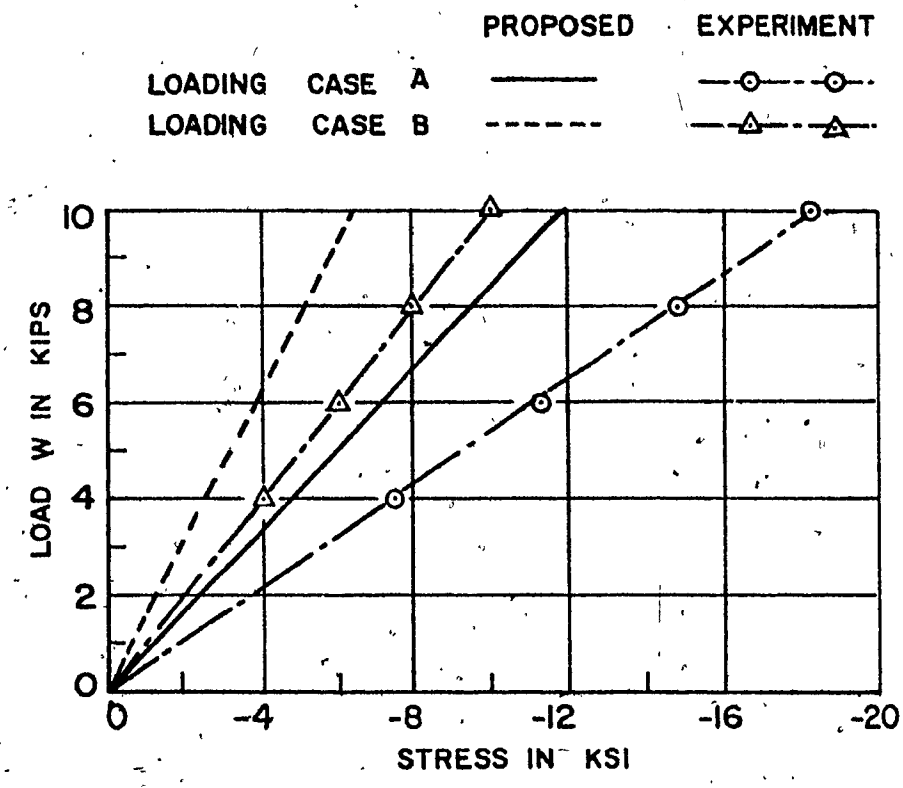

A. AT LOCATION 6

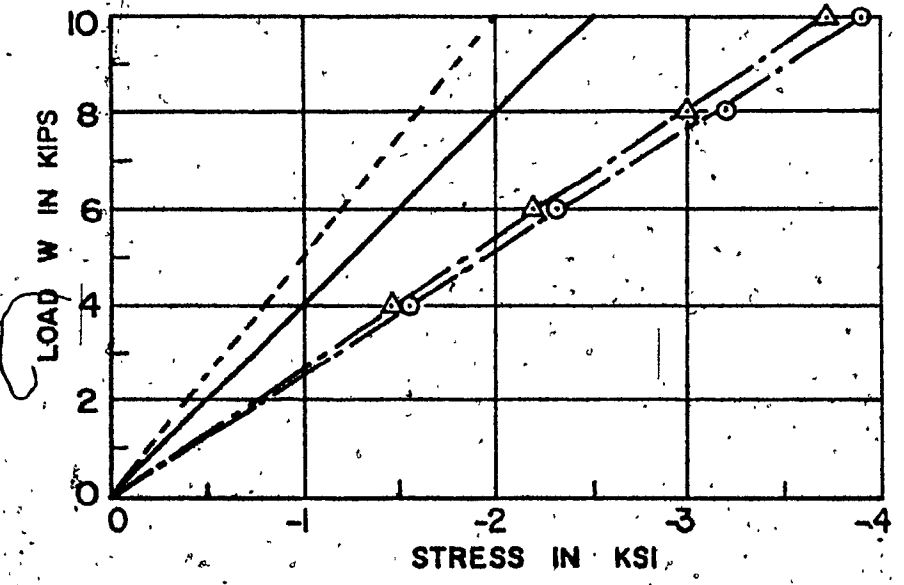

B. AT LOCATION 1

FIG. 6.10 - TRANSVERSE STRESS IN PLATE WITH RIB 1 LOADED

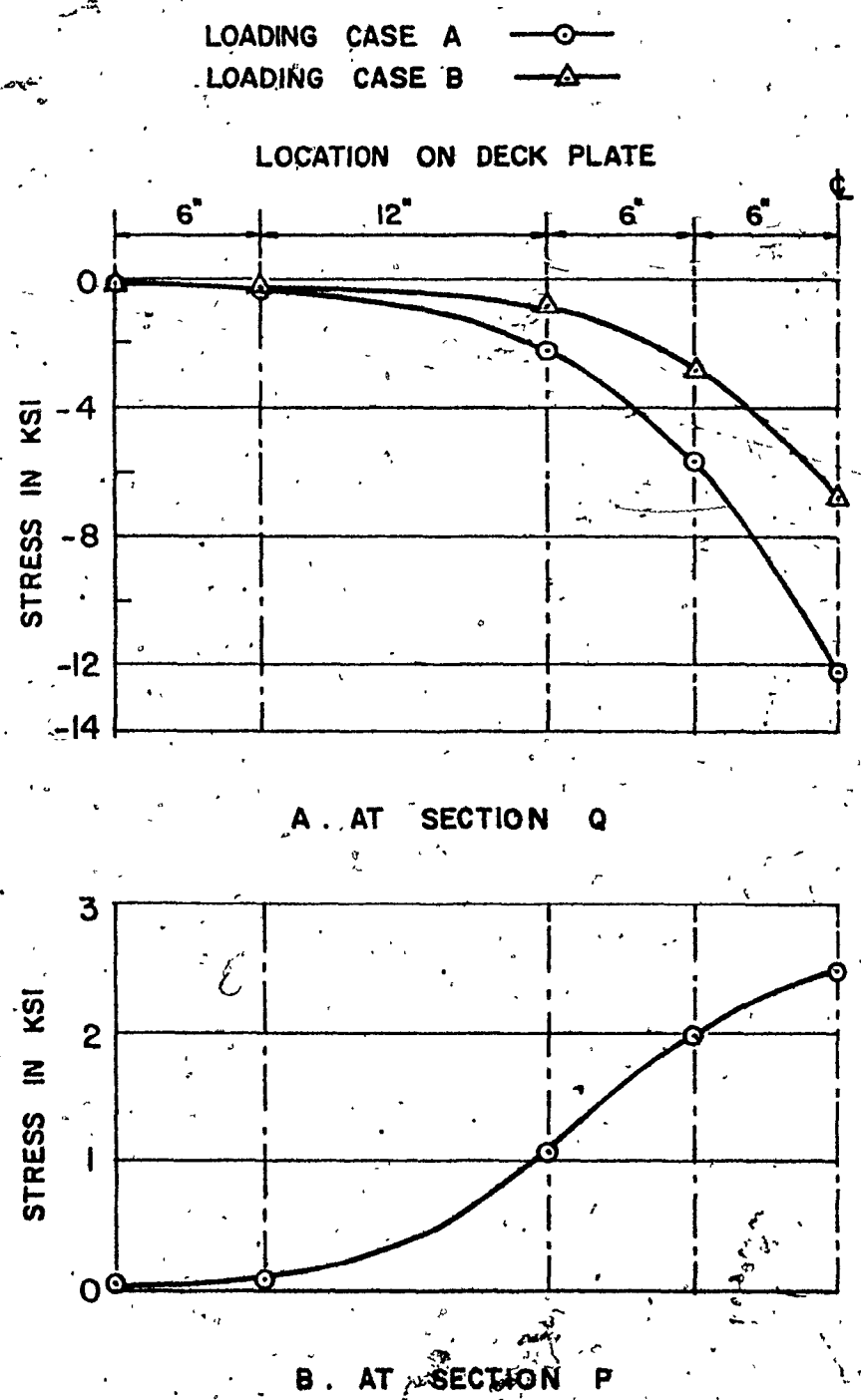

FIG. 6.11 - MEASURED LONGITUDINAL STRESS ACROSS THE WIDTH OF DECK PLATE WITH RIB I LOADED

References (6) and (7). The longitudinal stress in the deck plate was maximum at the location of the applied loading.

6.2.2. Second Phase of Test

Measured stresses in the deck due to the combined bending of the orthotropic deck and the girders, as obtained from this part of the test, are shown in Figures 6.12, 6.13 and 6.14 when Rib 1 is loaded. For theoretical values, it was necessary to calculate the additional stresses in the deck due to girder bending. This was accomplished in the following manner. The bending moment in the girder was computed, assuming that the applied load was transferred to the floor beams by ribs in a manner analogous to a continuous beam on several supports; the applied load, in turn, was transmitted to the main girders by the floor beams acting as simple beams. The section modulii of the girder were computed, considering the half-width of the deck to be effective as the top flange. The theoretical values obtained in this manner are shown in Figures 6.12-6.14 and appear to compare favourably with the measured stresses. It can be concluded from this comparison that the assumed load distribution was satisfactory for practical purposes.

To verify the above conclusion more meaningfully, an attempt was made to find the experimental stress distribution across the width of the deck at Sections P and Q, due to

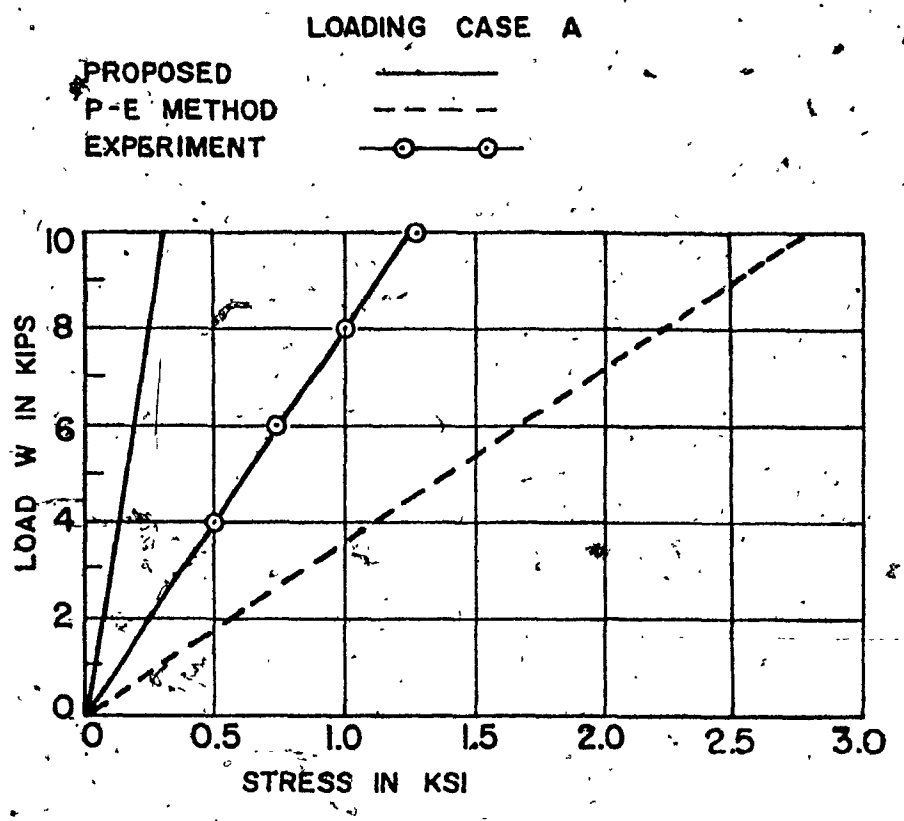

A . AT TOP OF PLATE - LOCATION 1

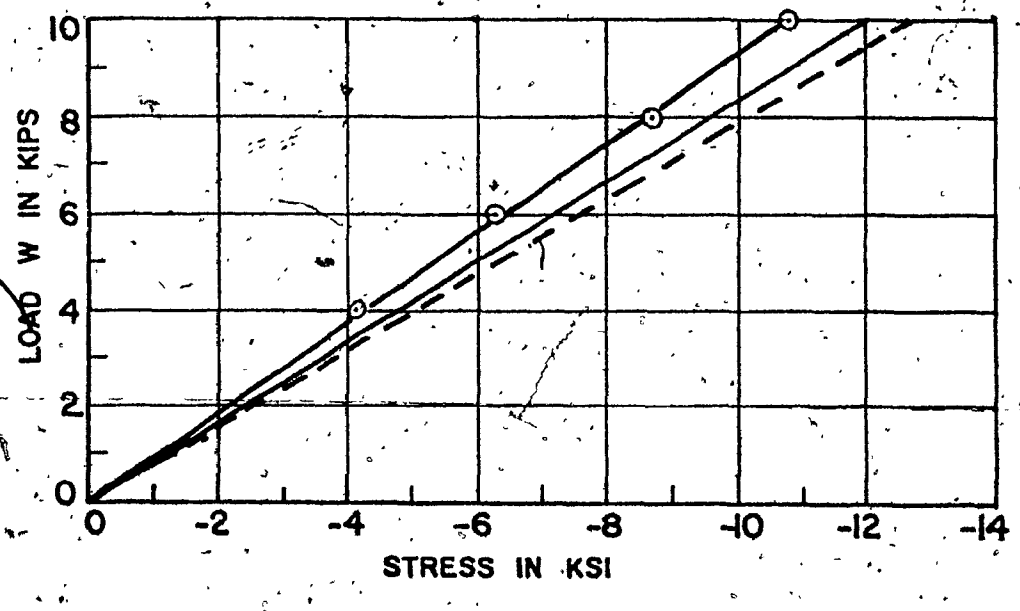

B . AT BOTTOM OF RIB

FIG. 6.12 - LONGITUDINAL STRESSES AT TOP AND BOTTOM OF RIB 1 DUE TO COMBINED BENDING AT SECTION P WITH RIB 1 LOADED

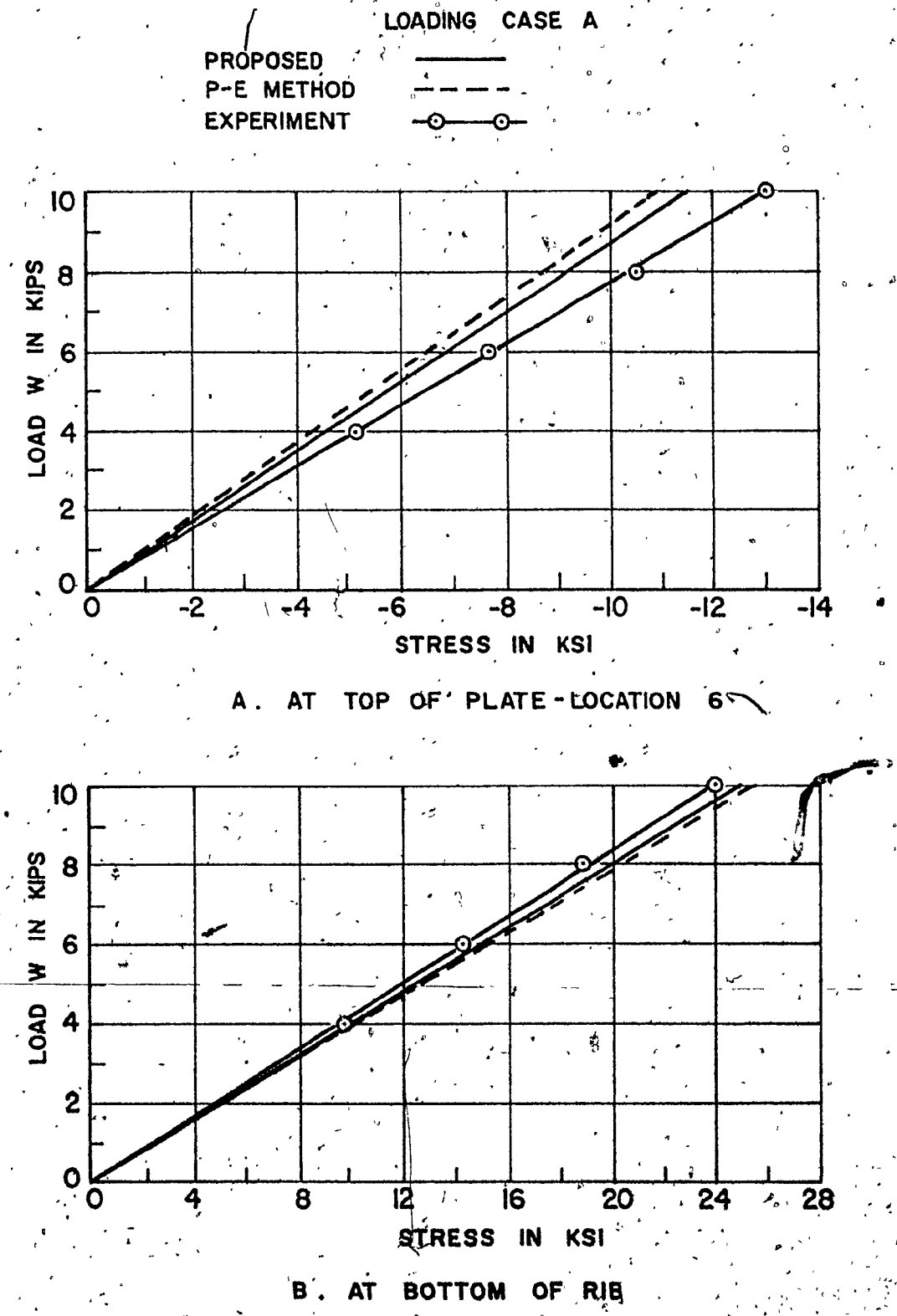

FIG. 6.13 - LONGITUDINAL STRESSES AT TOP AND BOTTOM OF RIB 1 DUE TO COMBINED BENDING AT SECTION Q WITH RIB 1 LOADED

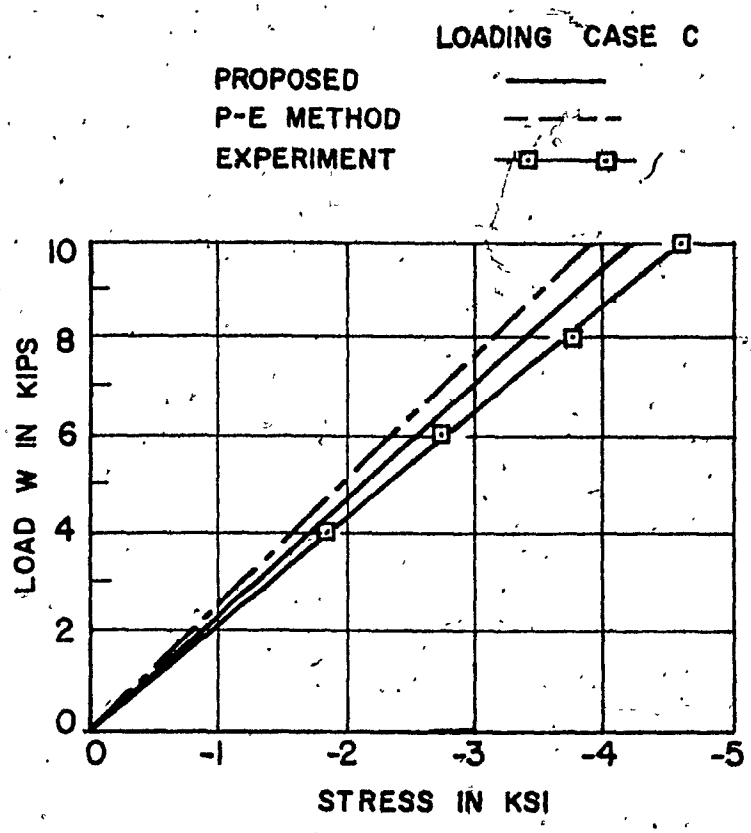

A . AT TOP OF PLATE - LOCATION II

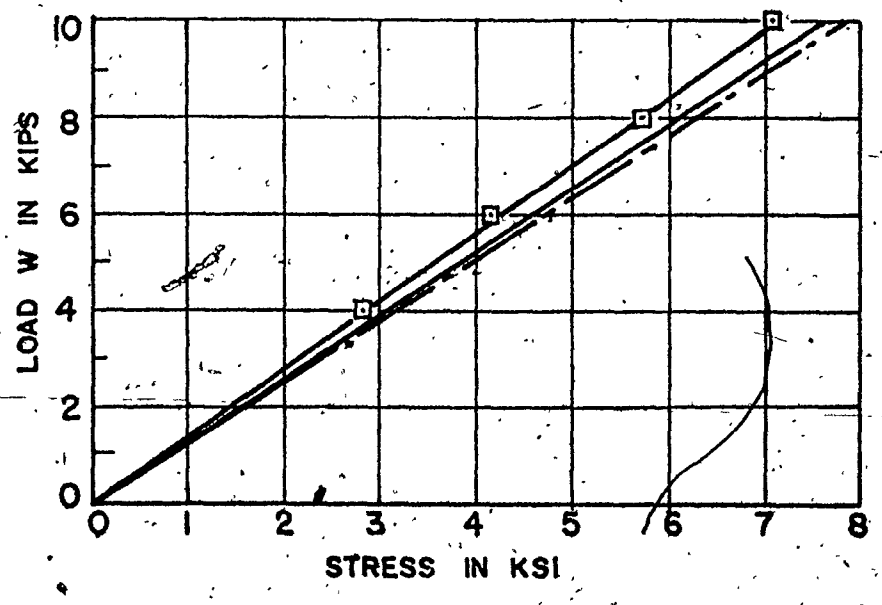

B . AT BOTTOM OF RIB

FIG. 6.14 - LONGITUDINAL STRESSES AT TOP AND BOTTOM OF RIB - I DUE TO COMBINED BENDING AT SECTION - R WITH RIB - I LOADED

the bending of the girder alone. This was done by subtracting the measured stresses in the first phase from those obtained from this phase of the test under an identical loading. The experimental values are plotted in Figure 6.15 together with the theoretical values. It is observed that the measured stress varies across the width of the deck and has a maximum value at the top of the girder, which exceeds slightly, the magnitude of the uniform theoretical stress. The ratios of the lowest to the highest measured stress corresponding to each stress distribution varied from 0.65 to 0.72.

The plots of the measured longitudinal stresses in the deck along the transverse sections for different positions of loading on the deck are shown in Figures 6.16 and 6.17. It is quickly observed that the deck plate stress is maximum again, at the location of the applied loading, which was also the case in the first phase of the test. The figures show that the deck plate stress decreases rapidly with the increase in the transverse distance from the centre line of the deck, indicating again that the directly loaded rib carries the major part of the applied load.

The bending stresses in the girder, as calculated and determined experimentally, are shown in Figures 6.18 and 6.19, for the various load positions on the deck. The bottom flange stress measured on the inside face of the flange, i.e.

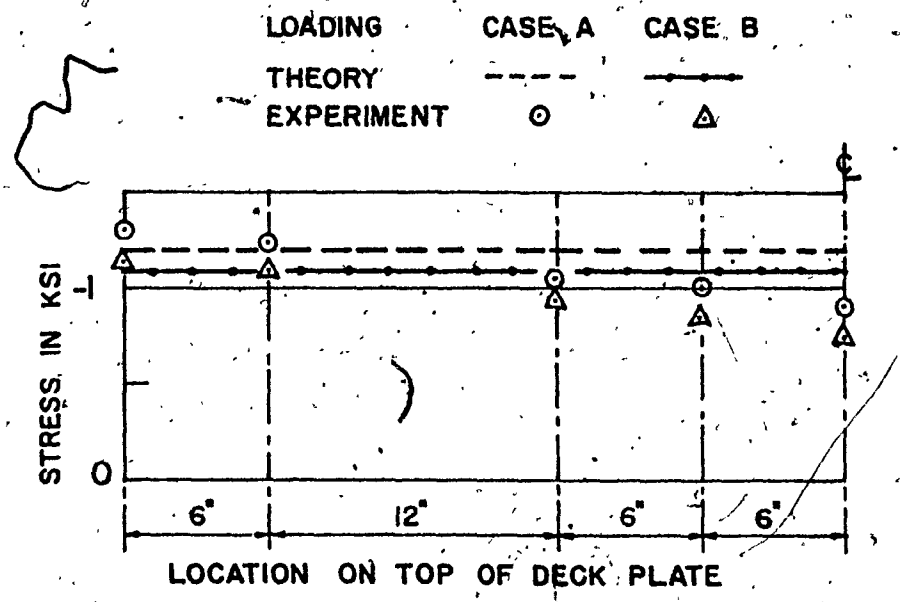

A . AT SECTION Q

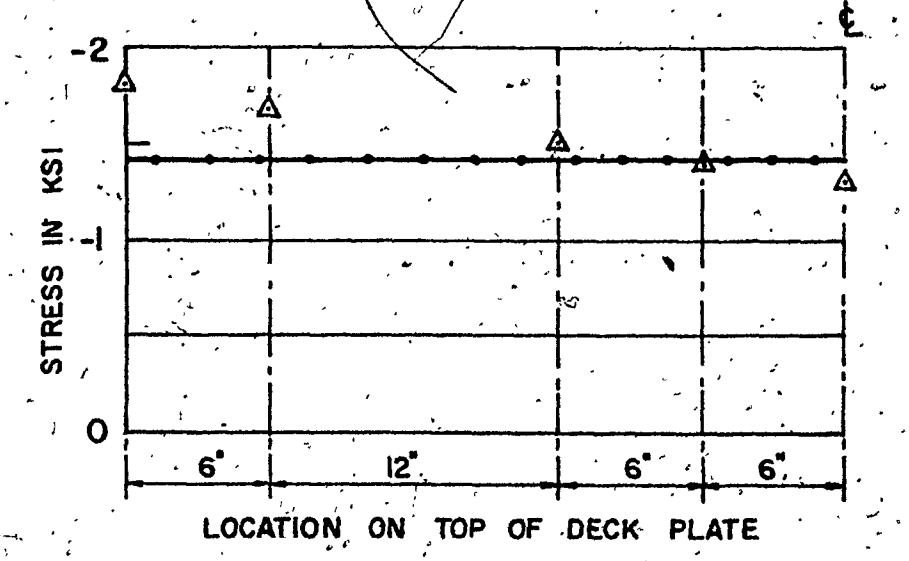

B. AT SECTION P

FIG. 6.15 - LONGITUDINAL STRESS DISTRIBUTION ACROSS DECK PLATE WIDTH DUE TO GIRDER BENDING WITH RIB 1 LOADED

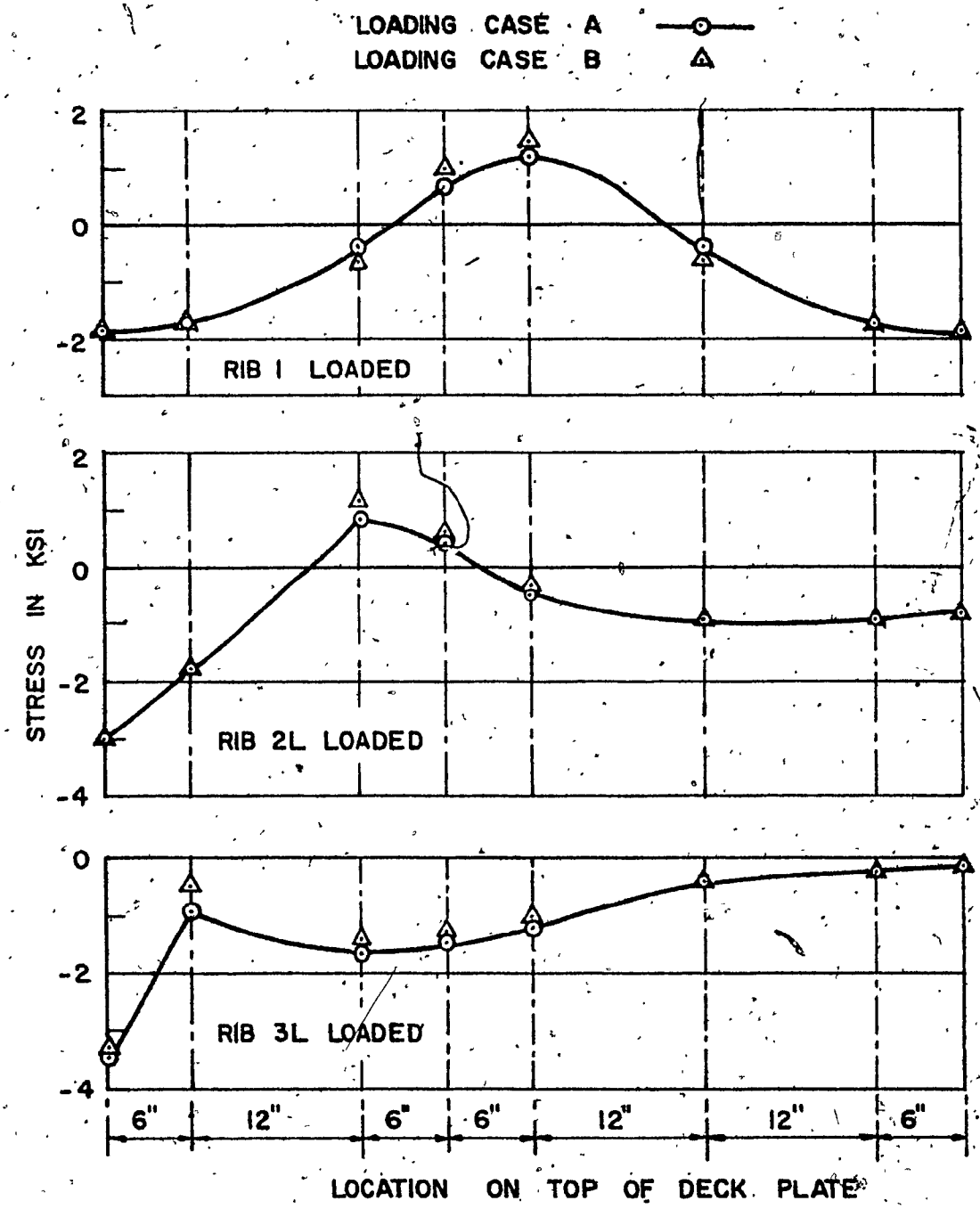

FIG. 6.16 - MEASURED LONGITUDINAL STRESSES ACROSS DECK PLATE WIDTH AT SECTION P FOR VARIOUS POSITIONS OF LOADINGS

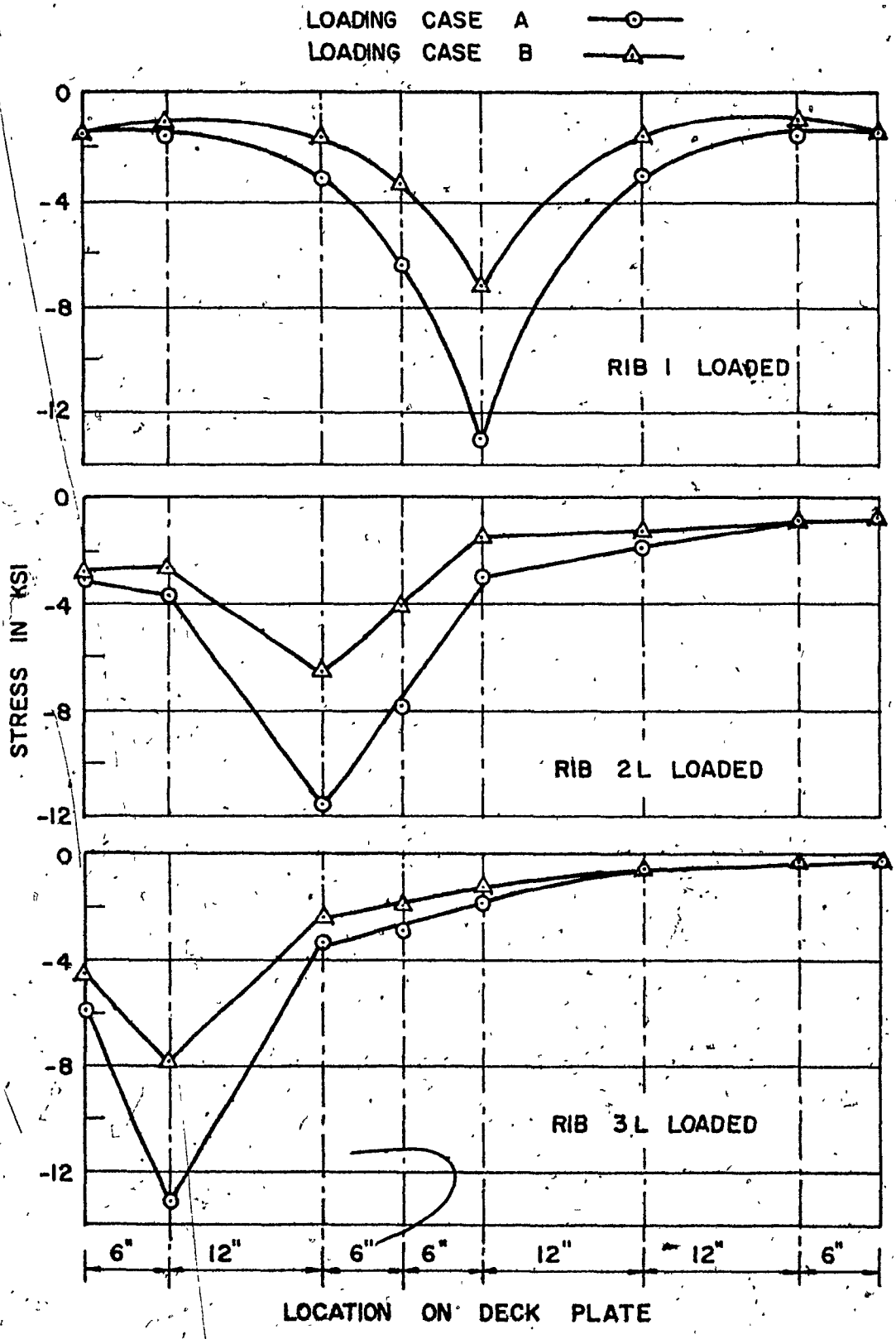

FIG. 6.17 – MEASURED LONGITUDINAL STRESSES ACROSS DECK PLATE WIDTH AT SECTION Q FOR VARIOUS POSITIONS OF LOADINGS

at the gage location, agrees closely with the theoretical values, as seen from Figures 6.18 (a) and 6.19 (a), when the applied loading was concentric, with respect to the longitudinal axis of the deck. The girder stresses were computed, assuming half-width of the deck was effective in acting as the top flange for such loading. A good agreement between the measured and calculated stresses shows that the orthotropic deck participated in the action of the main carrying member and the theoretical procedure to determine the girder bending stresses were satisfactory.

Figures 6.18 (b), 6.18 (c), 6.19 (b) and 6.19 (c) show that with the increase in the eccentricity of the applied loading, i.e., as the load was moved closer to one girder, the top and bottom stresses in the girder were not increased by the same proportion, and that the top stress increment was relatively higher. As the load was moved from Rib 1 to Rib 3L, the ratios of the new stress to the original stress varied from 2.8 to 3.0 for stresses measured at the top and those at the bottom of the girder varied from 2.0 to 2.3. If the load, placed at Rib 3L, is distributed between the girders in the same manner as in the case of a simple beam, the stresses at both the top and bottom of the near girder would be 1.8 times the stress caused by the same load when placed at Rib 1, using the same section modulii. This shows that the stress at the bottom of the girder can be predicted accurately by the conventional method, even for an asymmetrical loading about

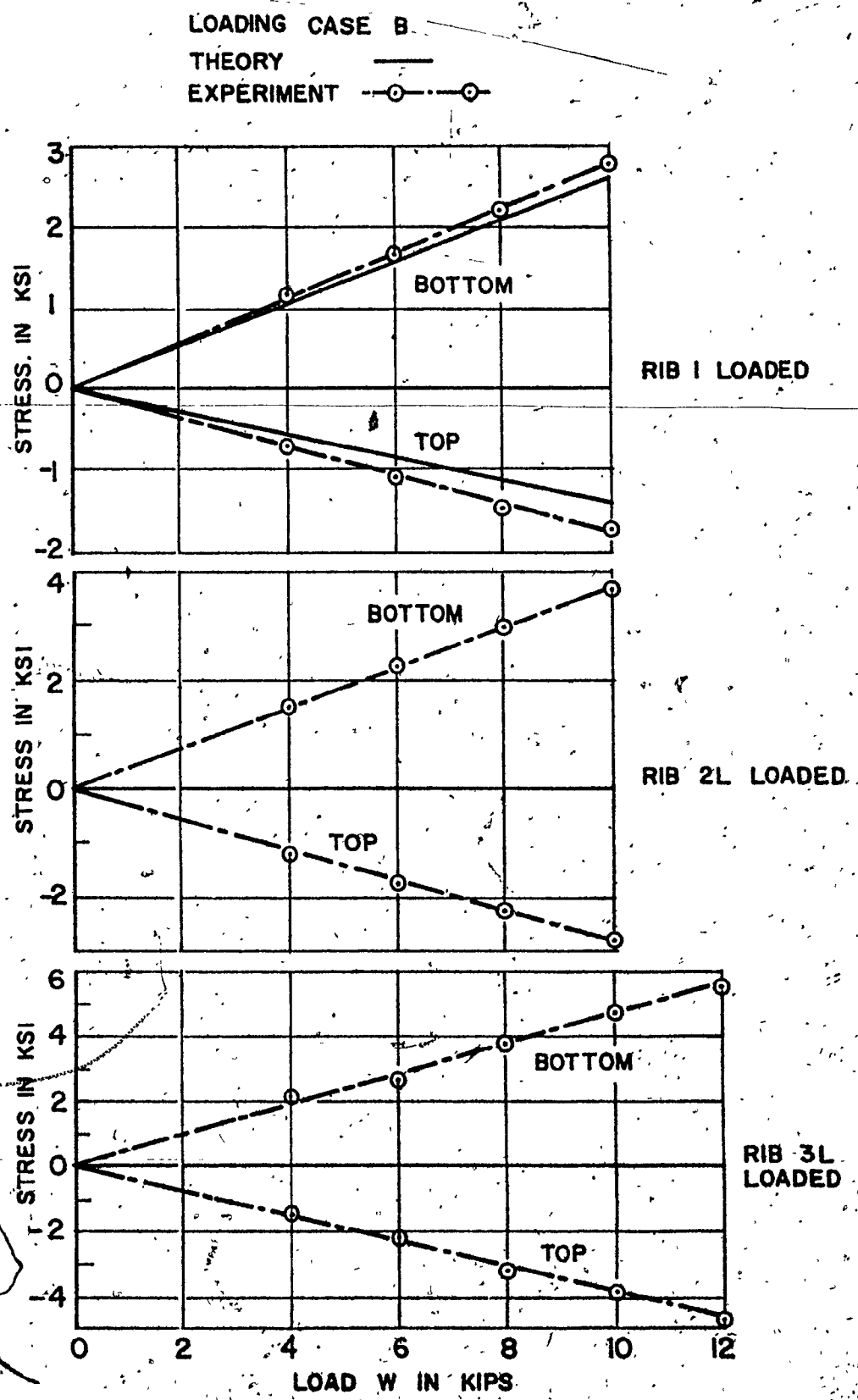

FIG. 6.18 - BENDING STRESSES IN GIRDER AT SECTION P FOR VARIOUS POSITIONS OF LOADING CASE B

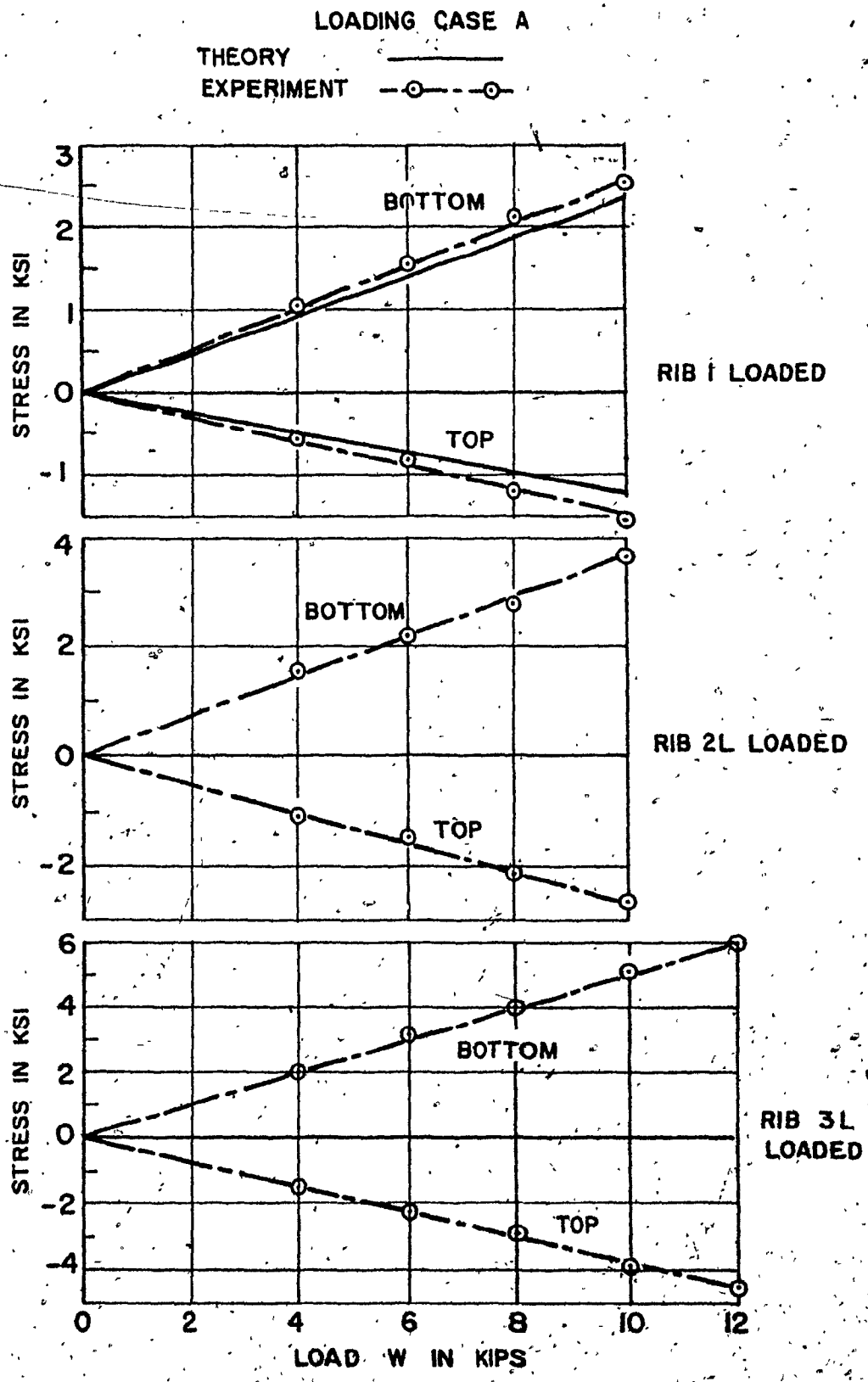

FIG. 6.19- BENDING STRESSES IN GIRDER AT SECTION Q FOR VARIOUS POSITIONS OF LOADING CASE A

the longitudinal axis of the deck.

Referring again to Figures 6.18 and 6.19, the larger stress increment at the top of the girder, compared with the bottom stress when the load moved nearer the girder, indicated that the effective width of the deck contributing to the action of the girder was reduced. This would apparently change the positions of the neutral axis of the girder.

An attempt was made to verify the above observation and to locate the neutral axis meaningfully, for different load positions on the deck, with the plot of the measured strains at the three locations on the girder. Figure 6.20 shows the approximate locations of the neutral axis at Section Q, for different positions of the loading Case A. For the symmetrical loading about the longitudinal axis of the girder, i.e., when Rib 1 was loaded, the experimentally determined neutral axis was located approximately 1/7 of the overall depth of the girder, from the top of the deck plate. This was close to the theoretical neutral axis at a depth of 7.70 in. from the top of the plate, determined with the consideration of the half-width of the deck, as the effective top flange of the girder. For the other positions of the loadings, it is observed from Figure 28 that the neutral axis moved downwards, i.e., towards the bottom flange, with the load approaching the girder. This indicated again, that the effective width of the orthotropic deck acting as flange, was reduced somewhat when the load moved from Rib 1 to Rib 3L.

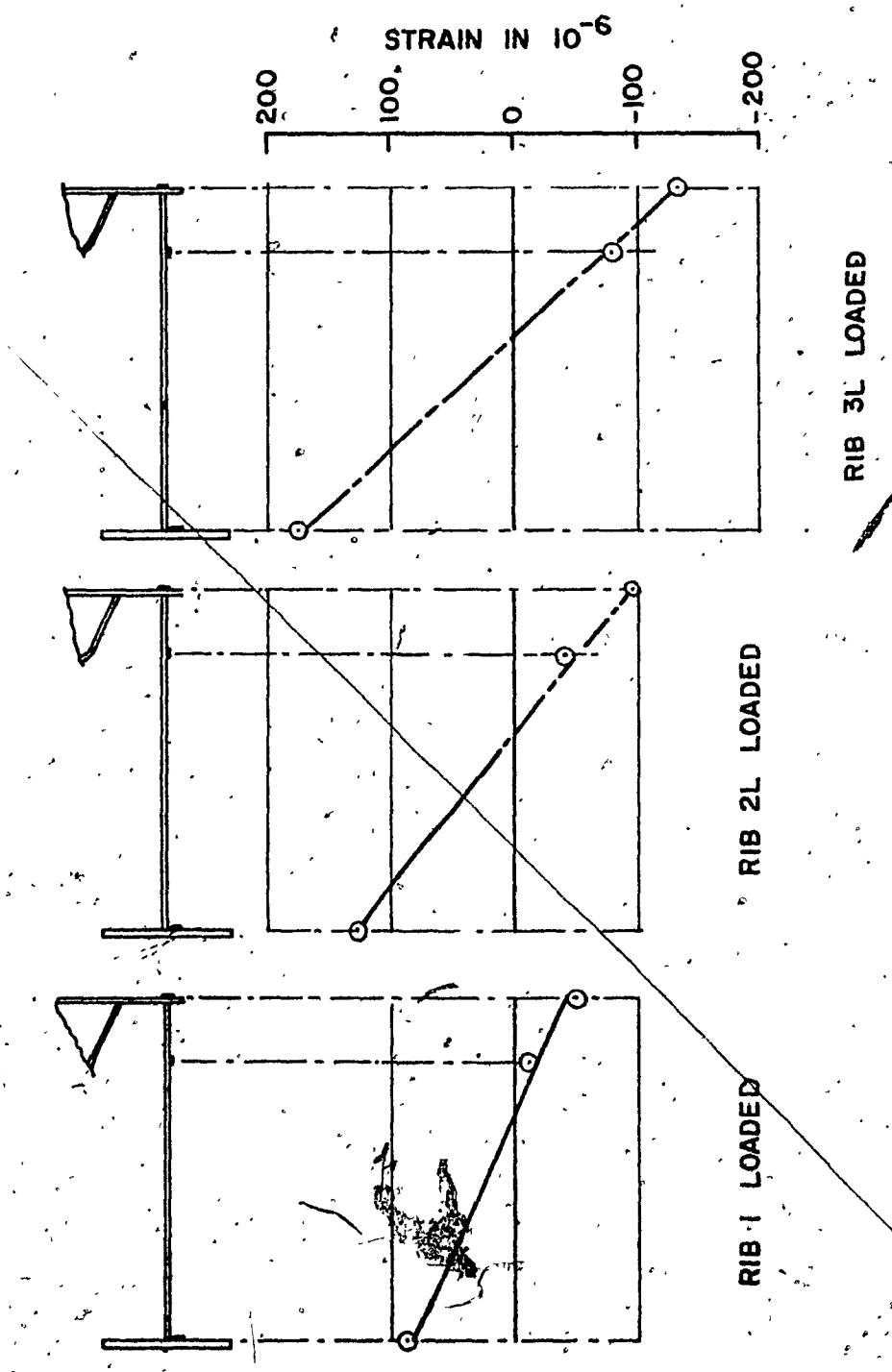

FIG. 6.20 - PLOTS OF LONGITUDINAL STRAINS IN GIRDER AT SECTION Q FOR LOADING CASE A

6.3 DEFLECTION

For a concentric load on the model, the deflections of the girder, as measured by dial gages, are shown in Figure 6.21, together with the calculated values. The measured deflections shown are the average of both the girders recorded by the dial gages, which were, however, almost identical. The deflections at P and Q for both loading Cases A and B, were almost similar, with little change, as revealed from both measurements and calculations, and, therefore, those at Section P are only shown in Figure 6.21. The deflections at Section R for loading Case C, are also shown. For theoretical values, the deflection due to both bending and shear deformations of the girder were considered, the latter being about 10% of the former. For these computations, the girder was assumed to be loaded by the floor beam reactions. For the deflection due to bending, the half-width of the deck was taken into account in computing the flexural rigidity of the girder. The calculation of shear deflection was based on the gross cross-sectional area of the web. The measured deflections, only being slightly higher, agreed favourably with the theoretical values, indicating again, that the assumed girder loading and the procedure to compute the girder deflection was satisfactory. It further showed the participation of the orthotropic deck in the action of the main carrying girder.

With the application of an eccentric loading, the

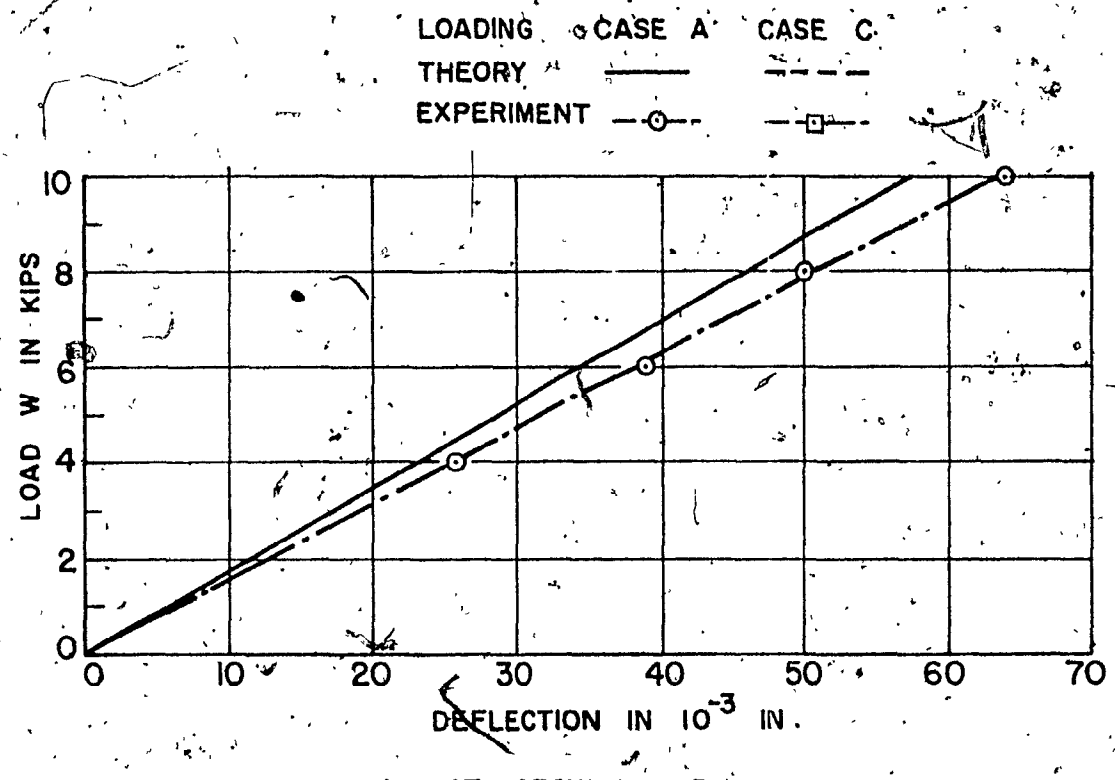

A. AT SECTION P

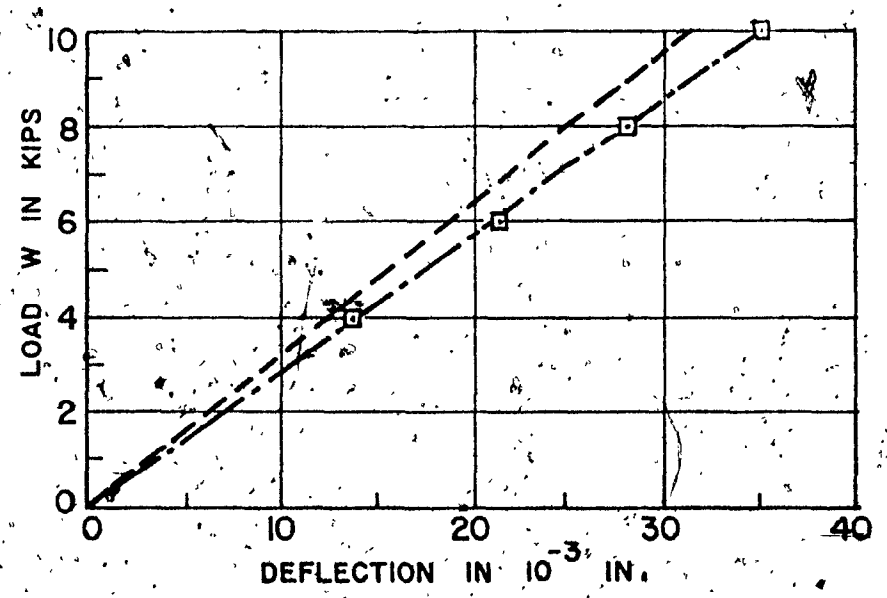

B. AT SECTION R

FIG. 6.21 - DEFLECTIONS OF GIRDER WITH LOAD AT RIB - 1

dial gages for both girders recorded different readings, as expected, Figure 6.22. It was observed that the deflection of the girder near the load was increased approximately by an identical amount, as the other girder decreased, compared to that due to concentric loading. This was mainly because the increase in the load carried by the near girder was equal to the magnitude of the load that the other girder was relieved of. The theoretical values of deflection for eccentric loading, based on simplified assumptions, are also shown in Figure 6.22, to check the acceptibility of such computations. It was again assumed that the floor beams transfer the load to the girder by simple beam actions, and that the flexural rigidity of the girder was the same as in the case of concentric loading. An examination of the curves in Figure 6.22 reveals that, despite some differences between the calculated and measured deflections, the simplified procedure may be used to predict a deflection satisfactory for practical purposes.

To indicate more clearly the change in the deflection, with respect to the various positions of a load across the width of the deck, Figure 6.23 is drawn, which shows both the measured and calculated deflections of a girder. It is observed that the load distribution between the girder for an eccentric loading, based on the assumption of a simple beam action, is not quite correct, which was also noted earlier in the case of bending stress measurements for

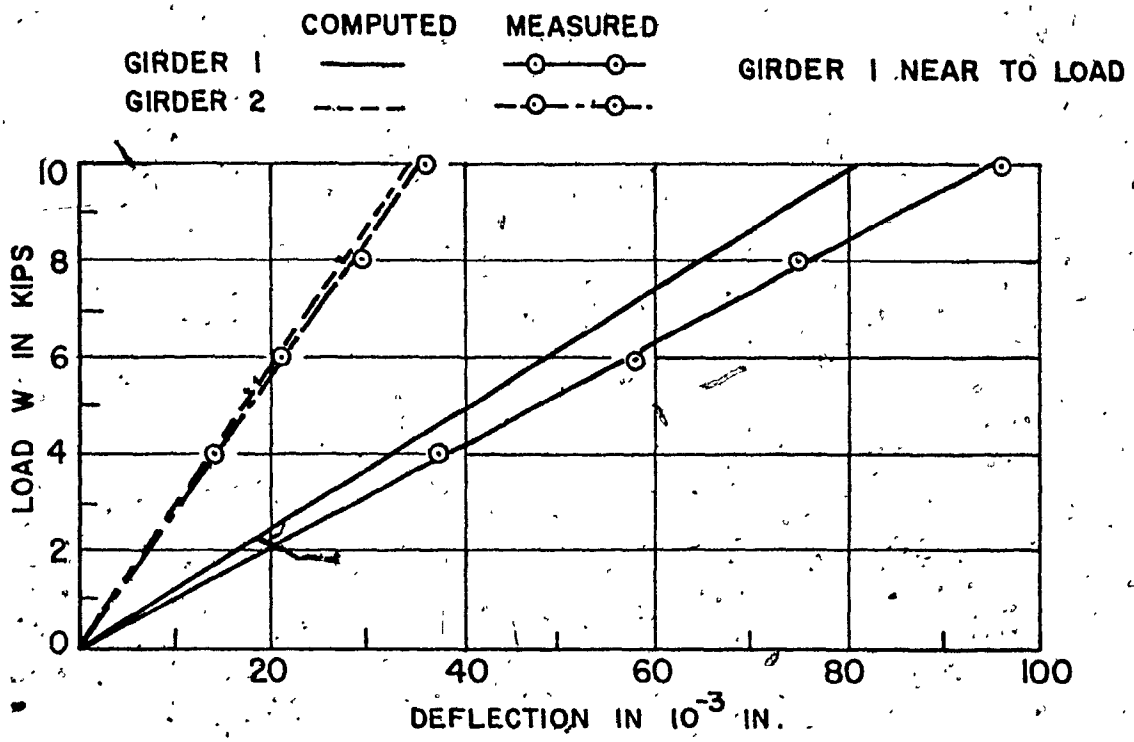

A. RIB 2L LOADED

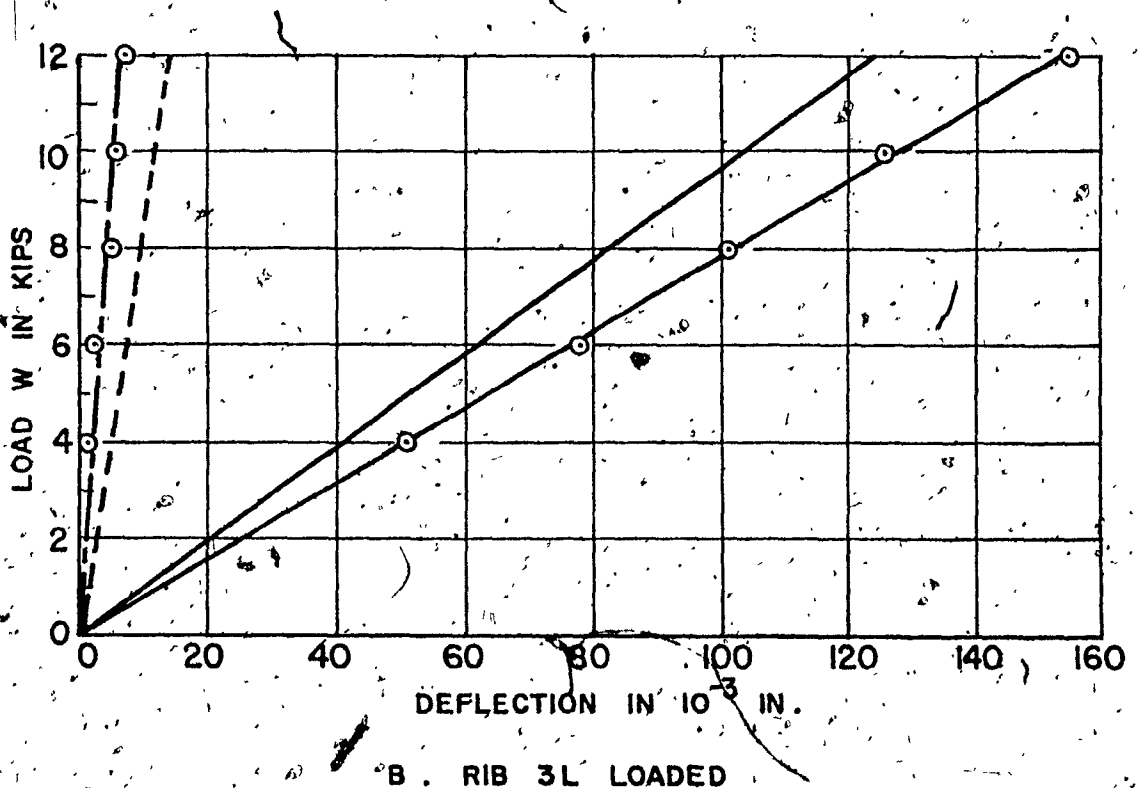

B. RIB 3L LOADED

FIG. 6.22 - DEFLECTIONS OF GIRDER AT SECTION P FOR ECCENTRIC LOADING (LOADING CASE A)

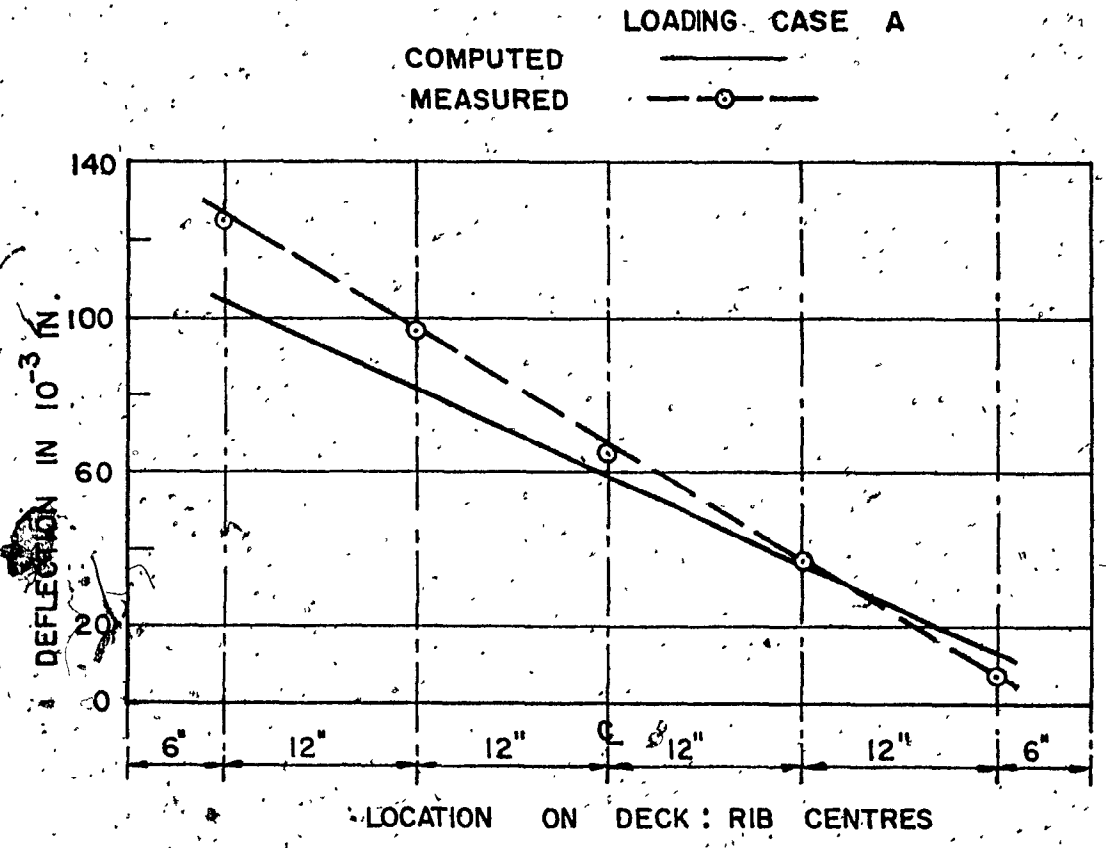

FIG. 6.23 - DEFLECTIONS OF GIRDER FOR VARIOUS LOAD POSITIONS ACROSS THE WIDTH OF DECK AT SECTION P

the girder. However, as seen from Figure 6.23, such a simplified assumption can be satisfactorily used for practical purposes without the loss of significant accuracy.

The deflections at the midspan and at the floor beam support of Rib 1, are shown in Figure 6.24, for loading Cases A and C. The theoretical deflections, as obtained from the refined analysis, are also shown. A favourable comparison between the two sets of values was observed, indicating that the deflection of a rib can be predicted satisfactorily by the proposed analytical method.

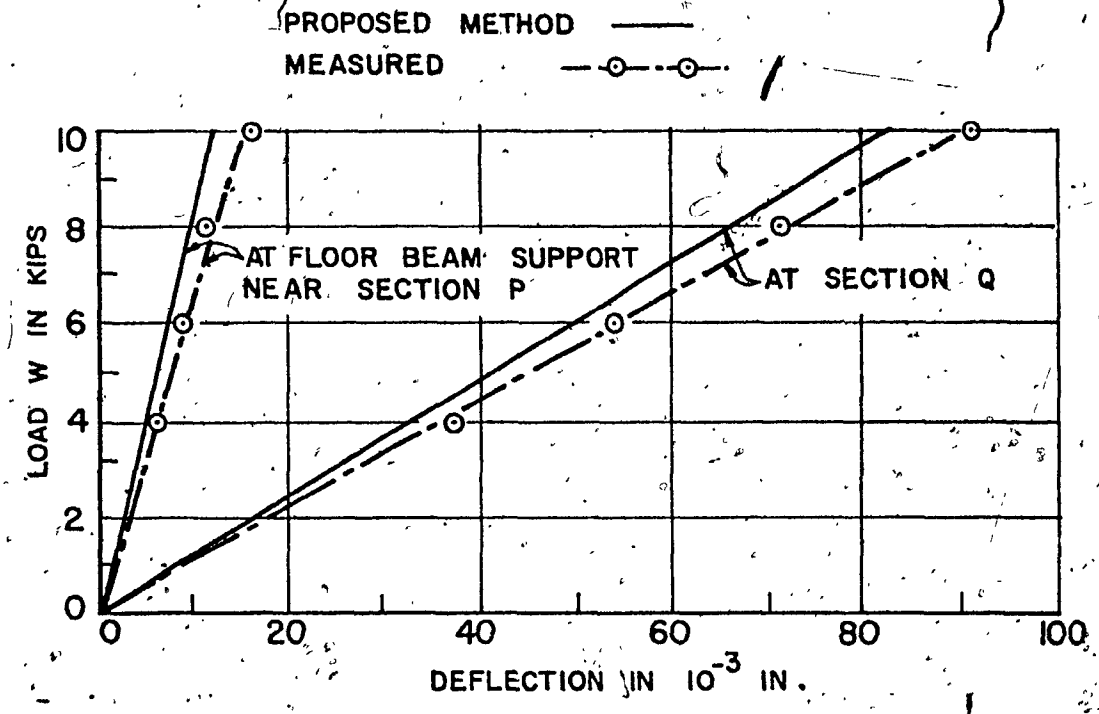

A. LOADING CASE A

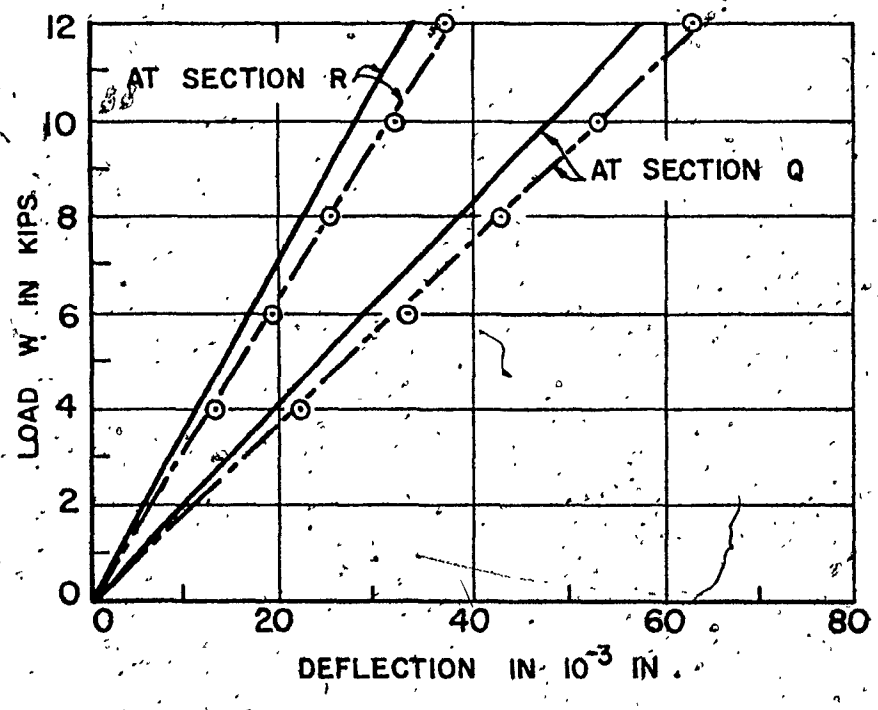

B. LOADING CASE B

FIG. 6.24 - DEFLECTIONS OF RIB I WHEN LOADED

CHAPTER 7

SUMMARY AND CONCLUSIONS

7.1 SUMMARY

A stiffness method of analysis of the conventional orthotropic steel bridge deck is proposed by idealizing the deck as a plate, stiffened only in the longitudinal direction and being continuous over flexible transverse floor beams. The main girders are assumed to provide simple supports to the deck. In this method, the basic theory of an eccentrically stiffened plate is incorporated, considering both open and closed type stiffeners or ribs. The method is readily programmed on CDC 6600 to obtain desired solutions conveniently from the computer.

The proposed method and the design method of Pelikan-Esslinger are compared by applying both of them to solve several hypothetical decks of various proportions. The parameters such as, the deck plate thickness, the rib size, the rib span and their spacings, are varied in order to compare both these methods in a wide range of deck proportioning.

An experimental investigation was also undertaken to observe the behaviour of an orthotropic deck and the stress distribution in it, and to compare it with the analytical solutions. A twin plate girder bridge model with an orthotropic steel deck having closed type ribs was tested

under static loads. The loadings on the deck was restricted so as to keep the stress in the deck well below the yield stress of the steel used.

7.2 CONCLUSIONS

Based on the theoretical investigations carried out in this research, the following conclusions are formulated:

1. The proposed stiffness method of analysis of orthotropic steel bridge decks can be used adequately to analyse a deck structure to obtain information relevant to the actual behaviour of the deck. The computerized method readily determines the desired stresses and deflections of the deck.

2. The simplified design method of Pelikan-Esslinger evaluates maximum stresses in the deck which are satisfactory for practical purposes. The results are usually higher in magnitude and thus can be used safely to design an orthotropic steel bridge deck. The method, however, becomes increasingly conservative with longer rib spans for open type ribs.

3. The width of the deck between simple supports of the main girders has little influence on the magnitude of the maximum stresses in the ribs located towards the middle of the deck, provided the

flexibility of the floor beams remains constant and that there is a sufficient number of ribs on either side of the loaded rib.

4. The effective transverse width of deck in carrying the applied load is relatively small, even for decks with closed ribs. However, closed ribs have better load distributing capacity than the open ribs. The transverse load distribution capacity of the closed ribs increases with the longer rib spans.

5. It appears economical to span the ribs longer as the stress increment with longer spans is relatively small after a certain span length.

The experimental investigations carried out in this research lead to the following conclusions, with regard to the simple span twin plate girder bridge with orthotropic deck.

6. The orthotropic deck participates in the action of the main carrying members and in the case of a simple span twin-girder bridge, with its span sufficiently larger than the width, half-width of the entire deck can be considered as flange material of one girder. This assumption is satisfactory for determining bending stresses in the girder.

7. The longitudinal stress in the deck plate and ribs can be determined satisfactorily following the conventional method of superposition of stresses due to the deck bending and girder bending.

8. The longitudinal stress in the deck due to bending of the main girders is not uniform over the full width of the deck for concentric loadings, as usually assumed in theory.

9. The effective width of the deck acting with a girder varies somewhat with the position of loading and as such the neutral axis of the girder is also dependent upon the load position. However, for practical purposes, half-width of the deck may be considered as top flange of a girder.

10. The load transfer on the deck is proportional to its stiffness. Almost the full load is carried by the ribs to the floor beams which, in turn, transmit it to the main carrying members.

11. The deflection of a simply supported twin-girder bridge with an orthotropic deck can be predicted with sufficient accuracy, considering half-width of the deck as effective in computing the flextural rigidity of the girder in question and using simple beam formulae for deflection due to bending and shear.

7.3 SUGGESTIONS FOR FUTURE RESEARCH WORK

In the light of this study, the following suggestions for future research work in the field of orthotropic steel deck bridges are proposed.

1. In recent years, more bridges have been built with cantilevered orthotropic decks. It is desirable, therefore, to develop a rigorous mathematical analysis of the cantilevered orthotropic deck, based on which the design method of Pelikan-Esslinger can be modified to be used in the design of such decks with sufficient accuracy. It can be mentioned here that the design of a cantilevered deck stiffened by open ribs can be furnished by Pelikan-Esslinger's method taking into consideration the modifications proposed by Troitsky and Azad.[52]

2. The influence of the wearing surface on the behaviour of the deck, in particular on the load distribution area of a wheel load, should be thoroughly investigated by both static and dynamic tests performed on model bridges. The allowable limit of the deck plate deflection between ribs and that of a rib between floor beams needs to be carefully established in order to have a wearing surface free of severe cracks.

3. It has been observed by this study and others made

in this area that the design method of Pelikan-Esslinger offers a safe and satisfactory design of the conventional orthotropic bridge decks of usual proportions. It is apparent, therefore, that for more economical design, attention should be oriented more on the new concept of orthotropic construction, improvement of fabrication methods and details, rather than on the improvement of the design method.

4. In order to take advantage of the proven high ultimate strength of orthotropic steel decks, it is necessary to develop a suitable wearing surface that would conform easily with the deformed structure without losing the necessary bond and serviceability limit. With such a wearing surface, it would also be possible to span ribs a longer distance, thus making an economical design of the deck.

REFERENCES

1. Hotchkiss, J.G., "New Ways to Cut Bridge Weight Lead to Record Spans", Engineering News-Record, No. 7, November, 1957.

2. Wolchuk, R., "Orthotropic Plate Design for Steel Bridges", Civil Engineering, February, 1959.

3. Troitsky, M.S., "Orthotropic Design in Modern Bridge Engineering", Paper No. 10, The Engineering Institute of Canada, Annual General Meeting, June, 1962.

4. Hardenberg, G., "Design of the Superstructure of the Port Mann Bridge", The Engineering Institute of Canada, Engineering Journal, July, 1961.

5. Foster, L., "First U.S. Orthotropic Design - The Poplar Street Bridge", Proc. of American Institute of Steel Construction, National Engineering Conference, 1962.

6. "Design Manual for Orthotropic Steel Plate Deck Bridges", American Institute of Steel Construction, New York, 1963.

7. Troitsky, M.S., "Orthotropic Bridge Theory and Design", Second Edition, The James F. Lincoln Arc Welding Foundations, Ohio, 1968.

8. Kunert, K., "Orthotropic Steel Decks in Germany", Proceedings of the Conference on Steel Bridges, The British Constructional Steelwork Association Ltd., London, June, 1968.

9. Grassl, H., "Entwurf von Leichtfahrbahnen", Publications, International Association for Bridge and Structural Engineering, Vol. 25, 1965.

10. Firmage, D.A., "Report on Investigation of Orthotropic Plate Bridges", American Iron and Steel Institute, Bulletin No. 7, February, 1968.

11. Huber, M.T., "Die Grundlagen einer rationellen Berechnung der Kreuzweise bewehrten Eisenbetonplatten", Zeitschrift des Osterreichischen Ingenieur-und Architekten-Vereines, Vol. 66, 1914.

12. Huber, M.T., "Die Theorie der Kreuzweise bewehrten Eisenbetonplatten, Der Bauingenieur, No. 4, 1923.

13. Lekhnitskii, S.G., "Anisotropic Plates", Gordon and Breach Publications, 1968.

14. Timoshenko, S.P., and Woinowsky-Krieger, S., "Theory of Plates and Shells", Second Edition, McGraw-Hill Book Co. Inc., 1959.

15. Cornelius, W., "Die Berechnung der Ebenen Flächentragwerke mit Hilfe der Theorie Orthogonal-Anisotropen Platte", Der Stahlbau, February, March, April, 1952.

16. Mader, F.W., "Berechnung Orthotroper Platten unter Flächenlasten, Randmomenten und Randdurchbeigungen", Der Stahlbau, Vol. 26, 1957.

17. Massonnet Ch., "Method de calcul des ponts à poutres multiples tenant compte de leur resistance à la torsion", Publications International Association for Bridge and Structural Engineering, Vol. 10, 1950.

18. Homberg, H., and Weinmeister, J., "Einflussflächen fur Kreuzwerke", Zweite Auflage, Springer, Berlin, 1956.

19. Girkmann, K., "Flachentragwerke", Vierte Auflage, Springer, Berlin, 1956.

20. Pelikan, W., and Esslinger, M., "Die Stahlfahrbahn, Berechnung und Konstruktion", M.A.N. Forschungsheft No. 7, 1957.

21. Pflüger, A., "Zum Beulproblem der anisotropen Rechteckplatte", Ingenieur-Archiv., Vol. 16, 1947.

22. Pflüger, A., "Die Orthotrope Platte mit Hohlsteifen", Osterreichisches Ingenieur-Archiv., Vol. 9, No. 2, 1955.

23. Trenks, K., "Beitrag zur Berechnung orthogonal anisotroper Rechteckplatten", Der Bauingenieur, Vol. 29, No. 10, 1954.

24. Giencke, E., "Die Grundgleichungen für die Orthotrope Platte mit exzentrischen Streifen", Der Stahlbau, Vol. 24, June, 1955.

25. Giencke, E., "Die Berechung von durchlaufenden Fahrbahnplatten", Der Stahlbau, Vol. 12, No. 27, September, November, December, 1958.

26. Giencke, E., "Die Berechnung von Hohlrippenplatten", Der Stahlbau, Vol. 29, January, February, 1960.

27. Giencke, E., "Einfluss der Steifen-Exzentrizität auf Beigung und Stabilität Orthotroper Platten", Beiträge Aus Statik Und Stahlbau, Verlags-GmbH, Köln, 1961.

28. Massonnet, Ch., "Plaques et Coques Cylindriques Orthotropes a Nervures Dissymetriques", Publications, International Association for Bridge and Structural Engineering, No. 19, 1959.

29. Clifton, R.J., Chang, J.C.L., and Au, T., "Analysis of Orthotropic Plate Bridges", Journal of the Structural Division, ASCE, Vol. 89, No. ST5, Proc. Paper 3675, October, 1963.

30. Vitols, V., Clifton, R.J., and Au, T., "Analysis of Composite Beam Bridges by Orthotropic Plate Theory", Journal of the Structural Division, ASCE, Vol. 89, No. ST4, Proc. Paper 3584, August, 1963.

31. Schumann, H., "Zur Berechnung orthogonal-anisotroper Rechtecksplatten unter Berücksichtigung der diskontinuierlichen Anordnung der Rippen", Der Stahlbau, Vo. 29, 1960.

32. Chu, K.H., and Krishnamoorthy, G., "Use of Orthotropic Plate Theory in Bridge Design", Journal of the Structural Division, ASCE, Vol. 88, No. ST3, Proc. Paper 3157, June, 1962.

33. Schaefer, W., "Berechnung von Einflussflächen für die Statischen Groessen mehrfeldriger orthotroper Fahrbahn Platten mit Hilfe von Eigenfunktionen", Stahlbau, Vol. 33, No. 6, June, 1964.

34. Adotte, G.D., "Second Order Theory in Orthotropic Plates", Journal of the Structural Division, ASCE, Vol.93, No. ST5, Proc. Paper 5520, p.343, October, 1967.

35. Coull, A., "Direct Analysis of Orthotropic Bridge Slabs", Journal of the Structural Division, ASCE, Vol. 90, No. ST2, April, 1964.

36. Heins, C.P., and Looney, C.T.G., "Bridge Analysis Using Orthotropic Plate Theory", Journal of the Structural Division, ASCE, Vol. 94, No. ST2, Proc. Paper 5822, February, 1968.

37. Dowling, P. J., "The Behaviour of Stiffened Plate Bridge Decks Under Wheel Loading", Ph.D., Dissertation, Imperial College of Science and Technology, University of London, London, 1968.

38. Heins, C.P., and Yoo, C.H., "Grid Analysis of Orthotropic Bridges", Publications International Association for Bridges and Structural Engineering, No. 30-1, 1970.

39. William, K.J., and Scordelis, A.C., "Analysis of Orthotropic Folded Plates with Eccentric Stiffeners", SESM Report No. 70-2, University of California, Berkeley, California, 1970.

40. McBean, R.P., "Analysis of Stiffened Plate by the Finite Element Method", Ph.D. Thesis, Stanford University, 1968.

41. Powell, G.H., and Ogden, D.W., "Analysis of Orthotropic Steel Plate Bridge Decks", Journal of the Structural Division, ASCE, Vol. 95, No. ST5, Proc. Paper 6563, p. 909, May, 1969.

42. Tinawi, R.A., "Behaviour of Orthotropic Bridge Decks", Ph.D. Thesis, McGill University, Montreal, 1972.

43. Klöeppel, K., "Zur orthotropen Platte aus Stahl. Die Neue Köln-Mülheimer Brücke", Commemorative Book published by the City of Cologne, 1951.

44. Naruoka, Okabe, T., and Hori, K., "An Experimental Study on Model Continuous Beam Bridge with Steel Deck", Publications International Association for Bridge and Structural Engineering, No. 18, 1958.

45. Kondo, K., Komatsu, S., and Nakai, H., "Theoretical and Experimental Researches on Effective Width of Girder Bridge with Steel Deck Plate", Japan Society of Civil Engineers, Transactions, No. 86, October, 1962.

46. Davis, R.E., and Bender, O., "California Builds Experimental Orthotropic Plate Bridge", Civil Engineering, (New York), Vol. 34, No. 11, November, 1964.

47. Bouwkamp, J.G., "Behaviour of a Skew Steel-Deck Bridge Under Static and Dynamic Loads", Report No. SESM 65-2, Dept. of Civil Engineering, University of California, Berkeley, California, June, 1965.

48. Bouwkamp, G.J., and Powell, G.H., "Structural Behaviour of an Orthotropic Steel Deck Bridge", Vols. I and II, Report No. SESM 67-27, University of California, Berkeley, California, November, 1967.

49. Sharp, M.L., "Field Tests of Aluminium Orthotropic Bridge Deck", Journal of the Structural Division, ASCE, Vol. 95, No. ST 11, Proc. Paper 6920, November, 1969.

50. Davis, H.L., and Toprac, A.A., "Fatigue Testing of Ribbed Orthotropic Bridge Elements", Research Report No.77-1, The Centre for Highway Research, The University of Texas, Austin, Texas, June, 1966.

51. Erzurumlu, H., and Toprac, A.A., "Fatigue of Orthotropic Steel Decks", Journal of the Structural Division, ASCE, Vol. 98, ST 4, Proc. Paper 8823, April, 1972.

52. Troitsky, M.S., and Azad, A.K., "Bending and Torsion in Orthotropic Deck Box Girder", Journal of the Structural Division, ASCE, Vol. 98, No. ST 9, Proc. Paper 9168, September, 1972.

53. Glockner, P.G., Verma, K.K., and de Paiva, H.A.R., "Study of the Behaviour of a Three-Panel Orthotropic Steel Plate Deck", Transactions of the Engineering Institute of Canada, Vol. 14, No. A-3, March, 1971.

54. Timoshenko, S.P., and Goodier, J.N., "Theory of Elasticity" McGraw-Hill Book Co. Inc., Second Edition, New York.

55. Gere, J.M., and Weaver, W.Jr., "Analysis of Framed Structures", D. Van Nostrand Company, Inc., Toronto, 1965.

56. Weaver, W.Jr., "Computer Programs for Structural Analysis" D. Van Nostrand Company, Inc., Toronto, 1966.

57. "Orthotropic Bridge Decks using Bethlehem Standard Ribs", Bridge Design Aids, Bethlehem Steel Corporation, Bethlehem.

58. Troitsky, M.S., and Azad, A.K., "A Stiffness Method of Analysis of Orthotropic Steel Bridge Deck", Paper presented at the Fourth Canadian Congress of Applied Mechanics, Montreal, May, 1973.

59. Troitsky, M.S., and Azad, A.K., "Analysis of Orthotropic Steel Bridge Decks by a Stiffness Method", Proceedings of the Institution of Civil Engineers, London, Vol. 55, June, 1973.

60. Troitsky, M.S., and Azad, A.K., "Refined Analysis of Orthotropic Steel Bridge Decks", Report No.1, Faculty of Civil Engineering, Sir George Williams University, Montreal, November, 1971.

61. Troitsky, M.S., and Azad, A.K., "Refined Analysis of Orthotropic Steel Bridge Decks", Report No. 2, Faculty of Civil Engineering, Sir George Williams University, Montreal, March, 1972.

62. Troitsky, M.S. and Azad, A.K., "Refined Analysis of Orthotropic Steel Bridge Decks", Report No. 3, Faculty of Civil Engineering, Sir George Williams University, Montreal, 1973.

APPENDIX A

ROOTS OF EIGHTH ORDER POLYNOMIAL

For an actual orthotropic bridge deck of usual proportions and stiffened by open type ribs, it can be shown that the polynomial in Eq. (2.46) yields always two pairs of real roots and two pairs of complex conjugate roots.

Replacing s^2 by x and using coefficients valid for the case of open ribs, Eq. (2.46) reduces to a quartic equation of the form

$$a_5x^4 + a_4x^3 + a_3x^2 + a_2x + a_1 = 0 \qquad (A.1)$$

Where the coefficients a_5 to a_1 are given by the expressions (2.23).

Dividing by a_5, Eq. (A.1) can be written as

$$x^4 + p_1x^3 + p_2x^2 + p_3x + p_4 = 0 \qquad (A.2)$$

where

$$p_1 = a_4/a_5;\quad p_2 = a_3/a_5 \qquad (A.3)$$
$$p_3 = a_2/a_5;\quad p_4 = a_1/a_5$$

In order that Eq. (A.2) has two real roots and two

complex conjugate roots, the discriminant, Δ, for the equation must always be a negative quantity. Δ is given as

$$\Delta = -4f^3 - 27g^2 \qquad \text{(A.4)}$$

where

$$f = p_1p_3 - 4p_4 - \frac{1}{3}p_2^2 \qquad \text{(A.5a)}$$

and

$$g = -p_1^2p_4 + \frac{1}{3}p_1p_2p_3 + \frac{8}{3}p_2p_4 - p^3 - \frac{2}{27}p_2^3 \qquad \text{(A.5b)}$$

The expressions for p_1, p_2, p_3 and p_4 obtained from Eqs. (A.2) and (2.23) indicate that, while p_1 and p_3 are always negative quantities, p_2 and p_4 have positive values. Since the moment of inertia, I, of the deck plate is small compared to other values, the numerical magnitudes of these coefficients are in a descending order with p_1 being the largest and p_4 being the smallest of all. Furthermore, it is also evident that the values of p_3 and p_4 are also small compared with the values of p_1 and p_2. Therefore f and g can be written approximately as

$$f = p_1p_3 - \frac{1}{3}p_2^2 \quad \text{and} \qquad \text{(A.6a)}$$

$$g = -p_1^2p_4 + \frac{1}{3}p_1p_2p_3 + \frac{8}{3}p_2p_4 - \frac{2}{27}p_2^3 \qquad \text{(A.6b)}$$

or

$$f = \delta_f - \frac{1}{3} p_2^2 \quad \text{and} \tag{A.6c}$$

$$g = \delta_g - \frac{2}{27} p_2^3 \tag{A.6d}$$

where

$$\delta_f = p_1 p_3 \quad \text{and} \quad \delta_g = p_1^2 p_4 + \frac{1}{3} p_1 p_2 p_3 + \frac{8}{3} p_2 p_4 \tag{A.6e}$$

Both δ_f and δ_g are relatively small compared with other terms in f and g.

$$f^3 = d_f^3 - d_f^2 p_2^2 + \frac{1}{3} \delta_f p_2^4 - \frac{1}{27} p_2^6 \tag{A.7a}$$

and

$$g^2 = \delta_g^2 - \frac{4}{27} \delta_g p_2^3 + \frac{4}{27^2} p_2^6 \tag{A.7b}$$

Ignoring the small terms in f^3 and g^2, Δ can be expressed from Eq. (A.4) as

$$\Delta = -4(\delta_f p_2)^2 - \frac{4}{3} (\delta_f p_2) p_2^3 + 4 \delta_g p_2^3 \tag{A.8}$$

Substituting values of δ_f and δ_g in the above equation of Δ and rearranging

$$\Delta = -4(p_1 p_2 p_3)^2 - 4 p_1^2 p_2^3 p_4 + \frac{32}{3} p_2^4 p_4 \tag{A.9a}$$

or

$$\Delta = 4p_1^2p_2^2\{-p_3^2 - p_4p_2 + \frac{8}{3}(\frac{p_1}{p_2})^2p_4\} \qquad (A.9b)$$

Further rearranging, Δ can be written in the form

$$\Delta = 4(p_1p_2)^2\,[-p_3^2 - p_4\{p_2 - \frac{8}{3}(\frac{p_2}{p_1})^2\}] \qquad (A.9c)$$

From the relative values of p_1 and p_2 obtained from Eqs. (A.2) and (2.23), it can be shown that the term in the second bracket is always positive for an actual bridge deck having open ribs. Thus, the term in the third bracket of the above equation becomes negative, which makes the discriminant, Δ, a negative quantity. Therefore, the polynomial in Eq. (A.1) has always a pair of real and a pair of complex conjugate roots.

APPENDIX B

PROPERTIES OF BRIDGE MODEL

The properties of the bridge model used in the theoretical analyses are given below.

B.1 PROPERTIES OF MAIN GIRDER

In calculating the moment of inertia and section modulii of each girder, half-width of the deck is considered as the top flange. Referring to Figure B.1

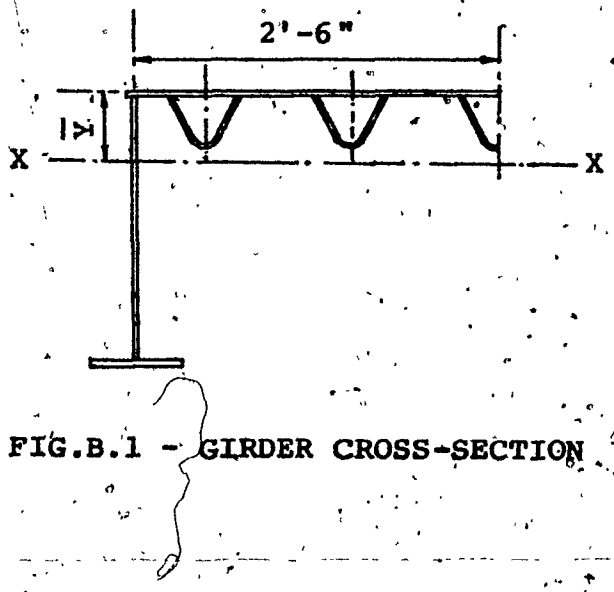

FIG.B.1 - GIRDER CROSS-SECTION

Depth of neutral axis from top of deck, $\bar{Y}$	= 7.70	in.
Moment of inertia about X-X axis, I_{xx}	= 1524.0	in^4
Section modulus at top of girder, S_{xt}	= 198.0	in^3
Section modulus at bottom of girder, S_{xb}	= 102.0	in^3
Section modulus at inside face of bottom flange	= 105.0	in^3
Cross-sectional area of web	= 5.5	in^2

B.2 PROPERTIES OF RIB AND FLOOR BEAM USED IN PELIKAN-ESSLINGER'S METHOD

B.2.1 Rib

Referring to Figure B.2

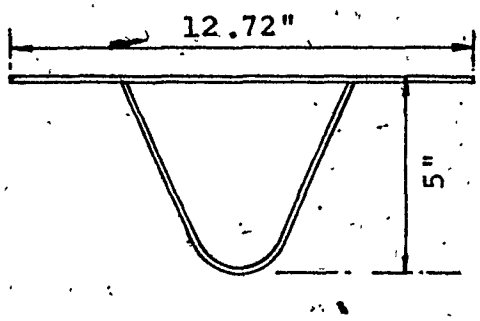

FIG.B.2 - RIB CROSS-SECTION

Effective width of deck plate = 12.72 in
Developed length of rib, L_d = 11.78 in
Area enclosed by rib, A = 17.83 in^2
Torsional constant, K_t = 13.50 in^4

$y = 1.373$ in
$I_{xx} = 12.84$ in^4
$S_{xt} = 9.35$ in^3
$S_{xb} = 3.54$ in^3

Torsional reduction factor, $1/\mu$, as defined in Reference (6) = 6.31

Effective torsional rigidity, H = 1.00×10^8 K-in^2/in.

Ratio of effective torsional rigidity to flexural

rigidity = 0.0323.

B.2.2 Floor Beams

Effective width = 13.20 in

$\bar{Y}$ = 1.348 in

I_{xx} = 86.18 in^4

Relative rigidity ratio, γ = 0.0045

B.3 DATA OBTAINED FROM PROPOSED METHOD

Roots of polynomial are

S_1 = 1.37113

S_2 = 0.590268

S_3 = 0.260614

S_4 = 0.081631

The coefficients K_{jm} and R_{jm} are evaluated as

K_{1_m} = 18.5209 $\bar{m}$

K_{2_m} = 1.55585 $\bar{m}$

K_{3_m} = -0.028831 $\bar{m}$

K_{4_m} = -0.000201 $\bar{m}$

R_{1_m} = 7.10718 $\bar{m}$

R_{2_m} = 3.56062 $\bar{m}$

R_{3_m} = -0.166150 $\bar{m}$ and

R_{4_m} = -0.003779 $\bar{m}$

The following material constants are used:

Young's modulus, E = 29,000 ksi

Poisson's ratio, μ = 0.30

Shear modulus, G = 11.20 ksi